Analysis of control rod ejection accidents in large boiling water reactors

Thorlaksen, B.

Publication date:
1977

Document Version
Publisher's PDF, also known as Version of record

Risø Report No. 344

Risø Report No. 344

Risø National Laboratory

Analysis of Control Rod Ejection Accidents in Large Boiling Water Reactors

by B. Thorlaksen

November 1976

Sales distributors: Jul. Gjellerup, 87, Sølvgade, DK-1307 Copenhagen K, Denmark

Available on exchange from: Risø Library, Risø National Laboratory, DK-4000 Roskilde, Denmark

INIS descriptors

BWR TYPE REACTORS
EXCURSIONS
HYDRAULICS
R CODES
REACTOR KINETICS
REACTOR SIMULATORS
ROD DROP ACCIDENTS
ROD EJECTION ACCIDENTS
THREE-DIMENSIONAL CALCULATIONS
TRANSIENTS

UDC 621.039.524.4-97:621.039.562.24:621.039.588:681.3.06

November 1976 Risø Report No. 344

Analysis of Control Rod Ejection Accidents in Large Boiling Water Reactors

by

B. Thorlaksen

Risø National Laboratory
Department of Reactor Technology

Abstract

Expressions are evaluated for the control rod velocity as well as the hydraulic pressure inside the control rod guide tube during a rod ejection accident and a rod drop accident. For the rod ejection transients, the effectiveness of the control rod velocity limiter is found to be strongly dependent on the discharge flow from a postulated rupture of the control rod drive thimble. The nuclear transient is analysed by means of the three-dimensional dynamic BWR simulator DANAID, which is based on nodal technique. The kinetics equations are written in modified one-energy group theory. Both Doppler feedback and moderator feedback are incorporated in the program. The Doppler effect is especially strong, but because of the power directly deposited in the coolant the moderator feedback is also significant and rapid. Removal of a 2% $\Delta k/k$ rod, with a velocity corresponding to the maximum drop velocity of a General Electric control rod, should not result in any significant damage to the reactor system. The result of the rod ejection analysis is a maximum fuel enthalpy below the fracture thresholds. However, the hot channels are voided and the radioactivity from 800-1200 fuel rods is released to the coolant.

This report is submitted to the Technical University of Denmark, in partial fulfilment of the requirements for obtaining the lic. tech. (Ph. D.) degree.

CONTENTS

Page

1. INTRODUCTION

Major technical problems in reactor safety are a satisfactory determination of a "maximum credible accident" and a plant design that will safely contain the resulting radioactivity. An accurate knowledge of the amount of energy and the modes of its release in such an accident is particularly important, since this will greatly influence containment design.

Perhaps the most serious accident in water reactors can result from a combination of circumstances which include an inadvertant addition of a large amount of excess reactivity.

There are many ways of inserting reactivity into a large LWR. However, most of them result in a relatively slow rate of reactivity insertion and are therefore no threat to the system. The one category of reactivity additions that must be considered in evaluating large nuclear excursions is that associated with the control rod system. It appears that the rapid removal of a high-worth control rod is the only way of obtaining a sufficiently fast rate of reactivity insertion to result potentially in a significant excursion.

Control rod accidents in a LWR are commonly divided into two categories, ROD DROP ACCIDENTS and ROD EJECTION ACCIDENTS, respectively. The control rod drop accident in a BWR is defined as the complete disconnection of a random, fully-inserted control rod from its cruciform control blade at or near the coupling and in such a way that the blade somehow gets stuck at its location. If the drive were withdrawn, the sticking blade would later fall to its drive position and cause a rod drop reactivity insertion accident. The PWR control rod drive is located at the top of the vessel and the fuel assembly fits like a glove to the finger-shaped blade. A disconnection of the blade from its drive would only result in a full insertion of the blade. If one finger breaks off, a small rod drop accident might occur. For the postulated control-rod ejection accident, a mechanical failure of a control-rod drive mechanism housing is assumed, so that the reactor coolant system pressure would eject the control-rod and drive shaft to the fully withdrawn position. The rod ejection accident is a possibility in both the PWR and the BWR, but because of higher control-rod reactivity worth, the potential risk is largest in the BWR.

The rapid removal of a high-worth rod results in a high local k_{∞} in a small region of the core. For large, loosely-coupled cores, this would result in a highly-peaked power distribution and subsequent shutdown mechanisms. Significant shifts in the spatial power generation would occur during the course of the excursion. Therefore, the method of analysis must be

capable of handling many spatial points of the reactor core and, as feed-back mechanisms, both moderator effects and Doppler effects must be included.

The objective of this report is to provide an estimate of the possible consequences of control-rod ejection accidents in a BWR. A break in the control-rod drive housing is assumed and the resulting control-rod velocity is calculated as a function of time with the program RODACC. RODACC incorporates velocity restrictions, and it takes into account maximum critical two-phase flow. With the estimated control-rod velocity as input, the three-dimensional dynamic BWR program DANAID simulates the reactor core and the coolant system. DANAID is based on nodal technique and calculates most of the essential parameters of the reactor. After a DANAID run, the reactor state (coolant velocity, coolant pressure, temperature distribution, etc.) is known and the consequences for the pressure vessel and its internal components can be estimated.

Because control-rod ejection calculations for power reactors are not commonly included in the literature, a rod-drop calculation was performed to verify the code complex.

2. THE BOILING-WATER REACTOR

Because modern boiling-water reactors have reactor cores with slight differences in the basic nuclear and hydraulic design parameters, it is possible to represent most reactors by one prototype. The size of the prototype must be a compromise between a large reactor, dictated by the desire for a loosely coupled reactor, and a small reactor, which is cheaper in computer time. Oskarshamn 1 is rather small compared with very recent power plants, but it has many modern characteristics and is large enough to demonstrate the effects of a highly-peaked power distribution. Thus this reactor was chosen as prototype in the present study.

The reactor vessel cutaway, fig. 2.1, shows the arrangement of the reactor assembly components.

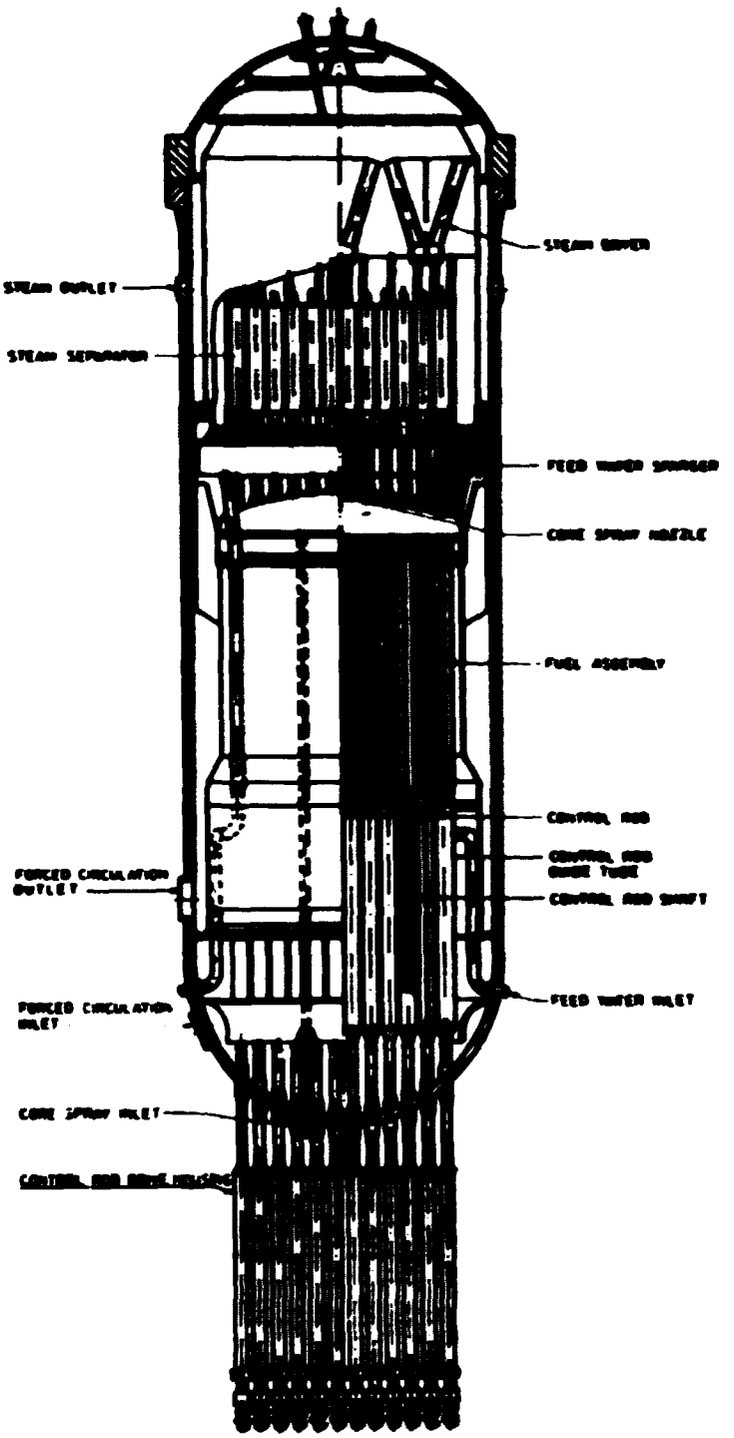

Fig. 2.1. Reactor vessel cutaway.

3. INITIATING EVENT

3.1. The Control Rod System

The control rod system in a typical BWR includes a control rod blade, a velocity limiter, a shaft, a control-rod guide-tube, and a drive system.

The cruciform control-rods contain stainless steel tubes filled with boron-carbide powder. Rollers provide guidance for control-rod insertion and withdrawal and reduce friction between the rod and the fuel boxes. The control-rod support is a hollow shaft extending up through the guide tube from the control-rod drive to the rod.

The velocity limiter is an integral part of the control-rod and it protects against a rod-drop accident. It is designed to limit the free fall velocity and reactivity insertion rate of a control-rod, so as to ensure minimum fuel damage. It is a one-way device, in that the control-rod scram time is not significantly affected. A velocity limiter is not installed in the Oskarshamn reactor.

The control-rod guide-tubes, located inside the vessel, extend from the top of the control-rod drive housings up through apertures in the core support plate. Each tube is designed as the guide for a control-rod and as the vertical support for the four fuel assemblies surrounding the control-rod. The bottom of the guide-tube is supported by the control-rod drive housing, which transmits the weight of theguide-tube and the fuel assemblies to the reactor vessel bottom head.

The control-rods perform dual functions of reactivity regulation and reactor "scram" (prompt shutdown). Because of this the control-rod drives must be capable of inserting or withdrawing a control-rod at a slow, controlled rate, as well as providing rapid insertion when required. The drives are located in the control-rod drive housings attached to the bottom of the reactor vessel.

The drive systems used in European constructions (ASEA-ATOM and KWU) are significantly different from those used in the USA. (GE). Figs. 3.1.1, 3.1.2 and 3.1.3 illustrates the operating principles of the different systems. The control-rod drive mechanism used by General Electric[31] is a double-acting, mechanically latched, hydraulic cylinder. The drive piston is mounted at the lower end of the control-rod shaft. This shaft functions as a piston rod. The drive piston and the shaft make up the main moving assembly in the drive. The piston has both inside and outside sealing rings and operates in an annular space between an inner cylinder (fixed piston tube) and an outer cylinder (drive cylinder). The shaft or the index tube,

as it is called in GE reactors, has circumferential locking grooves, spaced every 6 in along the outer surface to transmit the weight of the control-rod to the collet assembly. This assembly serves as the index tube locking mechanism and prevents the index tube from accidentally moving downwards. Locking is accomplished by fingers mounted on the collet piston at the top of the drive cylinder. In the locked position the fingers engage a locking groove in the index tube. The collet piston is normally held in the latched position by a spring and it will not unlatch until a pressure above reactor vessel pressure is applied to the collet piston to overcome spring force (fig. 3.1.1, drive withdrawn line), slide the collet up against the conical surface in the guide cap, and spread the fingers out so they do not engage a locking groove.

Rod insertion is initiated by a signal from the operator to two insert valves. The signal causes both insert valves to open. The insert drive valve applies pressurised water to the bottom of the drive piston (fig. 3.1.1, drive insert line). The insert exhaust valve allows water from above the drive piston to discharge to an exhaust pool (fig. 3.1.1, drive withdraw line). The collet assembly locking mechanism does not interfere with rod insertion.

Before rod withdrawal the collet fingers must be raised to reach the unlocked position. The notches in the index tube and the collet fingers are shaped so that the downward force on the index tube holds the collet fingers in place. The index tube must be lifted before the collet fingers can be released. This is done by opening the drive insert valves for approximately 1 s. The withdraw valves are then opened, applying driving pressure above the drive piston and opening the area below the piston to the exhaust pool. Pressure is simultaneously applied to the collet piston. As the piston raises, the collet fingers are jammed outwards, away from the index tube, by the guide cap.

During a scram, accumulator pressure is admitted under the drive piston, and the area over the drive piston is vented to the scram discharge volume.

The two European suppliers of boiling water reactors have control-rod drives which are largely similar. For normal reactor power level control and core power distribution control, the absorbers are moved into and out of the core by an electric motor via a screw and nut arrangement. This direct mechanical drive system facilitates exact positioning of the absorber rods. A revolution counter on the motor unit indicates the position within one per cent of the full absorber stroke. In adverse situations, when rapid

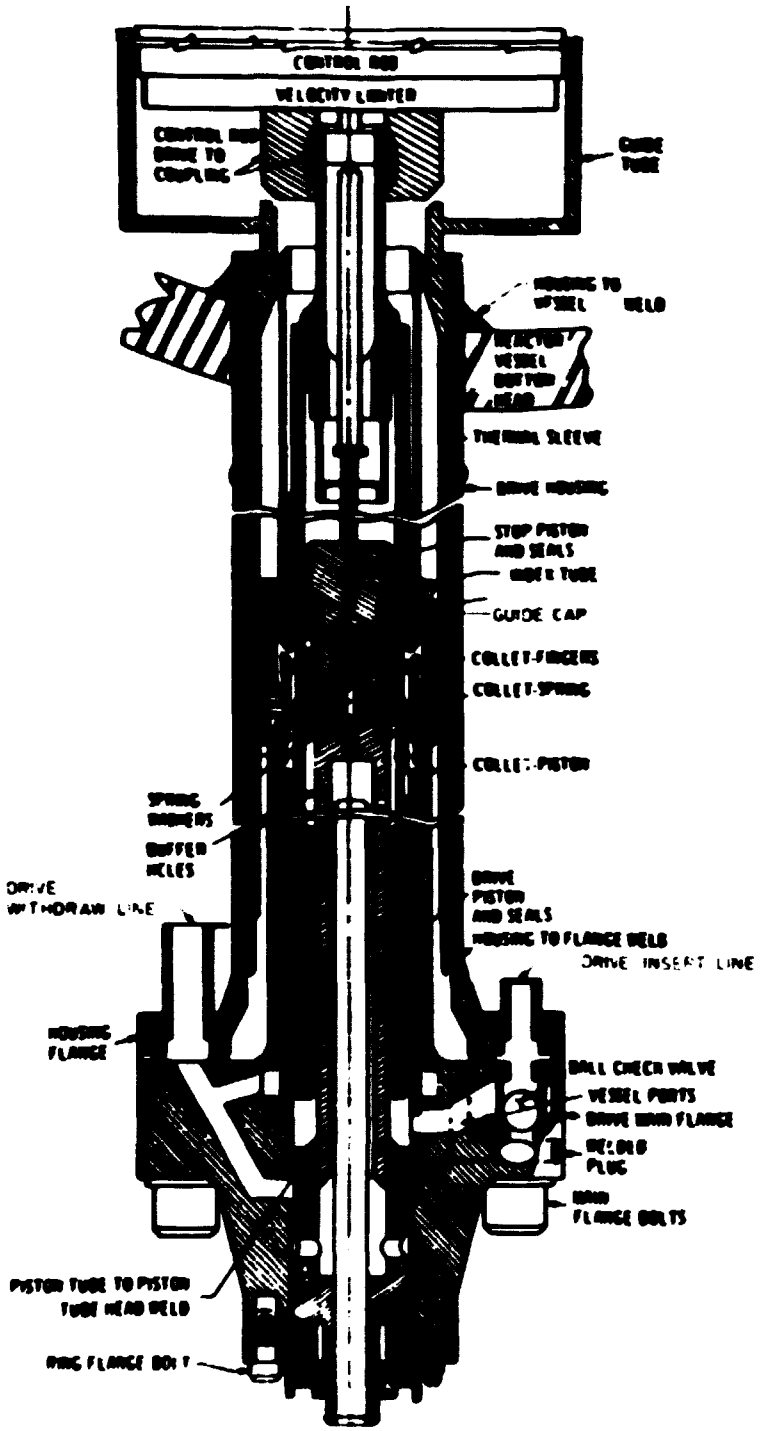

Fig. 3.1.1. General Electric control rod drive system.

insertion is required, the absorbers are driven into the core by admitting pressurized water below the absorber drive piston. In such cases the piston, on top of which lies the absorber, leaves the nut on which it normally rests. Latches that are normally retracted engage a rack in the housing to lock the piston in the uppermost position. Simultaneously with the activation of the hydraulic scram system, the electric drive motors are started to drive the nut to the top position. When the piston rests again on the drive nut, the latches are automatically retracted and the absorbers can be manoeuvred in the normal way.

To prevent control rod ejection in the event of a drive housing failure, reactor suppliers have different control-rod drive housing supports. The General Electric control-rod drive housing support system is shown in fig. 3.1.4. Horizontal beams are installed immediately below the bottom head of the reactor vessel, between the rows of drive housings. The beams are bolted to the reactor support pedestal. Hanger rods are supported from the beams on stacks of disc springs. The support bars are bolted between the bottom ends of the hanger rods. Individual grids rest on the support bars between adjacent beams.

At the bottom of the drive housing the ASEA BWR has a square flange as connection to the four adjoining drives (fig. 3.1.5) so that each housing is supported by two of its neighbours, while it constitues an emergency stop for the other two. A disconnection of the control-rod drive housing and the pressure vessel bottom head, or a break of the housing above the flange, will not result in accidental ejection of the control-rod in this system.

The Kraftwerk Union (KWU) philosophy concerning rod ejection accidents is that, owing to the performance and construction of the control-rod drive housing, the probability of a large break is insignificant. Therefore the present KWU reactors have no support systems for the drive housings. Instead, the joining between the housing and the pressure vessel bottom head has been improved by a nut that turns round the guide tube inside the vessel (fig. 3.1.6).

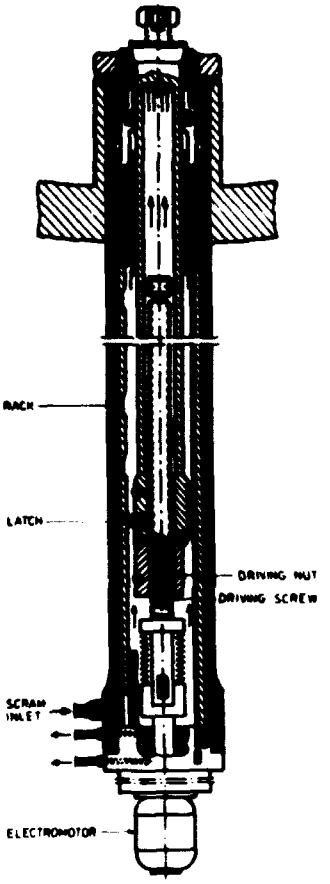

Fig. 3.1.2. KWU control rod drive system.

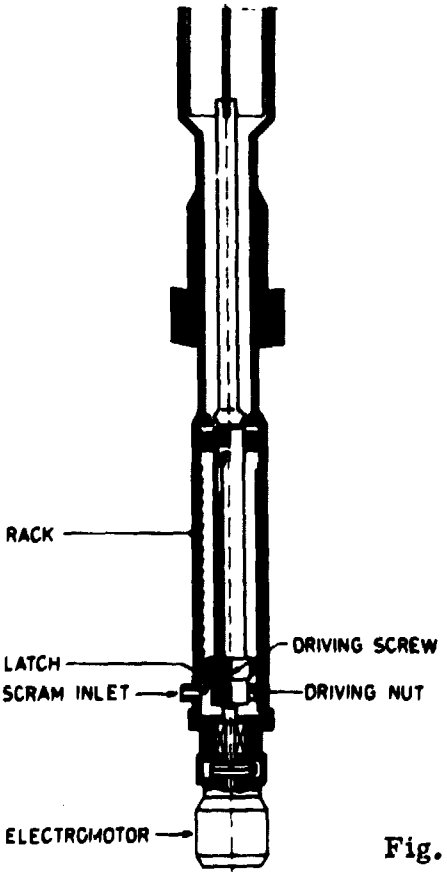

Fig. 3.1.3. ASEA-ATOM control rod drive system.

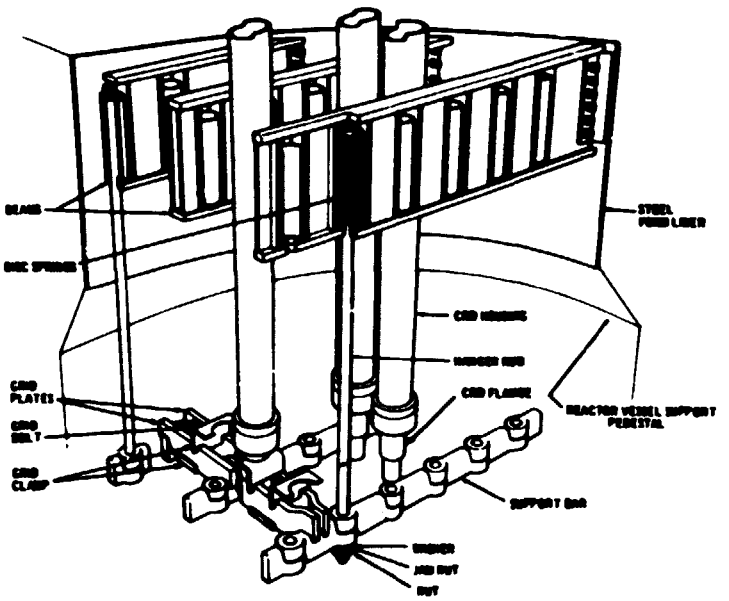

Fig. 3.1.4. GE control rod drive housing support system.

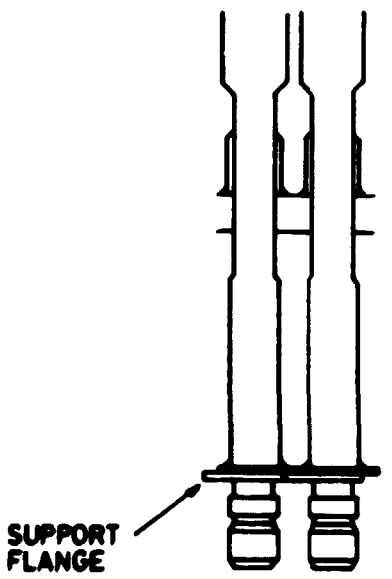

Fig. 3.1.5. ASEA-ATOM control rod drive housing support system.

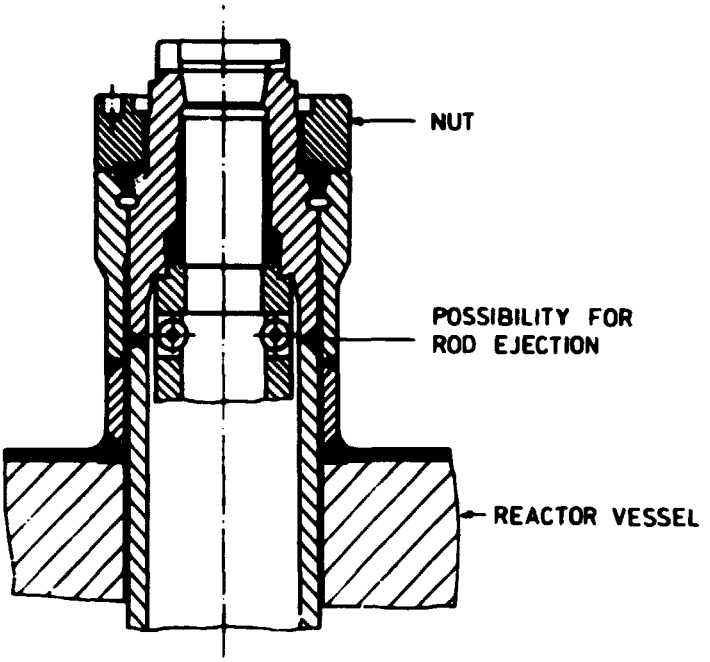

Fig. 3.1.6. KWU control rod drive housing support system.

3.2. The Control-Rod-Drop Accident

In conjunction with the loss-of-coolant accident, the steam-line-break accident and the fuel-bundle-drop accident, the control-rod-drop accident constitutes the design basis accidents in a BWR from General Electric.

The control-rod-drop accident is defined as a power excursion caused by the accidental removal of a control rod from the core at a more rapid rate than can be achieved by the use of the control-rod drive mechanism. In the control-rod-drop accident, a fully inserted control rod is assumed to fall out of the core after being disconnected from its drive, and after the drive has been removed to the fully withdrawn position.

To minimize the probability of a rod-drop accident, some design features and operating procedures have been developed.

The control rods are designed to minimize the probability of sticking in the core. The blades travel in gaps between the fuel channels with total clearance, and they are equipped with rollers which make contact with the channel walls.

The control-rod coupling to the drive shaft is made of high quality materials and tests have shown that the drive and coupling do not fail when

subjected to pull forces up to 30 times greater than that which can be achieved in a reactor.

Movements of the control rods when the reactor is critical or near critical cause changes in the neutron flux. Rod coupling is verified by observing the neutron flux changes during rod movement.

The control-rod bottoms on a seal, preventing the control-rod drive from being withdrawn to its overtravel position. Thus, attempting to withdraw a rod drive to the overtravel position provides an effective method for verifying rod coupling. This method is used prior to reactor startup, when rod following cannot be verified by observing the response of the neutron flux instrumentation. Operating procedures require rod-following verification checks during startup and during major rod movements, and daily verification checks on all rods not fully in to ensure that any rod-from-drive separation would be detected. Procedures require full insertion of rods when following cannot be verified.

Operating procedures require that control-rod movements follow preplanned patterns designed to flatten the power distribution, which tends to minimize the reactivity worth of individual rods, so that extensive fuel damage would not be expected, if a control-rod-drop were to occur.

To augment the above procedural controls, the General Electric BWR's are provided with a control-rod worth-minimizer interlock system and a control-rod velocity limiter. The interlock system consists of a computer that monitors the control rod withdrawal sequence and actuates interlocks to prevent abnormal control-rod patterns. The limiter is a hydraulic piston on the bottom of the control rod, which adds substantial drag against downward control-rod movement.

To result in a serious rod-drop-accident, the dropping rod must be an out of sequence rod, and because the maximum reactivity worth of individual rods decreases rapidly with increasing reactor power, the reactor must be operating at a few per cent only of full power. Thus a severe accident is determined by two operator errors, namely selection of a control rod out of sequence in the prescribed pattern and withdrawal of the drive without check of rod following. At the same time, the control rod-to-drive coupling must fail, the control-rod must stick in the core and drop at the right time and the control-rod worth-minimizer interlock system must be inoperable. All these requirements make the rod-drop accident unlikely and, according to WASH-1400[1], unlikely accidents contribute little to the total risk of nuclear power.

3.3. The Control-Rod-Ejection Accident

A failure of one of the control-rod drive housings results under almost all conditions in a small loss-of-coolant accident, and implies a potential control-rod ejection.

The reactor design and fabrication procedures require considerable attention to the design of the vessel and all its penetrations, including the bottom head penetrations such as the control-rod-drive housings. This provides a high degree of assurance that rod ejection will not occur. The most credible possibilities for failure of the housing are expected to be a break of the housing to vessel weld and a break of the flange bolts nethermost at the control rod thimble.

If the drive housing supports act satisfactorily, a circumferential crack at the attachment weld to the vessel does not result in a rod ejection, no matter which of the three previously described support structures is used, but a failure of the welding in the socket inside the vessel (fig. 3.1.6) might result in a rod ejection accident in KWU reactors.

When the control rod is not operated, the GE rod is locked by the collet fingers, while in the KWU and ASEA types the rod rests unlocked on the drive nut, but if the control rod shaft and the drive nut are separated, a pawl, similar to the GE collet fingers, holds the drive to a dentiformed outer tube. If the bolts in the main flange all break the drive will drop out and, if the rod is separated from the nut, the pawls are activated and will connect the rod to the outer tube. Unfortunately, this tube is not connected to the drive house and, because the support structure does not prevent it, such a failure must result in a rod ejection accident in KWU and ASEA reactors.

If the flange bolts break in cases where the GE support structure is installed, the collet assembly must be able to withstand substantial dynamic loads from the hydraulic pressure and the mass of the control assembly. The static load can be expressed as

$$F = M \cdot g + p_r \cdot A_s - p_{sp} \cdot A_{sp} + p_{out} \cdot A_{out} - p_{in} \cdot A_{in}$$

where

M = mass of control assembly
g = gravity acceleration
p_r = reactor pressure
p_{sp} = pressure above stop piston
p_{out} = pressure above drive piston

p_{in} = pressure below drive piston
A_s = cross sectional area of the control rod shaft
A_{sp} = cross sectional area of the stop piston
A_{out} = cross sectional area of the drive piston for withdrawal
A_{in} = cross sectional area of the drive piston for insertion

Under normal operating conditions, the pressures p_{sp}, p_{out} and p_{in} are approximately equal to the reactor pressure p_r, and the collets only sustain the dead weight of the control rod and drive. If a flange break is followed by a disrupture of the insert line and the withdraw line, the ball check valve is most likely to close. The pressure below the drive piston is then unchanged, while the pressure above the piston decreases to the containment pressure level and at the same time reduces the load on the collets. If the ball check valve remains open, p_{in} and, as a conservative assumption p_{sp}, slowly drop and equal the containment pressure. The maximum static load on the collets then becomes approximately F = 33000 N. The ability of the collet mechanism to prevent an accidental rod withdrawal has been demonstrated by a series of drop tests[2] where it was found that the collet locking mechanism can stop a control rod assembly accelerated to a velocity of 4.5 m/s followed by a 31000 N static load. In other words, the collet assembly may not be able to sustain the static load under the above conditions. If such a basic line failure occurred while the control rod was being withdrawn, and if the collets remained open, which is unlikely, calculations[3] indicate that the steady-state control rod withdrawal velocity would be 60 cm/s compared with a calculated control rod drop velocity of 150 cm/s.

A control-rod ejection caused by a break of the flange bolts is not believed to result in an excursion, as severe as if the failure is at the housing to vessel weld. Owing to the long, narrow cylinder, the resistance to the coolant flow out through the house is large, i.e., much of the water in the guide tube below the velocity limiter must pass the limiter when the control rod is ejected. When the rod drops through the water, large hydraulic drag forces will act on the limiter, and a terminal velocity is reached when the drag forces exactly balance the sum of the external hydraulic forces on the control assembly and gravity.

3.4. Accident Probability

The purpose of this study is not to discuss the probability of a control-rod ejection, but to describe the development of such a postulated accident.

However, if the accident probability is not discussed, there may be an unnecessary overestimation of the risk.

The most valuable work currently concerning reactor safety is undoubtedly the Reactor Safety Study WASH-1400[1]. This concludes that the two accident catagories of interest are both unlikely, and because of their improbability such accidents contribute very little to the total risks involved in nuclear power. Unlikely accidents are given no special treatment in the Reactor Safety Study, but failure rates are estimated for some of the events involved in control-rod-ejection accidents.

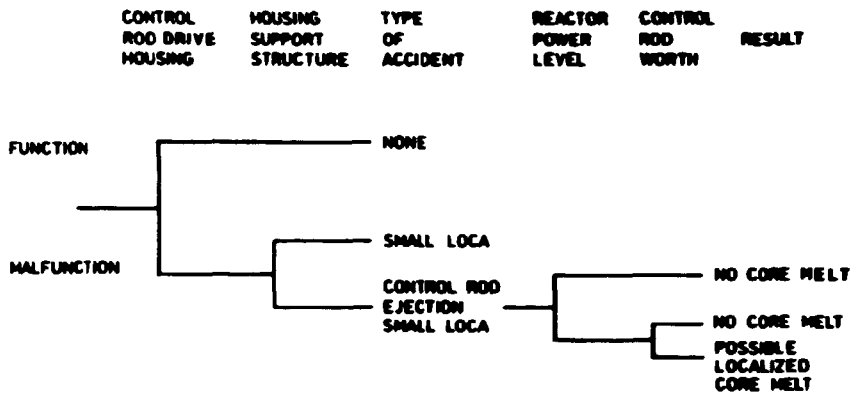

Fig. 3.4.1. Control rod ejection fault tree.

Fig. 3.4.1 shows a simplified event tree for a control-rod ejection. The failure probability of the control-rod drive is assigned a value of $3 \cdot 10^{-4}$ per reactor year. Since the support structure is designed with large structural safety margins, it is considered highly unlikely that it would fail and allow rod ejection to occur. However, the GE structure is periodically removed for reactor maintenance purposes; it is thus possible for a portion of the structure to be incorrectly replaced after maintenance. This failure probability is estimated to be less than 10^{-2} per event. The KWU and ASEA support structures are never removed for maintenance, but then they do not prevent a rod ejection if the housing fails nethermost at the thimble. If it is assumed that a break of the flange bolts and a circumferential crack of the attachment to vessel weld have the same probability, the support structure must be assigned an effective failure probability as high as 0.5. The probability of a control-rod ejection is then $3 \cdot 10^{-6}$ for the GE reactors, and $1.5 \cdot 10^{-4}$ for the KWU and ASEA types.

In order for a control-rod ejection accident to result in fuel damage, the ejected rod must, according to [1], have a reactivity worth greater than 1.5% Δk/k. This requires that the reactor is critical, but at less than 20% power, and that the ejected control rod is one of the rods having a reactivity worth large enough to cause localized melting. There are approximately 12 events per year that involve operation of the reactor in the range from criticality to 20% power. Assuming a median value of 4 h in this power range per event, it is estimated that the plant will be in this power range for approximately 52 h per year. Therefore, the probability of being in this mode is approximately $52/(365 \cdot 24) = 6 \cdot 10^{-3}$ per event. For the analysis, it is conservatively assumed that 10% of the rods are high worth rods for the power range of concern. Thus, the probability of the ejected rod being a high worth rod is assumed to be approximately 10^{-1}. The probability for a control-rod ejection accident with "maximum damage" can then be assigned a value of $2 \cdot 10^{-9}$ for General Electric reactors and a value of $9 \cdot 10^{-8}$ for KWU and ASEA reactors.

The Reactor Safety Study assessed the total probability for core melting in connection with very likely transients to be approximately 10^{-5}. Thus the risk of a rod-ejection accident is insignificant compared with the total risk of nuclear power.

The rod-drop accidents have smaller consequences than the rod-ejection accidents and, because of a more complicated fault tree (fig. 3.4.2), the probability of a rod-drop accident is perhaps even lower. Therefore the risk of such an accident is negligible too.

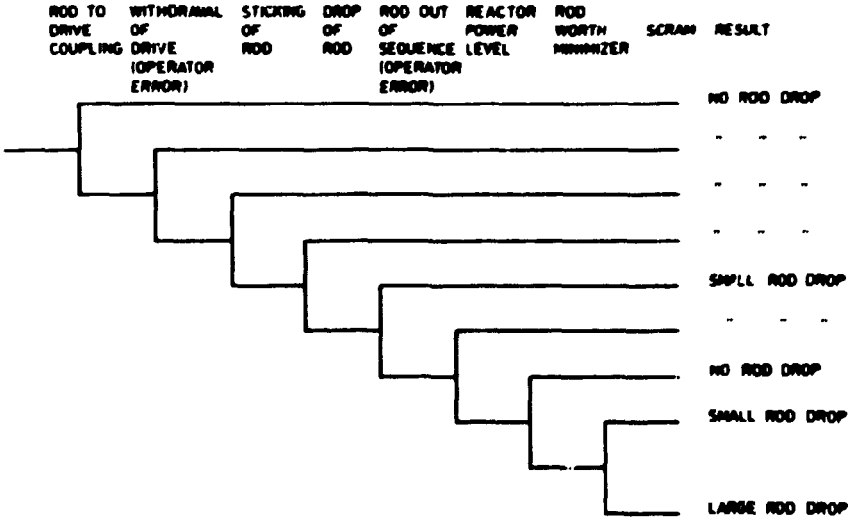

Fig. 3.4.2. Control rod drop fault tree.

4. CONTROL ROD VELOCITY CALCULATION

4.1. The Control Rod Velocity Limiter

As previously stated, some reactor suppliers, i.e. GE and KWU, have a special device, the control rod velocity limiter, to limit the control rod drop velocity.

The velocity limiter, fig. 4.1.1, is an integral part of the bottom assembly of each control rod. It has the shape of two conical elements acting as a large-clearance piston inside the control rod guide tube. The lower conical element is separated from the upper by four radial spacers 90^{o} apart and located at a 15^{o} angle relative to the upper conical element.

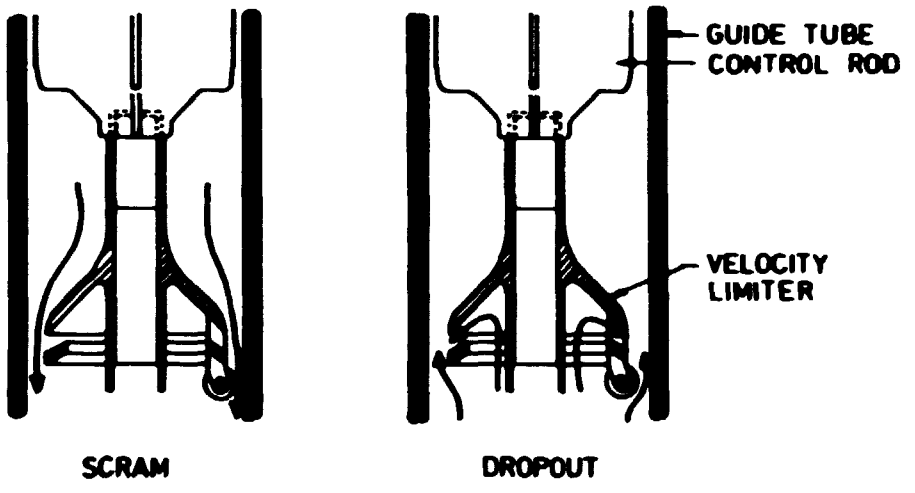

Fig. 4.1.1. General Electric control rod velocity limiter.

The hydraulic drag forces on a control rod are approximately proportional to the square of the rod velocity and are negligible at normal rod-withdrawal or rod-insertion speeds. However, during the scram stroke, the rod reaches high velocity, and the drag forces must be overcome by the drive mechanism.

To limit control rod velocity during dropout but not during scram, the velocity limiter is provided with a streamlined profile in the upward direction. Thus, when the control rod is scrammed, water flows over the smooth surface of the upper conical element into the annulus between the guide tube and the limiter. In the dropout direction, however, water is trapped by the lower conical element and discharged through the annulus

between the two conical sections. Because this water is jetted in a partially reversed direction into water flowing upward in the annulus, severe turbulence is created, thereby slowing the withdrawal of the control rod assembly.

The BWR's of ASEA-ATOM have no special control rod velocity limiter, but the control rod console is provided with a piston to close the gap to the drive housing, when the control rod is totally withdrawn. This piston influences the dropout velocity, but does not effectively restrict it, and because the device yields resistance to relative flow in both directions, the scram insertion is affected too.

4.2. Control Rod Drop, Analytical Solution

There is no leak of coolant from the pressure vessel to the reactor containment in the rod-drop accident. Thus, the reactor pressure is not decreased and the control rod guide tube still contains non-streaming single-phase water. Because the specific volume of liquid is rather indifferent to changes in the coolant system pressure, it is possible to find an analytical expression for the control rod drop velocity.

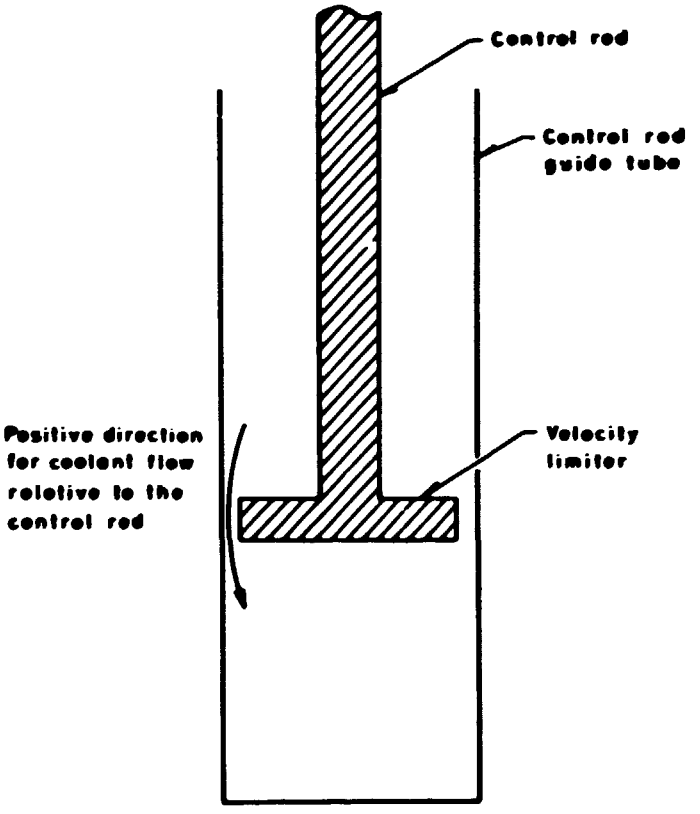

Fig. 4.2.1. Model for the control rod and its guide tube used in obtaining an analytical approach to the rod drop velocity.

Fig. 4.2.1 shows a simplified model of the control rod and its guide tube. During the rod-drop accident the discharged water from below the rod must pass the piston, i.e. the velocity limiter, but because of the very special construction of the limiter the leak rate is low and a high pressure barrier, Δp_{vl}, is built up across the limiter. The pressure drop in a constriction is proportional to the square of the mass flow through the constriction[4], so when the hydrostatic pressure is neglected, and Δp_{vl} is the pressure difference between the lower part of the piston and the upper part, Δp_{vl} may be expressed as

$$\Delta p_{vl} = f \frac{w^2}{\rho (A_{gt}-A_{vl})^2} \qquad (4.2.1)$$

Here -w is the discharged mass flow in the upward direction relative to the piston and f is the single phase friction factor for the velocity limiter applied to flow in the same direction. The coolant density is ρ, and A_{gt} and A_{vl} are the cross sectional areas of the guide tube and the piston, respectively.

A fluid mass balance can be made over the volume below the piston. This volume is increased at the rate

$$\dot{\Omega} = -u A_{gt}, \qquad (4.2.2)$$

where u is the control rod velocity. The change of fluid mass, $\rho\dot{\Omega}$, must be equal to the net flow across the surface, w. Thus, preservation of fluid mass is contained in the equation

$$w = -\rho \cdot A_{gt} \cdot u. \qquad (4.2.3)$$

The cross sectional area of the control rod is termed A_{rod}, and the pressure drop along the rod from above the piston to the top of the rod is Δp_{rod}. When M is the total mass of the moving assembly, Newton's second law applied to the assembly becomes

$$M \frac{du}{dt} = M \cdot g - A_{vl} \Delta p_{vl} - A_{rod} \Delta p_{rod}, \qquad (4.2.4)$$

where g is the specific gravity. Here friction between the rod itself and the fluid is excluded, but it might be included in the velocity limiter friction by an appropriate choice of f.

Combination of eqs. 4.2.1, 4.2.3 and 4.2.4 yields

$$\frac{1}{1-\left(\sqrt{\frac{f c_1}{c_2}}\,u\right)^2}\;\frac{d}{dt}\left(\sqrt{\frac{c_1 f}{c_2}}\,u\right) = \sqrt{c_1 c_2 f} \qquad (4.2.5)$$

$$c_o = \left(\frac{A_{gt}}{A_{gt}-A_{vl}}\right)^2 \qquad (4.2.6)$$

$$c_1 = c_o \frac{A_{vl}}{M} \qquad (4.2.7)$$

$$c_2 = g \cdot \frac{A_{rod}}{M}\,\Delta p_{rod}\,. \qquad (4.2.8)$$

Assuming ρ and Δp_{rod} constant, c_o, c_1 and c_2 are positive constants, and f is positive, too. Hence, the complete solution to eq. 4.2.5 may be expressed as

$$\text{Artgh}\,[u/u_2] = t/\tau_2 + B \qquad (4.2.9)$$

$$u_2 = \sqrt{\frac{c_2}{c_1 f}} \qquad (4.2.10)$$

$$\tau_2 = \sqrt{\frac{1}{c_1 c_2 f}} \qquad (4.2.11)$$

Applying the convenient boundary condition

$$t = 0 \rightarrow u = 0 \qquad (4.2.12)$$

the arbitrary constant B is determined, and the proper solution found

$$u = u_2\,\text{tgh}\,(t/\tau_2)\,. \qquad (4.2.13)$$

Then the pressure difference at the velocity limiter becomes

$$\Delta p_{vl} = \Delta p_{max}\,\text{tgh}^2\,(t/\tau_2) \qquad (4.2.14)$$

$$\Delta p_{max} = c_o \frac{c_2}{c_1} \qquad (4.2.15)$$

The control rod drop velocity and the pressure barrier at the velocity limiter can be calculated as a function of time, when numerical values have been attributed to the quantities u_2, τ_2 and Δp_{max}. Most of the data necessary for calculation of these quantities are simple design data available from the reactor suppliers, but it is difficult to obtain an accurate value of f by calculation because of the special design of the velocity limiter. The best way to obtain an acceptable approximation to f is to measure the steady state rod drop velocity, u_2, and then to calculate f from eq. 4.2.10. In this way f becomes an effective friction factor for both the control rod and the velocity limiter, and that is exactly what is needed here. The maximum control rod drop velocity achievable in a GE BWR is mentioned in [5] and presented here in table 4.2.1. Also presented in the same table are design data taken from [3].

For calculation of the pressure drop along the rod, Δp_{rod}, only the hydrostatic part is incorporated, thus, $\Delta p_{rod} = l \cdot (1-\alpha) \cdot \rho \cdot g$, where l is the length of the rod and α the steam fraction. At the same time it is assumed that the reactor is at low power, allowing the void to be neglected. In addition, Δp_{rod} will only have little influence on the rod velocity.

Table 4.2.1

Data for Rod Drop Velocity Calculation

Quantities obtained from reactor vendor	Symbol	Numerical value
Cross sectional area of velocity limiter	A_{vl}	0.0439 m^2
Cross sectional area of guide tube	A_{gt}	0.0552 m^2
Cross sectional area of control rod	A_{rod}	0.0011 m^2
Mass of moving assembly (control rod)	M	85.5 kg
Length of control rod	l	3.65 m
Coolant density	ρ	740 kg/m^3
Maximum measured rod drop velocity	u_2	0.95 m/s

Calculated quantities

Velocity limiter friction, relative upstream	f, f_{up}	1.2
Time constant	τ_2	105 ms
Maximum pressure build-up at velocity limiter	Δp_{max}	0.2 bar

4.3. Control-Rod Ejection, Analytical Solution

There are two major differences between the categories of excursion accidents of interest in this study. In the rod-drop accident, gravity is the only force to withdraw the rod; however, in case of a rod-ejection accident, gravity is negligible and the essential pull come from the huge hydraulic pressure gradient acting on the control assembly. Further control-rod drop is not combined with any loss of coolant, but rod ejection probably is. The reason for considering the leak of the coolant is not because it would lead to a severe loss-of-coolant accident - the loss would not be that large - but because leaking from the bottom of the guide tube counteracts a rapid pressure build-up below the velocity limiter, which then has a reduced value.

When coolant starts to leak from the guide tube, the hydraulic pressure drops and steam is generated. In this case it is not a good approximation to keep the coolant density as a constant, but, in an attempt to obtain an analytical expression for the control rod velocity, this assumption is nevertheless maintained.

The model used in this section for calculation of the control rod velocity is shown in fig. 4.3.1.

The pressure gradient, Δp_{vl}, caused by the velocity limiter, is calculated almost identically to that in the previous section. However, because of the leak of coolant, w_{vl} may be positive in the transition phase, i.e. the coolant can have the direction of relative downflow at the velocity limiter. Thus the pressure gain is calculated as

$$\Delta p_{vl} = f \frac{w_{vl}^2}{\rho (A_{gt} - A_{vl})^2} \qquad (4.3.1)$$

$$f = \begin{cases} -f_{down} & \text{for } w_{vl} > 0 \\ f_{up} & \text{for } w_{vl} < 0 \end{cases} \qquad (4.3.2)$$

The coolant volume below the piston is increased at the rate

$$\dot{Q} = - u(A_{gt} - A_{shaft}) , \qquad (4.3.3)$$

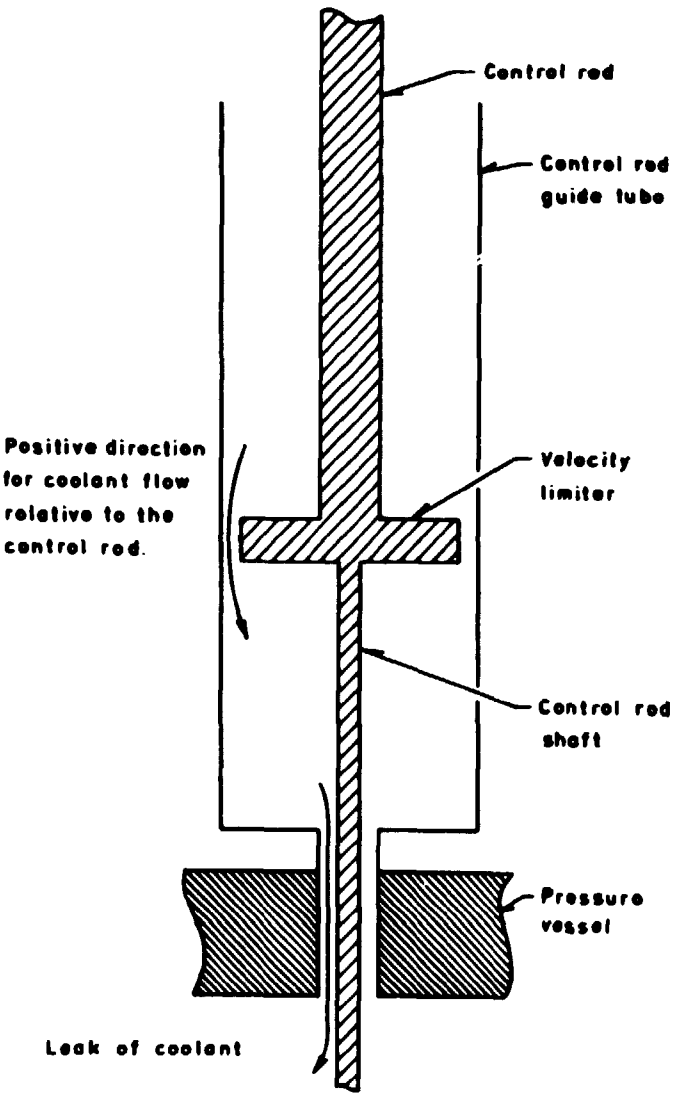

Fig. 4.3.1. Model for the control rod and its guide tube used in obtaining an analytical approach to the rod ejection velocity.

where A_{shaft} is the cross-sectional area of the control rod shaft. The "loss" of coolant, $\rho\dot{Q}$, is equal to the net flow across the surface, thus, when w_{leak} is the leak rate to the containment, a mass balance yields

$$w_{vl} - w_{leak} = - \rho u(A_{gt} - A_{shaft}) . \qquad (4.3.4)$$

Using the pressure, p_{vl}, just below the velocity limiter and the containment pressure, p_{con}, the dynamic equation becomes

$$M\frac{du}{dt} = Mg - A_{rod}\,\Delta p_{rod} - A_{vl}\,\Delta p_{vl} + A_{shaft}(p_{vl} - p_{con}) . \qquad (4.3.5)$$

Here M is the total mass of the moving assembly, i. e. the control rod, the control rod shaft and possibly the drive housing.

A control-rod ejection is so rapid that most of its reactivity worth is inserted before the reactor pressure increases. An acceptable approximation to p_{vl} is therefore

$$p_{vl} = p_o + \Delta p_{vl} \qquad (4.3.6)$$

where p_o is the constant reactor pressure. The pressure above the velocity limiter is not constant as assumed here, but the change in this pressure is mainly due to a change in the hydrostatic pressure caused by the removal of the rod, and such a change is small compared to Δp_{vl}.

w_{leak} is zero at the initiation of the event, but in a very short time maximum critical flow is attained in the orifice. Thus, except at the beginning, w_{leak} has an almost constant value. To give w_{leak} this maximum value at the start time, too, is equal to letting the pressure below the velocity limiter drop immediately, resulting in an overestimation of the control rod acceleration, but the steady state velocity of the rod remains unaltered. In the following, w_{leak} is assumed constant.

Equations 4.3.1, 4.3.4, 4.3.5 and 4.3.6 might be reduced to

$$\frac{du}{dt} = c_2 - fc_1(u_o - u)^2 \qquad (4.3.7)$$

$$c_o = \rho\left(\frac{A_{gt} - A_{shaft}}{A_{gt} - A_{vl}}\right)^2 \qquad (4.3.8)$$

$$c_1 = c_o\,\frac{A_{vl} - A_{shaft}}{M} \qquad (4.3.9)$$

$$c_2 = g - \frac{A_{rod}}{M}\,\Delta p_{rod} + \frac{A_{shaft}}{M}\,(p_o - p_{con}) \qquad (4.3.10)$$

$$u_o = \frac{w_{leak}}{\rho\,(A_{gt} - A_{shaft})} \qquad (4.3.11)$$

With the previous assumptions, c_o, c_1, c_2 and u_o are positive constants.

For further simplification, it is necessary to split the problem into two in order to make f consistent in each domain. From a physical point of view it is obvious that if there is a relative downflow, it must occur immediately after the break and until a time, t_o, when the control rod has reached the velocity u_o.

The problem might now be redefined to

$$\frac{1}{1 + \left(\frac{u_o - u}{u_1}\right)^2} \frac{d}{dt}\left(\frac{u_o - u}{u_1}\right) = \frac{1}{\tau_1} \quad \text{for } t < t_o \tag{4.3.12}$$

$$\frac{1}{1 - \left(\frac{u_o - u}{u_2}\right)^2} \frac{d}{dt}\left(\frac{u_o - u}{u_2}\right) = -\frac{1}{\tau_2} \quad \text{for } t > t_o \tag{4.3.13}$$

$$u_1 = \sqrt{\frac{c_2}{c_1 f_{down}}} \tag{4.3.14}$$

$$u_2 = \sqrt{\frac{c_2}{c_1 \cdot f_{up}}} \tag{4.3.15}$$

$$\tau_1 = \sqrt{\frac{1}{c_1 c_2 f_{down}}} \tag{4.3.16}$$

$$\tau_2 = \sqrt{\frac{1}{c_1 c_2 f_{up}}} \tag{4.3.17}$$

The complete solutions to the two differential equations are

$$\text{Arctg}\left(\frac{u_o - u}{u_1}\right) = -\frac{t}{\tau_1} + B_1 \tag{4.3.18}$$

and

$$\text{Artgh}\left(\frac{u_o - u}{u_2}\right) = -\frac{t}{\tau_2} + B_2 \tag{4.3.19}$$

respectively, where B_1 and B_2 are arbitrary constants. Applying the boundary conditions

$$t = 0 \rightarrow u = 0 \tag{4.3.20}$$

$$t = t_o \rightarrow u = u_o \tag{4.3.21}$$

the proper solution and t_o are determined

$$u = \begin{cases} u_o - u_1 \, tg \left(\frac{t_o - t}{\tau_1} \right) & \text{for } t < t_o \\ u_o + u_2 \, tgh \left(\frac{t - t_o}{\tau_2} \right) & \text{for } t > t_o \end{cases} \tag{4.3.22}$$

$$t_o = \tau_1 \, Arctg \left(\frac{u_o}{u_1} \right). \tag{4.3.23}$$

Then Δp_{v1} might be expressed as

$$\Delta p_{v1} = \begin{cases} - \Delta p_{max} \, tg^2 \left(\frac{t_o - t}{\tau_1} \right) & \text{for } t < t_o \\ \Delta p_{max} \, tgh^2 \left(\frac{t - t_o}{\tau_2} \right) & \text{for } t > t_o \end{cases} \tag{4.3.24}$$

with

$$\Delta p_{max} = c_o \frac{c_2}{c_1}. \tag{4.3.25}$$

If A_{shaft} and w_{leak} are removed from eqs. 4.3.22 and 4.3.24, the equations reduce to the corresponding rod drop expressions, eqs. 4.2.13 and 4.2.14, respectively.

In addition to table 4.2.1, table 4.3.1 is needed for calculation of the quantities involved in the rod ejection formulae. Most of the elements in table 4.3.1 are described below.

The control rod and its shaft are chosen as moving assembly, while the drive housing is excluded. Probably part of the housing will be removed too, but the strength of the coupling to the drive depends on which kind of break is postulated. Besides, it is a conservative assumption to reduce

the mass of the moving assembly to a minimum, because then the acceleration time is shorter, while the maximum speed is unaffected.

The friction factor, f_{up}, is known from the rod drop calculations. f_{down} is not very important and a calculation based on geometrical considerations is believed to be accurate enough. A model for the flow area around the constriction is shown in fig. 4.3.2, indicating that the velocity limiter might be separated in a contraction and an expansion. f_{down} is calculated making use of [6] and the result is incorporated in table 4.3.1.

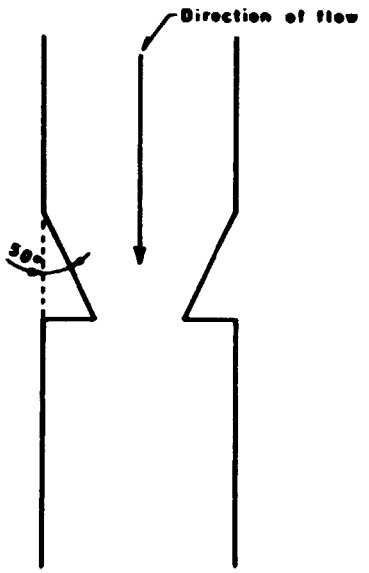

Fig. 4.3.2. Model for the flow area change around the control rod velocity limiter.

The coolant leak rate in the orifice must be known for the estimation of u_o. When the final pressure at the bottom of the guide tube and the friction factor for the outlet duct are estimated, the discharged mass flow, w_{leak}, can be calculated by means of expressions for the maximum critical two-phase flow. In this study the Moody expression[7] has been used. The final pressure nethermost in the guide tube is approximately $p_o + \Delta p_{max}$, which is known. The applied friction factor for the orifice, f_{exit}, is calculated from geometrical considerations by means of [6].

The results presented in table 4.3.1 are believed to be the best data for calculation of the control rod velocity after a circumferential break of the housing to vessel weld. A further discussion of the influence of parameter variations is given in section 4.5.

Table 4.3.1

Data for Rod Ejection Velocity Calculation

Quantities from reactor vendor	Symbol	Numerical value
Cross sectional area of control rod shaft	A_{shaft}	0.00456 m^2
Cross sectional area of guide tube exit	A_{exit}	0.0118 m^2
Mass of moving assembly (rod + shaft)	M	140.5 kg
Reactor pressure	p_o	70 bar
Containment pressure	p_{con}	1 bar
Calculated quantities		
Velocity limiter friction, relative downstream	f_{down}	0.75
Guide tube exit friction	f_{exit}	0.4
Steady state pressure barrier at velocity limiter	Δp_{max}	8.3 bar
Coolant leak rate from guide tube	w_{leak}	248 kg/s
eq. 4.3.11	u_o	6.6 m/s
eq. 4.3.14	u_1	8.5 m/s
eq. 4.3.15	u_2	6.7 m/s
eq. 4.3.16	τ_1	37 ms
eq. 4.3.17	τ_2	29 ms
eq. 4.3.23	t_o	24 ms

4.4. RODACC, A Fortran Computer Code

The behaviour of the control rod during a rod drop and a rod ejection accident is now known in great detail, but some trammels still remain. However, treating the coolant as a two-phase mixture and incorporating a more realistic model for the leak rate make an analytical solution of the problem impossible. Therefore, a computer code was made for analysis of the more sophisticated aspects of the problem.

Guide Tube Model

For a mathematical description, the guide tube is devided into N_t sections, fig. 4.4.1. Section number 1 and section number N_t cover the tube inlet and outlet, respectively, while the volume above the velocity limiter is shared by N_a sections of equal size. The volume of each of these sections increases, as the control rod is withdrawn. The volume of

the next section, section number $N_{vl} = N_a + 2$, is independent of time, but the section deals with the velocity limiter and consequently it follows the rod down during withdrawal. What is left of the guide tube, i. e. the part below the piston, is shared by N_b identical sections with volumes diminishing with time.

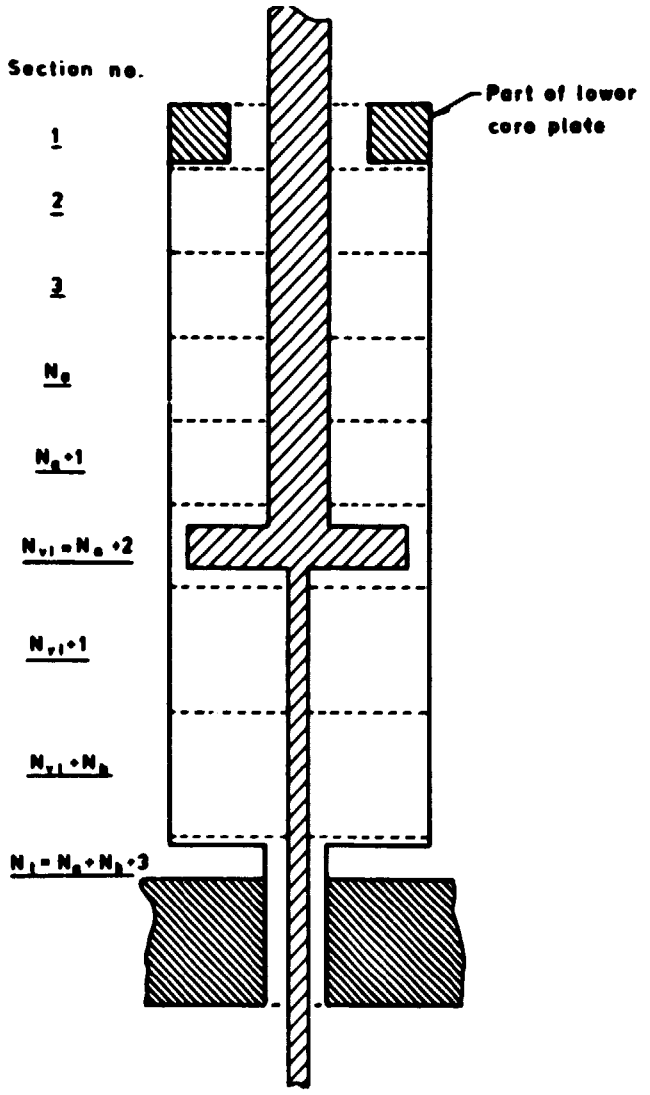

Fig. 4.4.1. Model for the control rod and its guide tube used in RODACC.

Hydrodynamic Model

In the hydrodynamic model for the water-steam mixture subcooling or superheating of steam are omitted, so the steam, if present, is always at the saturation temperature T_s, while the fluid state is allowed to deviate somewhat from equilibrium.

The thermodynamic state functions at saturation are assumed to be functions of pressure only (including T_s), and the water functions are expressed as Taylor series of first degree in the water temperature T_f. For the fluid mass density this is

$$\rho_f = \rho_{f_s} + \left(\frac{\partial \rho_f}{\partial T_f}\right)_p (T_f - T_s) . \qquad (4.4.1)$$

where ρ_{f_s} is the fluid mass density at saturation and p is the pressure. A similar expansion for the internal energy yields

$$e_f = e_{f_s} + C_p (T_f - T_s) . \qquad (4.4.2)$$

The zero point of energy is arbitrary and is here taken to be the reference temperature T_{so}, so

$$e_f = C_p (T_f - T_{so}) . \qquad (4.4.3)$$

The specific enthalpy is defined as

$$h_f = e_f + \frac{p}{\rho_f} \qquad (4.4.4)$$

hence

$$h_f = C_p (T_f - T_{so}) + \frac{p}{\rho_f} . \qquad (4.4.5)$$

Other quantities of the liquid are calculated at the saturation temperature.

From an intermolecular point of view, evaporation might be explained as molecules from the liquid running up towards the van der Waal potential, and some that have sufficient kinetic energy break through the surface tension and change phase from liquid to gas. At the same time some gas molecules hit the boundary and join the liquid. Thus the net evaporation rate, ϕ, (or if negative the condensation rate) is the difference between the two processes. At saturation ϕ is zero.

In principle, a fluid is a compressed gas, and for a gas a Maxwellian velocity distribution applies [8]. Assuming that such a velocity distribution function is valid for the fluid too, the probability of finding molecules with

a velocity component in the direction of the boundary and in the range dv at v is $\eta(v)dv$, where

$$\eta(v) = \left(\frac{m}{2\pi kT}\right)^{1/2} \exp\left(-\frac{mv^2}{2kT}\right). \qquad (4.4.6)$$

T and m are the absolute temperature of the liquid and the mass of one molecule, respectively, while k is the Boltzmann constant.

The probability of finding molecules with velocity components greater than a reference velocity v_o is

$$\eta(v > v_o) = \int_{v_o}^{\infty} \left(\frac{m}{2\pi kT}\right)^{1/2} \exp\left(-\frac{mv^2}{2kT}\right) dv = \frac{1}{2} - \frac{1}{2}\,\mathrm{erf}\left(\sqrt{\frac{\epsilon_o}{kT}}\right) \qquad (4.4.7)$$

with $\epsilon_o = \frac{1}{2} m v_o^2$. Thus it is most obvious to expect ϕ to be proportional to

$$\mathrm{erf}\left(\sqrt{\frac{m}{k}\frac{h_{fg}}{T_s}}\right) - \mathrm{erf}\left(\sqrt{\frac{m}{k}\frac{h_{fg}}{T}}\right), \qquad (4.4.8)$$

where $h_{fg} = \frac{\epsilon_o}{m}$ is the specific evaporation enthalpy. The function $\mathrm{erf}(x^{-1/2})$ is rather linear in x, so it is an acceptable approximation to assume that is linear in steps in $(T - T_s)/h_{fg}$.

The evaporation rate is a function of the boundary area too. For small void fractions, α, the steam is assumed to form spherical bubbles of equal size and with a diameter, d_s, which is independent of α. Thus, the surface area per unit volume of the coolant becomes

$$A = 6\frac{\alpha}{d_s} \qquad \text{for} \quad \alpha \ll 1 . \qquad (4.4.9)$$

When the steam is dominant, the liquid forms spherical bubbles with the surface area

$$A = 6\frac{1-\alpha}{d_f} \qquad \text{for} \quad \alpha \gg 0 . \qquad (4.4.10)$$

For small void fractions, $1 - \alpha$ is nearly independent of α, just as α is unaffected by variations in $1 - \alpha$ when $\alpha \simeq 1$. Because $\alpha(1-\alpha)$ obtains a maximum value when the coolant volume is equally shared by the liquid and the gas, it seems reasonable to expect A to be a function of that product.

The following expression for the bulk fluid evaporation terms is proposed in [8]:

$$\phi = \begin{cases} f(a)(1+\varkappa)(T_f - T_s) & \text{for } T_f > T_s \\ f(a)(1-\varkappa)(T_f - T_s) & \text{for } T_f < T_s \end{cases} \qquad (4.4.11)$$

with

$$f(a) = \frac{1}{h_{fg}} (R_o + R_1 a(1 - a)) . \qquad (4.4.12)$$

R_o, R_1 and $\varkappa$ are constants. The term associated with R_o covers evaporation and condensation around foreign bodies such as walls, impurities, etc. Note that if ϕ, as calculated from eq. 4.4.11, is negative and no steam is present, ϕ must be put at zero, as there are no voids to condense. The expression for ϕ is in excellent agreement with what is expected from above, therefore eqs. 4.4.11, 4.4.12 are used for the evaporation term in RODACC.

The two-phase friction is calculated as

$$F = f \cdot R \cdot \frac{G_f^2}{\rho_f} \qquad (4.4.13)$$

$$G_f = \frac{w_f}{A} .$$

The correlation was made by Becker et al.[10] and is valid for a wide range of pressure, quality and mass flow rates and heat fluxes.

According to Becker, the two-phase friction multiplier

$$R = 1 + a \left(\frac{x}{p}\right)^{.96} . \qquad (4.4.14)$$

Here x is the quality and p the pressure, while a is an input quantity.

For the single-phase friction factor f, Weisbach's formula for smooth pipes has been used

$$f = \frac{g_1}{2 \cdot D_e R_e^{g_2}} . \qquad (4.4.15)$$

D_e is the equivalent hydraulic diameter of the channel, R_e the Reynolds number, and g_1, g_2 the input constants.

The slip ratio is defined as $S = v_g/v_f$, where v_g and v_f are velocities of the gas and the fluid, respectively. Because the mass flow rates are very

high during the ejection, it is believed that the steam is snapped up by the fluid, so that the coolant flow is homogeneized. Thus S = 1 has been used in the code, but the slip is treated explicitly, so that it is easy to use another expression.

System Equations

The equations for conservation of mass, momentum and energy are used to calculate the coolant flow throughout the guide tube.

The lower boundary of each section is included in the section and it is assumed that the physical properties of the coolant are consistent inside each section.

The mass equation for the steam in section k becomes

$$\frac{d}{dt}\left(\Omega_k \alpha_k \rho_{gk}\right) = \phi_k \Omega_k - \left(\Phi_{gk} - \Phi_{gk-1}\right) \tag{4.4.16}$$

where Ω_k is the volume of section k and

$$\Phi_{gk} = A_k \alpha_k \rho_{gk} \left(v_{gk} - u_k\right) \tag{4.4.17}$$

u_k is the velocity of the boundary k. Hence,

$$\frac{d\alpha_k}{dt} = \frac{\phi_k}{\rho_{gk}} - \alpha_k \left(\frac{1}{\rho_{gk}} \frac{d\rho_{gk}}{dt} + \frac{1}{\Omega_k} \frac{d\Omega_k}{dt}\right) - \frac{\Phi_{gk} - \Phi_{gk-1}}{\rho_{gk}\,\Omega_k} \quad . \tag{4.4.18}$$

The mass equation for the total coolant is very simple

$$\frac{d}{dt}\left(\Omega_{k+1}\,\rho_{k+1}\right) = -\Phi_{k+1} + \Phi_k \tag{4.4.19}$$

where

$$\rho_k = \alpha_k \rho_{gk} + \left(1 - \alpha_k\right) \rho_{fk} \tag{4.4.20}$$

$$\Phi_k = A_k \left(G_k - \rho_k u_k\right) \tag{4.4.21}$$

which is tantamount to

$$G_k = \rho_k u_k + \frac{A_{k+1}\left(G_{k+1} - \rho_{k+1}\,u_{k+1}\right) + \frac{d}{dt}\left(\Omega_{k+1}\,\rho_{k+1}\right)}{A_k} \tag{4.4.22}$$

The momentum equation is rather complex, because the coolant interferes with both the guide tube and the control rod, and because maximum, critical two-phase flow must be taken into account. Another complication is that the flow resistance at the velocity limiter does not only depend on the flow speed but also on the flow direction relative to the control rod.

The coupling between the coolant and the control rod is very strong at the velocity limiter and weak elsewhere, therefore this coupling is concentrated to the velocity limiter section in the model. If there is no velocity limiter, however, the friction between the coolant and the control rod could be included in section N_{vl}. Maximum critical two-phase flow is allowed to occur in sections N_{vl} and N_t only (fig. 4.4.1).

The momentum equation might be expressed as

$$F_{hyd_k} + F_{grav_k} - F_{fric_k} = Q_k \frac{dG_k}{dt} \qquad (4.4.23)$$

where F_{hyd} is the hydraulic force, F_{grav} the gravitational pull and F_{fric} the influence from the control rod and the guide tube. The forces can be expressed more explicitly as

$$F_{hyd_k} = A_{k-1} p_{k-1} - A_k p_k \qquad (4.4.24)$$

$$F_{grav_k} = \zeta_k \rho_k g \qquad (4.4.25)$$

and, in the case of smooth pipes,

$$F_{fric_k} = A_k \, dz_k \, f_k \, R_k \frac{G_{fk}^2}{\rho_{fk}} , \qquad (4.4.26)$$

where dz_k is the height of the section. If there is a special flow restriction in the section, another expression is necessary for F_{fric}. In such a case the steady state pressure drop across the restriction (neglecting gravity) is calculated as

$$\Delta p = \gamma f R \frac{G_f^2}{f} , \qquad (4.4.27)$$

where γ is an input quantity with the dimension of length. The steady state momentum equation reduces to

$$F_{fric_k} = F_{hyd_k} \qquad (4.4.28)$$

hence,

$$F_{fric_k} = A_{k-1} p_{k-1} - A_k p_k = (A_{k-1} - A_k) p_{k-1} + A_k \gamma_k f_k R_k \frac{G_{fk}^2}{\rho_{fk}} \tag{4.4.29}$$

In pressure terms, the momentum equation becomes

$$p_k = p_{k-1} + \frac{1}{A_k} (\zeta_k \rho_k g - \frac{d}{dt}(\rho_k G_k)) - dz_k f_k R_k \frac{G_{fk}^2}{\rho_{fk}} , \tag{4.4.30}$$

but in the case of a special flow restriction in the section, dz_k must be replaced by γ_k.

In the next section (number N_t) p_k is not the pressure at the lower boundary of the section, but the pressure just below the convergent duct at the top of the section (fig. 4.4.2). This pressure is calculated as

$$p_k = p_{k-1} - \gamma_2 f_k R_k \frac{G_{fk}^2}{\rho_{fk}} , \quad k = N_t \tag{4.4.31}$$

where γ_2 is an input quantity. The exit pressure in section N_t is given by

$$p_{ex} = p_{con} + \gamma_1 f_k R_k \frac{G_{fk}^2}{\rho_{fk}} , \quad k = N_t , \tag{4.4.32}$$

p_{con} is the containment pressure and γ_1 an input constant. The momentum equation for the cylinder part of the section is then equal to eq. 4.4.23, but with another expression for F_{hyd_k}

$$F_{hyd_k} = A_k (p_k - p_{ex}) , \quad k = N_t . \tag{4.4.33}$$

In the transition time from the initiation of the accident and until maximum critical two-phase flow is achieved, the momentum equation is used to express the flow out through the orifice

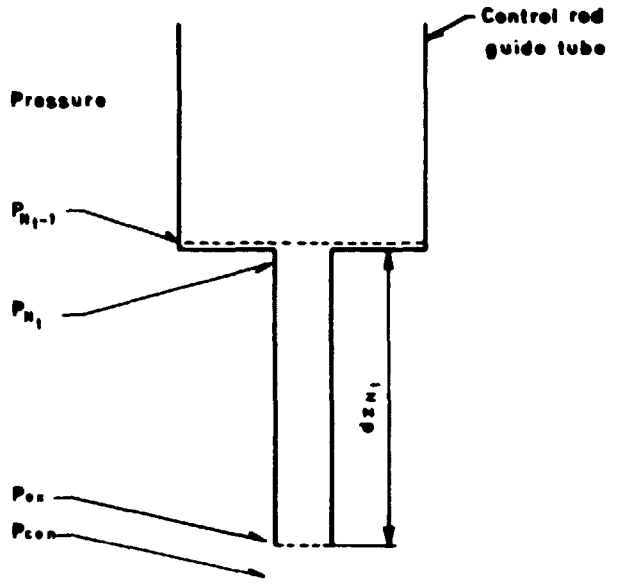

Fig. 4.4.2. Coolant pressures within the control rod guide tube exit section.

$$G_k(t) = \frac{1}{\Omega_k} \int_o^t (F_{hyd_k} + F_{grav_k} - F_{fric_k})\, dt$$

$$= G_k(t-dt) + dt \cdot \left(\frac{p_k - p_{ex}}{dz_k} + \rho_k g - f_k R_k \frac{G_{fk}^2}{\rho_{fk}}\right). \qquad (4.4.34)$$

When $G_k(t)$, calculated in the above way, exceeds the critical flow rate, G_{crt}, $G_k(t)$ is put equal to G_{crt}. G_{crt} is assumed known as a function of the driving pressure (p_k), a friction factor, the mass densities of steam and liquid and of the steam quality. In the present version of the code G_{crt} is calculated as by Moody[7], but it can easily be substituted by another expression. Because calculation of critical flow rates is not well established, a correction factor C_{crt} is included in the program

$$G_k(t) = C_{crt} \cdot G_{crt}. \qquad (4.4.35)$$

In the velocity limiter section the coolant has a considerable coupling to both the guide tube and the control rod and the friction term must therefore account for these two couplings

$$F_{fric_k} = F_r + F_a , \tag{4.4.36}$$

where F_r (r for relative) is the force between the control rod and the coolant and F_a (a for absolute) the friction between the guide tube and the coolant (in section N_{vl}). F_a is calculated from eq. 4.4.26.

For the calculation of F_r, it is necessary to introduce coolant flows relative to the control rod. The relative fluid flow, G_{rf}, and the relative mixture flow, G_r, are defined by

$$G_{rfk} = G_{fk} - u \cdot \rho_{fk} \tag{4.4.37}$$

$$G_{rk} = G_k - u \cdot \rho_k \tag{4.4.38}$$

where u is the control rod velocity. The special friction factor is given by two input constants γ_3 and γ_4

$$\gamma = \begin{cases} \gamma_3 & \text{for } G_{rf} > 0 \\ -\gamma_4 & \text{for } G_{rf} < 0 \end{cases} \tag{4.4.39}$$

In analogy with eq. 4.4.29, F_r can now be calculated as

$$F_r = (A_{k-1} - A_k) p_k + A_k \gamma f_k R_k \frac{G_{rfk}^2}{\rho_{fk}} . \tag{4.4.40}$$

In pressure terms the momentum equation becomes

$$p_k = p_{k-1} + \frac{\Delta_k}{A_k} (\rho_k g - \frac{dG_k}{dt}) - R_k(\gamma f_k \frac{G_{rfk}^2}{\rho_{fk}} + dz_k f_k \frac{G_{fk}^2}{\rho_{fk}}) \tag{4.4.41}$$

When maximum critical flow is not achieved in the section, p_k is calculated by the formula above.

The effect of critical flow is only taken into account when G_{rfk} is negative, i. e. relative upflow. As stated previously, G_{crt} is known as a function of the driving pressure p_k and an effective friction factor γ_{eff}

$$\gamma_{eff} = (\gamma_4 - dz_k (\frac{G_{fk}}{G_{rfk}})^2) f_k R_k . \tag{4.4.42}$$

When G_{rk} is known, p_k can be found by iteration in

$$G_{rk} = C_{crt}\, G_{crt} . \tag{4.4.43}$$

Thus, in the case of relative upflow, two pressures are calculated corresponding to the critical flow correlation and to the non-critical correlation, respectively. Normally, when critical flows are involved, the driving pressure is given and from that pressure two flows, a critical and a non-critical, are found. The correct flow is then the minimum of the two values. Here the situation is the reverse, the flow is given and the pressure must be selected in consistency with the rules presented above, i. e. the flow formula resulting in the minimum flow for the correct pressure must be used. Because the mass flow always increases with increasing driving pressure, the correct correlation is that which, for the true flow, results in the maximum pressure.

To fulfil the momentum equation, F_r is finally corrected by

$$F_r = A_{k-1}\, p_{k-1} - A_k p_k + \Omega_k \left(\rho_k g - \frac{dG_k}{dt}\right) - F_a . \tag{4.4.44}$$

F_r is used in the calculation of the control rod momentum.
The specific enthalpies of liquid and gas are calculated as

$$h_f = C_p (T_f - T_{so}) + \frac{p}{\rho_f} \tag{4.4.45}$$

$$h_g = C_p (T_s - T_{so}) + \frac{p}{\rho_{fs}} + h_{fg} \tag{4.4.46}$$

and for the mixture

$$h = x h_g + (1 - x)\, h_f . \tag{4.4.47}$$

When the kinetic and gravitational energies are neglected, the energy flow density in section k is

$$G_{ek} = G_k h_k = \rho_k v_k h_k . \tag{4.4.48}$$

According to [11] it is common to describe the flow in pipes and jets as an adiabatic flow. Hence, the energy equation becomes quite analogous to the mass equation

$$\frac{d}{dt}(\iota_k \rho_k e_k) = -(\Phi_k - \Phi_{k-1}) \tag{4.4.49}$$

$$\Phi_k = A_k \rho_k h_k (v_k - u_k) \tag{4.4.50}$$

This can be transformed to

$$\frac{dh_k}{dt} = -h_k \left(\frac{1}{\rho_k}\frac{d\rho_k}{dt} + \frac{1}{\iota_k}\frac{d\iota_k}{dt}\right) - \frac{\Phi_k - \Phi_{k-1}}{\rho_k \iota_k} + \frac{1}{\rho_k \iota_k}\left(\iota_k \frac{dp_k}{dt} + \rho_k \frac{d\iota_k}{dt}\right) \tag{4.4.51}$$

After integration h_k is known and the water temperature T_f is calculated

$$T_f = T_{so} + \frac{1}{C_p}\left(\frac{h}{1-x} - \frac{x}{1-x}\left(C_p(T_s - T_{so}) + \frac{p}{\rho_{fs}} + h_{fg}\right)\right). \tag{4.4.52}$$

Control Rod Momentum Equation

The control assembly is under the influence of hydraulic forces, friction forces and gravity.

At the top of the rod, reactor pressure acts on the horizontal surfaces of the rod with a force that helps to eject the rod. Simultaneously, in the rod ejection type of accident, the control assembly is affected by the containment pressure with an upward force to slow down the control rod speed. The friction between the rod and the coolant could be included by means of the friction force F_r (eq. 4.4.40), which is very significant if a velocity limiter is present.

The control assembly momentum equation then becomes

$$M \frac{du}{dt} = p_r A_{rod} - p_{con} A_{shaft} \cdot \delta + F_r + M \cdot g \tag{4.4.51}$$

where

$$\delta = \begin{cases} 0 & \text{in rod drop accidents} \\ 1 & \text{in rod ejection accidents} \end{cases} \tag{4.4.52}$$

The control rod position (insertion) in the core, z(t), is given by integration of the differential equation

$$\frac{dz}{dt} = - u \qquad (4.4.53)$$

and the application of an appropriate initial condition.

Calculation Scheme

From the overall reactor calculations, the coolant temperature, the pressure and the void fraction are known in the lower plenum. These quantities are used as input for the guide tube calculation. The flow from lower plenum to guide tube is known only at the time of accident initiation, when the flow is zero.

Applying the flow from the last time step, the water temperature, the pressure and the void fraction are calculated from top to bottom of the tube by making use of the energy equation, the momentum equation and the steam mass equation, respectively.

The containment pressure is known, and after calculation of the pressure in the exit section it is possible to estimate the leak rate from the guide tube. By means of the mass equation for the total coolant, the new mass flow in each section can be calculated from the bottom of the tube to the top.

Then it is easy to finally calculate the control rod speed and position before proceeding to the next time step.

Numerical Calculations

The simple Euler method was used for integration of the energy equation and the steam mass equation, while a third order method, evaluated from a Taylor expansion, was applied to solve the control rod momentum equation.

The expression for the total mass flow includes the term $\frac{d}{dt}(\zeta\rho)$, i.e. the time derivative of the total coolant mass in one node. Splitting the term yields

$$\frac{d}{dt}(\zeta\rho) = \omega\rho \left(\frac{1}{\omega} \frac{d\omega}{dt} + \frac{1}{\rho} \frac{d\rho}{dt} \right) \qquad (4.4.54)$$

where

$$\frac{1}{\rho} \frac{d\rho}{dt} \simeq \frac{1}{\rho} \left(\alpha \frac{d\rho_g}{dt} + (\rho_g - \rho_f) \frac{d\alpha}{dt} \right) \qquad (4.4.55)$$

neglecting $(1 - \alpha) \frac{d\rho_f}{dt}$ in the brackets. Because of a very sudden removal of coolant at the time of accident initiation, the pressure drops drastically at the bottom of the guide tube. When the pressure drops, the coolant saturation temperature drops and the evaporation rate becomes significant. This implies that $\frac{d\alpha}{dt}$ increases in a step and the code becomes unstable. To avoid this, $\frac{d\alpha}{dt}$ is averaged over several time steps. The pressure is rapidly increased and the void collapses, so this relaxation has negligible influence on the control rod speed.

Another instability is introduced into the code by calculation of the pressure and the mass flow in series and not in parallel. The coupling between the pressure and the flow implies a risk of oscillations in the system, if there is a disturbance. For instance, when the conventional flow formula is replaced by the critical one, $\frac{dG}{dt}$ is slowed down from a large to a smaller value. Then the pressure increases, $\frac{dG}{dt}$ increases, the pressure decreases and so on, leading to an oscillating system. Such an oscillation is avoided by making a smooth transition from the one flow regime to the other.

Results of RODACC runs are compared to the analytical solution in the next chapter.

4.5. Discussion of Results

The physical data from the reactor vendor presented in tables 4.2.1 and 4.3.1 were used as input to RODACC for a rod ejection run. The friction factors applied are listed in table 4.5.1.

Table 4.5.1

Friction factors used in RODACC

location	friction factor
Guide tube inlet section	-.64
Velocity limiter section, relative upflow	1.2
Velocity limiter section, relative downflow	0.75
Guide tube exit section, inlet	0.45
Guide tube exit section, outlet	-.01

The approximations made for obtaining the analytical solution are expecially incorrect when the coolant leak rate is high, because the variation in the coolant flow is then very marked and simultaneously the void fraction obtains a maximum value. The Moody expression for the critical flow is believed to overestimate the flow rate by perhaps a factor of 2; thus the use of the uncorrected Moody flow, i.e. $C_{crt} = 1$ in eq. 4.4.35, should result in the worst discrepancy between the analytical and numerical solutions. Therefore such a run has been used for comparison of the two models. The result is presented in figs. 4.5.1 to 4.5.3.

Fig. 4.5.1 shows the pressure variation in the guide tube. Both the pressure in the bottom section and the pressure gain of the velocity limiter are obtained from the numerical calculation, while the analytical model only yields the velocity limiter pressure difference. Immediately after the break, the pressure drops drastically especially at the guide tube exit. When the pressure drop has its most extreme value, a small ripple is seen on the curve. This phenomenon has been observed in blow-down tests and is due to the very high acceleration of the coolant, resulting in removal of water from the tube at a rate more rapid than that at which the steam can be generated. When evaporation starts, the pressure increases very slightly, but the water is still accelerated and soon the pressure continues dropping. Later on, steam generation combined with a supply of coolant from above exceeds the leak rate and a steady increase of the pressure is initiated. The ripple cannot be demonstrated by the analytical mode, due to the fact that it assumes a steady leak rate right from the beginning and because it does not incorporate evaporation. The initial pressure drop at the velocity limiter calculated from the analytical model is very much the mean value of the two pressure drops taken from the code. This is not surprising, because the analytical model treats the region below the velocity limiter as a hole, while in the numerical version this volume is shared by several sections (5 in the actual case).

In approximately 30 ms (somewhat faster for the analytical model, which is reasonable) the relative flow in the velocity limiter section changes sign, at which time all the pressure curves have a very characteristic saddle. Then the pressure increases at a slower rate, until a final level is obtained. The final pressure difference across the velocity limiter is higher in the analytical than in the numerical model, which is a result of the interaction of the coolant with the guide tube; an interaction that is neglected in the analytical model.

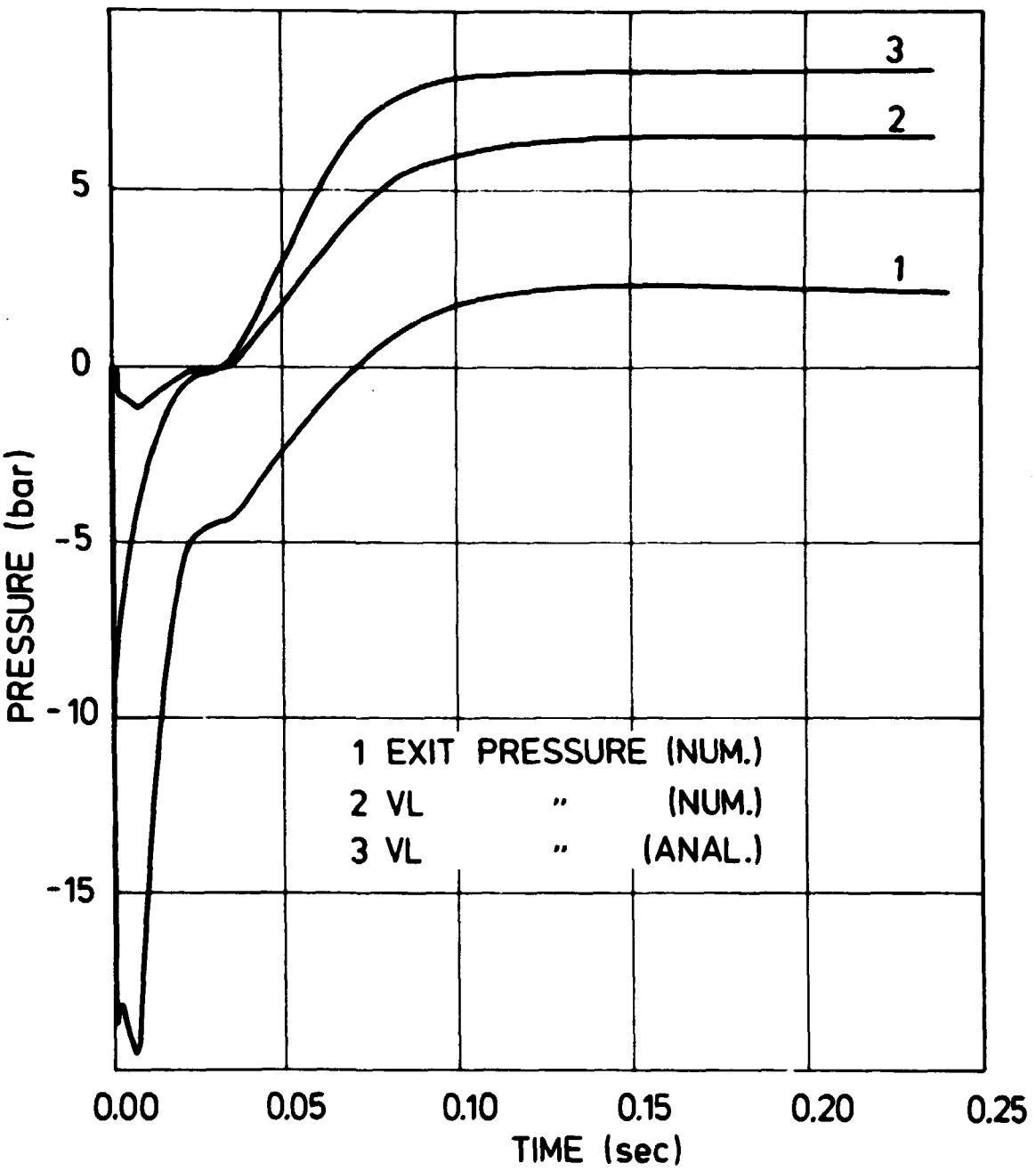

Fig. 4.5.1. Pressure variation in the guide tube during a rod ejection accident.

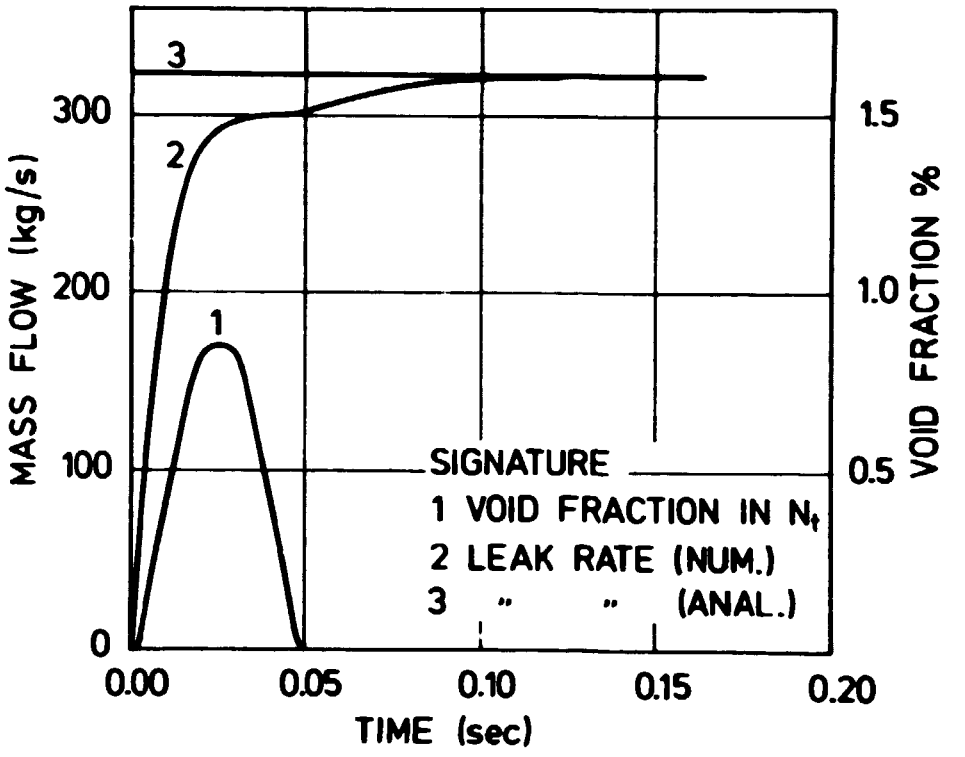

Fig. 4.5.2. Guide tube exit void fraction and coolant leak rate during a rod ejection accident.

Fig. 4.5.2 shows that, for most of the time, no steam is present and the maximum void fraction is lower than 1 per cent, thus it is no bad approximation to use single-phase flow correlations in the guide tube. Simultaneously it is seen that, except for the first 30 ms, the flow in the guide tube is nearly constant; thus the second assumption made in the analytical model is reasonable too.

Finally, the control rod velocity appears from fig. 4.5.3. As expected, the analytical model overestimates the initial control rod acceleration, but the steady velocity is very much the same in the two models. The only result from the RODACC runs that is necessary for the further calculations is the control rod velocity, or more correctly the control rod position as a function of time. The leak of coolant from the pressure vessel is not significant for the calculation of the power generation, because the nuclear transient is completed in a very short space of time. Due to the excellent accordance between the two models regarding control rod velocity, the sensitivity to parameter variations was demonstrated by means of the analytical model.

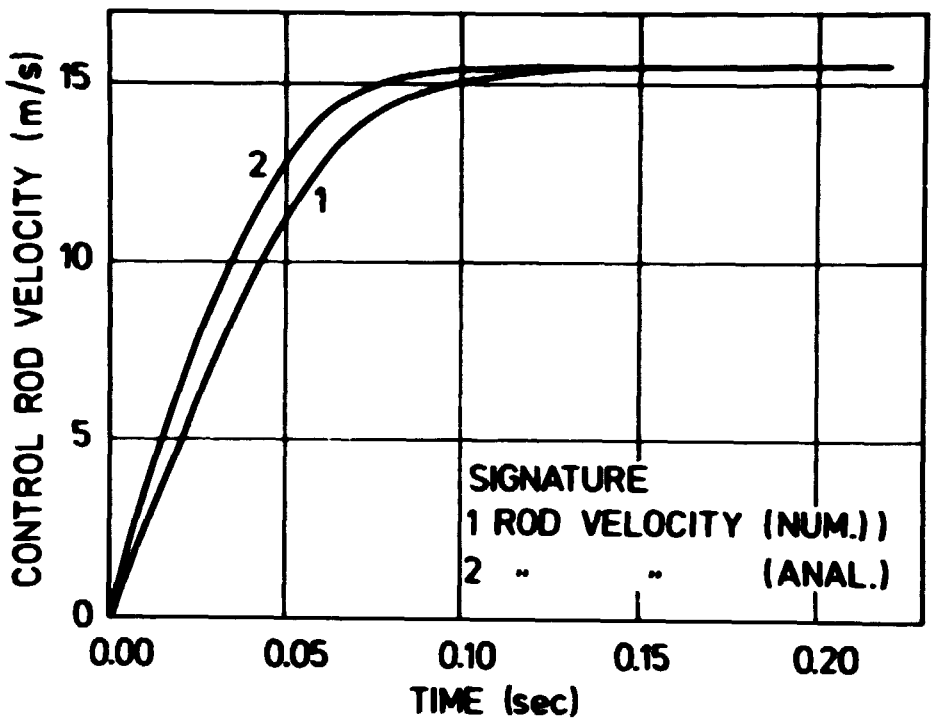

Fig. 4.5.3. Control rod ejection standard velocity.

From eq. 4.3.22 the maximum control rod ejection velocity is

$$u_{max} = u_o + u_2 = \frac{w_{leak}}{\rho(A_{gt} - A_{shaft})} + \sqrt{\frac{c_2}{c_1 f_{up}}} \qquad (4.5.1)$$

u_{max} is plotted in fig. 4.5.4 as a function of $\Delta = w_{leak}/w_{Moody}$ and $\Delta = f_{up}/f_{up_{standard}}$, respectively. It is seen that further improvement of f_{up} will not much reduce u_{max}, but with a poor velocity limiter, or in the absence of such a device, the increase in the rod ejection velocity is substantial. u_{max} is very sensitive to variations in w_{leak} and the best way to reduce the velocity seems to be to decrease the coolant flow from the guide tube.

Perhaps even more important than the final velocity of the control rod is the acceleration of the rod. This is given by eqs. 4.3.7 and 4.3.2 to be

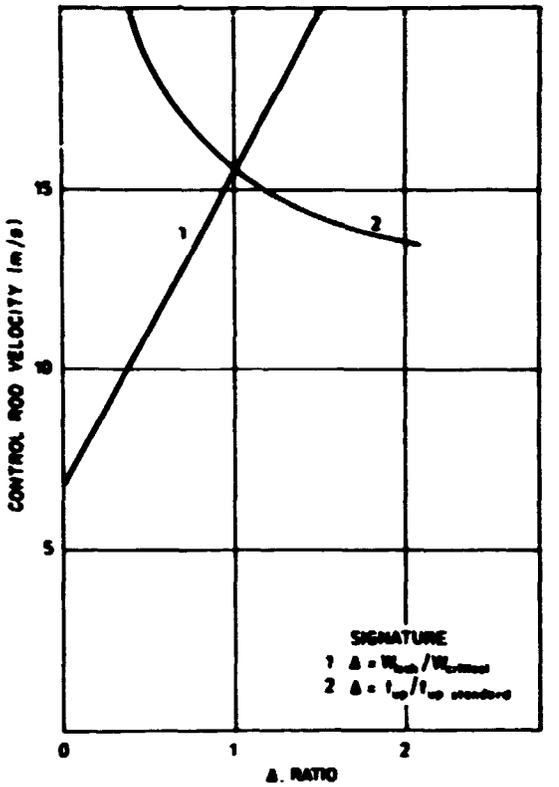

Fig. 4.5.4. Control rod ejection velocity dependency of coolant leak rate and velocity limiter efficiency, respectively.

$$\frac{du}{dt} = \begin{cases} c_2\left(1 + f_{down}\,\frac{c_1}{c_2}\,(u_o-u)^2\right) & t < t_o \\ c_2\left(1 - f_{up}\,\frac{c_1}{c_2}\,(u_o-u)^2\right) & t > t_o \end{cases} \qquad (4.5.2)$$

c_2 can be interpreted as effective gravity acceleration including gravity and pressure terms. Gravity constitutes less than 5 per cent of c_2, thus the positioning of the control rods below the reactor core does not add significantly to the consequences of a rod ejection accident. The initial acceleration is increased with f_{down} and u_o, i. e. w_{leak}, but a high value of f_{up} reduces the acceleration after $t = t_o$ at a rapid rate.

To check the consistency, RODACC runs were carried out with different numbers of nodes in the guide tube, and for $N_a = N_b \geq 4$ the result proved to be independent of the divisions used.

In normal reactor states, and during rod ejection accidents too, the coolant is subcooled in the lower plenum, and for subcooled water the coolant

temperature has been found to have an insignificant influence on the control rod velocity. The maximum rod velocity increases with increasing reactor pressure, and from table 4.5.2 it appears that the increase is almost equally shared by the effect of a higher driving pressure and the increased coolant flow.

Table 4.5.2

Maximum Control Rod Ejection Velocities

w_{leak} \ p_r =	70 bar	75 bar	80 bar
330 kg/s	15.55 m/s	15.78 m/s	16.01 m/s
338 kg/s	15.77 m/s	16.00 m/s	
345 kg/s	15.95 m/s		16.41 m/s

The conservative choice of $C_{crt} = 1$ has not been retained as standard for the following calculations in this report. Instead, the more realistic, but perhaps still conservative value of $C_{crt} = .75$ has been selected. The coolant leak rate then becomes $w_{leak} = 248$ kg/s, and the maximum rod speed reduces to $u_{max} = 13.3$ m/s.

The most doubtful question concerning the control rod ejection velocity calculation is probably whether the guide tube can sustain the pressure difference acting across the tube or not. However, collapse of the guide tube makes the velocity calculation much more uncertain, and because the initial pressure drop in the tube is several times greater than the final pressure increase, a possible failure is a squeezing of the tube. The result of such a tube failure is probably an increased resistance to the rod movement and a reduced control rod velocity.

5. DANAID, A THREE-DIMENSIONAL BWR SIMULATOR

5.1. General Description of the Model

For control-rod-removal accident analysis, the most important component of the BWR system is the reactor core including coolant channels, fuels and control rods. Consequently, the core calculations must be as accurate as possible with proper consideration of the computer capacity available, while the dynamics of less essential equipment can be treated more roughly.

The code complex consists of three main parts, namely the neutronic kinetics, the hydraulics and the fuel thermodynamics. For neutronic and hydraulic calculations, the core is divided into vertical channels, which again are cut up into sections by horizontal layers. Neutrons are allowed to move along and across the channels, but, for simplification, cross-flow is not implemented in the hydraulics. Inside each section fuel thermodynamic calculations are performed on an average fuel rod. To obtain detailed information about each rod, which is desirable for rod performance calculations, it is necessary to represent each fuel rod as a channel. However, such a demand is far from reality; a more realistic choice of channel size is four adjacent fuel boxes surrounding a control rod position. Corrections for local power peaking effects can then be made manually when the local power shape is known. For computer savings, hydraulic channels in the same environment can be collapsed to single channels.

The neutron kinetic theory is reduced tc a diffusion equation written in one energy group, obtained by collapsing a fast and a thermal group. The equation is solved by nodal technique with physical quantities considered as averages over the node volume. The reactor feedback mechnism is incorporated in the code through the nuclear parameters, i. e. cross sections and diffusion coefficients, which are treated as functions of the fuel temperature (Doppler feedback), the moderator density (void feedback) and the moderator temperature. In the present version the reflector is accounted for by an albedo representation with albedoes constant in time. This poor representation of the core boundary makes the code unfitted for rod ejection calculations, when the rod to be ejected is a peripheral one, but because marginal rods control small amounts of reactivity such an accident is not in the worst category. It is planned to modify the code so that albedoes can be calculated by a static flux program and changed during a transient.

The control rods are cruciform, as is usual in boiling water power reactors, and they are inserted from the bottom of the core. The absorber effect of the rods is calculated by the method of Henry.

For calculation of fuel temperature and internal heat conduction, the fuel rod is split into annular regions of equal volume; however, heat generation is assumed to be homogeneous over a cross section of the rod. The fuel conductivity is calculated as a simple function of the actual temperature. The conductivity of the gas gap between the fuel pellet and its cladding depends on the area of contact, which is mainly a function of the averaged rod temperature, and therefore in the program the gap conductivity is given as a function of that temperature. The cladding is treated as an ideal heat conductor with no heat capacity.

Most of the power generated is deposited as heat in the fuel and then after a delay-time convected to the coolant, but a small fraction, the neutron slowing-down energy and some of the Y-energy is immediately converted to heat in the coolant. Contrary to slower reactor transients, the direct heating of the coolant overrides the convective heating in the first phase of a rod ejection accident.

The convective heat transfer from the cladding to the coolant does not significantly exceed the heat transfer under normal reactor conditions, and in the absence of dynamical heat transfer correlations, conventional static correlations have been used in the subcooled and nucleate boiling region.

Besides the hydraulic channels in the core, the hydrodynamic model comprises an outer loop including two downcomers, two lower plena, a riser part and an upper plenum. The outer loop parts can be divided into smaller sections, but the mesh used is much coarser than that used in the core. Only the reactor system is included in the hydraulics, but very simple models for the steam load and the feedwater injection system are incorporated as auxiliary units. A not necessarily ideal pump can be installed in one of the downcomer sections, then an isentropic efficiency factor must be ascribed to the pump, so that it is possible to heat the coolant with the pump too. The pump power is essential when the reactor operates in the low power range.

The conservation laws for mass, momentum and energy are written in their one-dimensional form along the flow path and in conjunction with physical correlations they constitute the basic computational model. Special attention was paid to the energy calculation. This is due to the fact that the only way to initiate a severe rod-ejection accident is to eject the control rod from a reactor at low power, but in this condition a large amount of energy (the coolant is nearly saturated) flows in the loop without energy exchange with the surroundings. A small error in calculation of the coolant temperature might then introduce a significant and unphysical change of energy in the system, thus preventing a stable static solution.

Fig. 5.1.1 shows a schematic process diagram of the BWR system.

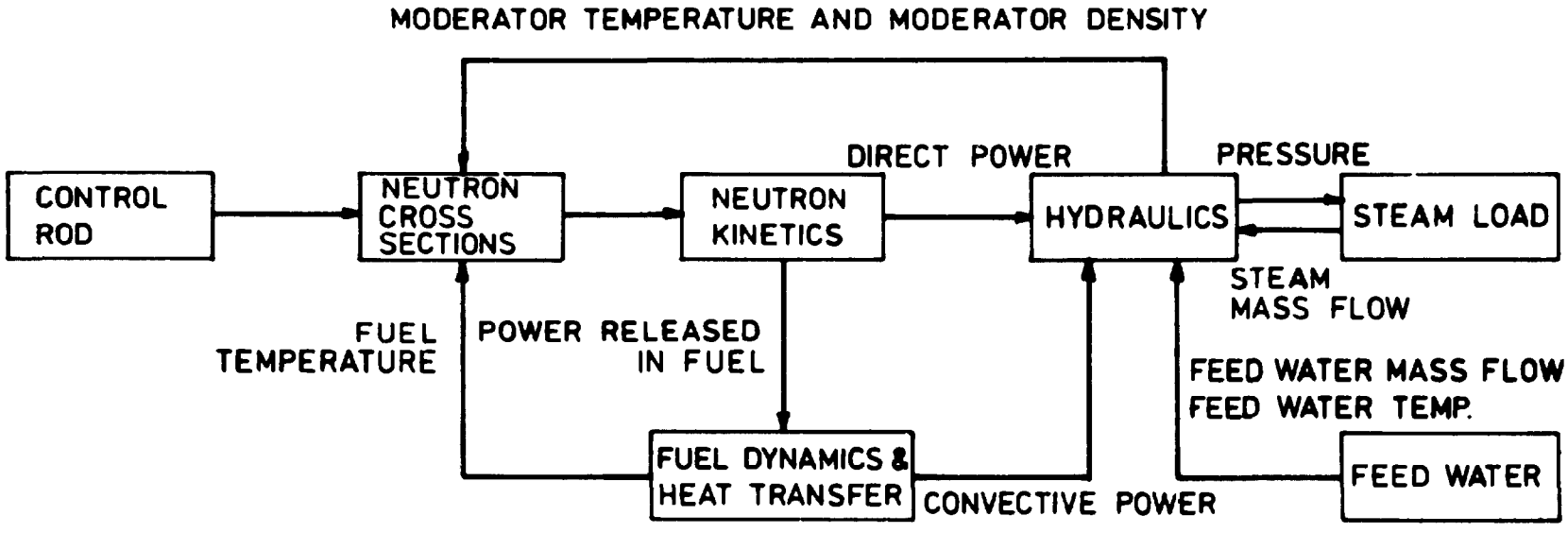

Fig. 5.1.1. DANAID. A schematic process diagram.

5.2. Neutronics

The nodal method.

The formal basis of the neutronic kinetic equation is a balance between source terms and loss terms. The time-dependent group-diffusion equations describe the average reaction rate over an interval of energy referred to as a group in terms of neutron-diffusion theory. They have the form [12]

$$\nabla \cdot D^g(r,t)\nabla\Phi^g(r,t) - (\Sigma_a^g(r,t) + \Sigma_s^g(r,t))\,\Phi^g(r,t)$$

$$+ \sum_{g' \neq g}^{G} \Sigma_s^{g'/g}(r,t)\,\Phi^{g'}(r,t) + (1-\beta)\chi_p^g \sum_{g' \neq 1}^{G} \nu^{g'}\,\Sigma_f^{g'}(r,t)\Phi^{g'}(r,t)$$

$$+ \sum_{m=1}^{M} \lambda_m \chi_m^g\, C_m(r,t) = (1/v^g)\,\frac{\partial\Phi^g(r,t)}{\partial t} \qquad (5.2.1)$$

$$g = 1, \ldots\ldots, G$$

where the quantity D^g is the diffusion coefficient in group g, Σ_a^g, Σ_s^g and Σ_f^g are the macroscopic absorption, scattering removal, and fission cross sections, respectively, in group g and $\Sigma_s^{g'/g}$ is the scattering cross section from group g' to g. The quantity $\nu^{g'}$ is the averaged number of neutrons produced in a fission induced by a neutron in group g', and v^g is the speed of neutrons in group g. The neutron flux in group g is denoted by Φ^g and the quantity C_m represents the concentration of delayed neutron precursors of type m with decay constant λ_m, β_m represents the fraction of fission neutrons that is delayed in group m ($\beta = \sum_{m=1}^{M} \beta_m$). The fractions of neutrons that are born within group g and produced directly by fission and by precursor decay are denoted χ_p^g and χ_m^g, respectively.

The concentrations of delayed neutron emitters satisfy the simple balance equation

$$\frac{\partial C_m(r,t)}{\partial t} = \beta_m \sum_{g=1}^{G} \nu^g \Sigma_f^g(r,t)\,\Phi^g(r,t) - \lambda_m C_m(r,t) \qquad (5.2.2)$$

$$m = 1, \ldots\ldots, M$$

Associated with equations 5.2.1 and 5.2.2 are boundary conditions of the general form

$$\phi^g(R, t) + d\nabla\phi^g(R, t) = 0 , \tag{5.2.3}$$

where R is the external boundary of the reactor and d the extrapolation distance, and the initial conditions

$$\phi^g(r, o) = \phi^g_o(r) \tag{5.2.4}$$

$$C_m(r, o) = C^o_m(r) \tag{5.2.5}$$

Flux and current continuity conditions must be satisfied at internal interfaces.

The purpose of nodal technique is to solve the neutron kinetic equations with respect to the averaged flux in each region. A detailed derivation of the nodal approach is given in [2] and [3], and only a few essential items shall be treated here.

The group flux within each node is assumed written as the product of a shape function $\phi^g_j(r)$ and an amplitude function $N^g_j(t)$

$$\Phi(r, t) = \phi^g_j(r)\, N^g_j(t) . \tag{5.2.6}$$

The expression for $\Phi(r, t)$ is substituted into equations 5.2.1 and 5.2.2 and integration over the volume (V_j) of the node is performed. By means of Green's theorem the part involving the leak term can be expressed as

$$\begin{aligned} L^g_j(t) &= N^g_j(t) \int_{V_j} \underline{\nabla} \cdot D^g(r, t)\, \underline{\nabla} \phi^g_j(r)\, d^3r \\ &= N^g_j(t) \left(\int_{S_j} D^g(r, t)\, \underline{\nabla} \phi^g_j(r) \cdot dS - \int_{V_j} D^g(r, t)\, \nabla^2 \phi^g_j(r)\, d^3r \right) \end{aligned} \tag{5.2.7}$$

The L_j term represents the contribution of neutrons that diffuse in and out of node j to the neutron balance in node j. Evaluation of $L_j(t)$ requires an assumption of the net neutron current on the bounding surface of the node, as well as an assumption about the flux shape within the node. The simplest scheme for relating the net current across a nodal surface to the average fluxes in the nodes, which this interfaces separates, is to define a constant of proportionality, so that the net current across the interface equals the constant multiplied by the difference in the two nodal fluxes. Such an

expression would reduce to Fick's law in the limit of zero mesh sizes. However, the coupling constant so defined would equally depend on the properties of both adjacent nodes. Since the success of the nodal scheme will depend on being able to estimate the coupling constants in some approximate manner, it would be far preferable to introduce quantities that only depend on the properties of a single node. To achieve this end, the net current across a nodal interface is divided into two partial currents, one only consisting of neutrons moving into the particular node and the other of neutrons moving in an opposite direction. A reasonable approximation to $L_j(t)$ is then

$$L_j^g(t) = \sum_{i \neq j} \left(l_{ji}^g(t)\, N_i^g(t) - l_{ij}^g(t)\, N_j^g(t) \right) . \qquad (5.2.8)$$

When the coupling coefficients $l_{ij}^g(t)$ are defined through equations 5.2.7 and 5.2.8, the latter is a formally exact relationship between the neutron current at the node border and the corresponding flux in the node and in the six nearest neighbouring nodes. However, although it is in principle possible to change the coupling coefficients during a transient, it is a considerable task. The difficulty has been at least partially circumvented by choosing the coupling coefficients so that the nodal calculation matches, as far as possible, several known extreme reaction rate distributions that bound any distributions that might be obtained during a transient, rather than matching any single distribution exactly.

According to [14] a valid relationship between the fast and the thermal flux is

$$\frac{\phi_j^1}{\phi_j^2} = \left(\frac{\Sigma_a^2}{p\, \Sigma_s^{1/2}} \right) \qquad (5.2.9)$$

where p is the resonance escape probability. Equation 5.2.9 is based on static calculations, but because the neutron generation time is less than the reactor period during rod ejection transients (~ 5 ms) the relation can be used in the dynamics too. With a relation between the neutron flux in groups 1 and 2, it is possible to reduce the two-group calculations to one-group calculations, and this has been done. It might seem to be an oversimplification to use one-group theory for such highly peaked transients as those of interest here, but essential parameters from one-group analysis are within 1 % of those from a three-group solution[5], with an order of magnitude reduction in computer costs.

The nuclear parameters are given as functions of the fuel temperature T_f, the moderator temperature T_m, and the moderator density ρ_m. Additional correction can be made for the xenon concentration.

The control rod absorption cross section, Σ_p^g, are calculated by the Henry method[15]

$$\Sigma_p^1 = \frac{\Sigma_1}{S_1 - 1} \tag{5.2.10}$$

$$\Sigma_p^2 = \frac{\Sigma_2}{\frac{S_2}{\Delta} - 1} \tag{5.2.11}$$

where

$$\Sigma_1 = \Sigma_a^1 + \Sigma_s^{1/2} \tag{5.2.12}$$

$$\Sigma_2 = \Sigma_a^2$$

$$S_g = \frac{m^2 - 2ah + a^2}{2h} \left[\frac{\Sigma_g}{a_g} + \frac{1}{L_g} \coth\left(\frac{m-a}{2L_g}\right) \right], \quad g = 1, 2 \tag{5.2.13}$$

$$L_g = \left(\frac{D_g}{\Sigma_g}\right)^{1/2}, \quad g = 1, 2 \tag{5.2.14}$$

$$\Delta = 1 + \frac{\Sigma_p^1}{\Sigma_1} \left(1 - \frac{m^2 - 2ah + a^2}{2h(L_1^2 - L_2^2)} \left(L_1 \coth\left(\frac{m-a}{2L_1}\right) - L_2 \coth\left(\frac{m-a}{2L_2}\right)\right)\right). \tag{5.2.15}$$

The parameter a_g, $g = 1, 2$ is an input constant to the program and it should be the ratio of the net neutron current into the control rod and the neutron flux at the rod surface. The constants a and h are the half-thickness, respectively, the half-span of the control rod and m is the half-width of the channel.

For changing the reactivity of single rods, it is possible to multiply Σ_p^g by an input constant without changing the cross sections of other rods.

Fission Energy Deposition

The fission energy is deposited partly in the fuel rod, partly in the moderator, and most of it is released promptly after the fission process. Fig. 5.2.1, which is taken from [16] shows the types of radiation present following a fission. The radiation can be categorized into three groups involving charged particles, neutrons and γ-radiation, respectively.

The group of charged particles is dominated by the fission fragments that deposit approximately 170 MeV per fission in U^{235}. Alpha-particles are emitted from the uranium and plutonium particles, but their energy deposition can be neglected. Both the fission fragments and the α-particles are stopped in the fuel rod and all their energy is released here. Beta-particles are emitted from decaying fission products and from nuclei created by neutron capture. The beta energy released from the decay of fission products is approximately 8.2 MeV/fission in U^{235}, and most of it, 7.6 MeV,

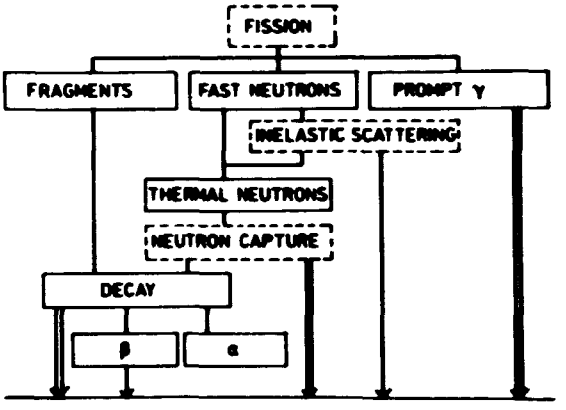

Fig. 5.2.1. Radiation following a fission process.

is released more than 1 s after the fission. The neutron capture process in U^{238} is

$$^{238}_{92}U + ^{1}_{0}n \rightarrow ^{239}_{92}U \xrightarrow[\beta^-,\gamma]{} ^{239}_{93}N_p \xrightarrow[\beta^-,\gamma]{} ^{239}_{94}P_u \qquad (5.2.16)$$

In the U^{239} decay process 0.5 MeV is released as β-energy and 0.35 MeV as γ-energy, which in a typical BWR at the beginning of a fuel cycle corresponds to 0.3 MeV and 0.2 MeV, respectively, per fission in U^{235}. The part of the β-energy released directly into the coolant is less than

0.05 MeV/fission, thus it is a reasonable approximation to assume that all the energy of the charged particles is deposited in the fuel rod.

The neutron energy per thermal fission in U^{235}, Pu^{239}, and Pu^{241} is given in table 5.2.1.

Table 5.2.1

Neutron energy per thermal fission

Target nucleus	U^{235}	Pu^{239}	Pu^{241}
Neutron energy (MeV/fission)	4.7	5.8	5.2

In inelastic scattering of fast neutrons and U^{238}, approximately 0.2 MeV/fission of the neutron energy is believed to be converted into γ-energy. The fission neutrons are born with an energy of 2 MeV per neutron and, because the resonance absorption is ineffective for neutron energies higher than 1 keV, the resonance capture process can be neglected in the energy accounts. It is assumed that all the energy released during the slowing down of the neutrons is deposited in the moderator. The neutron energy is shared by the coolant inside the fuel box (index i) and the coolant outside (index o) in the ratio

$$\frac{Q_i}{Q_o} = \frac{(1-\alpha_i)\, A_i}{(1-\alpha_o) A_o} \qquad (5.2.17)$$

where Q is the coolant deposition, α the void fraction and A the flow area. The delayed neutrons can be neglected from an energetic point of view.

When a neutron is captured in the control material, B^{10}, He^4, and Li^7 nuclei are created with a total energy of 2.3 MeV, or approximately 1.2 MeV/fission in a typical BWR cell containing a control rod. All this energy is deposited in the control rod.

Most of the γ-radiation is the result of the decay of fission fragments, fission products, and compound nuclei from neutron capture processes.

If the γ-radiation emitted within 1 μs after the fission process is categorized as fission γ-radiation and the rest as fission-product γ-radiation, the two categories are responsible for an energy decomposition of 8.0 MeV/fission and 7.2 MeV/fission respectively. After the capture of a neutron, the binding energy of the neutron is emitted from the compound nucleus. This process is responsible for approximately 4 MeV/fission in U^{238}. Decay of

U^{239} and inelastic scattering of neutrons results in 0.2 MeV/fission of γ-energy for each of the two processes. A smaller part of the γ-energy arises from capture in fission products, especially Xe^{135} and Sm^{149}, and outside the fuel in the cladding, the coolant, the fuel box, and in the control rod if present.

Because of the high penetration ability of γ-radiation, it is a rather complicated matter to determine how the γ-energy is deposited in the reactor system. Special care must be taken in the calculation of the energy deposition of the high energetic γ-quanta as the fission gamma, the fission product gamma, and the gamma radiation originating from neutron capture in the fuel. To calculate the energy deposition from these high energetic γ-quanta, the fuel cell is divided into three annular regions containing fuel, cladding, and moderator, respectively. The energy deposition is calculated by means of collision probability theory in six energy groups. It is assumed that the radiation from the cell is isotropic and that all the energy radiated to the cell from the adjacent cells is homogeneously absorbed over a cross section of the cell.

The sources of low energetic γ-radiation are compound nuclei from neutron capture processes in materials other than the reactor fuel and radiation from inelastic scattering of neutrons. Such sources are dispersed in the reactor and the energy deposition from them is small compared to that of the other γ-energy sources, therefore this energy deposition is assumed to be homogeneous in the cell.

The result of the calculations is a rather detailed picture of the fission energy distribution inside the cell and of how this distribution depends on the coolant density and on fuel composition. In the DANAID program the heat capacities of the control rod and structure materials are not incorporated, thus in a static calculation it is most natural to transmit the power deposited in the control rod to the moderator part outside the box and to share the power from the box itself between the coolant inside and outside the box. However, such a simplification would result in too fast a transmission of power to the coolant. For rapid transients, a better method is to include the power deposited in these materials in the fuel power and then let it be convected to the coolant. The fuel temperature then becomes a little high, but because the power addition to the fuel is small, compared to the real fuel power, the error is insignificant, and using this calculation method the power transmission to the coolant is represented in a more realistic time scale. With such a definition for the fuel power, approximately 97.5% of the total fission energy is deposited in the fuel rod and the rest in the coolant.

The result seems independent of the void fraction in the coolant, but the distribution between the moderator inside the box and outside the box varies with the coolant mass in the two regions. The dependency of the void fraction in the inside coolant is given in fig. 5.2.2 for a fuel box with new fuel (fission in U^{235}) and withdrawn control rod.

After the fission process most of the fission energy is promptly released as thermal energy, but a small fraction is delayed. In the time interval $\Delta t = (t, t + \Delta t)$ this fraction is calculated as $A(t)\Delta t$, where t is the time that has elapsed since the occurrence of the particular fission process. In the present version of DANAID the function A(t) is simply taken as a constant independent of time.

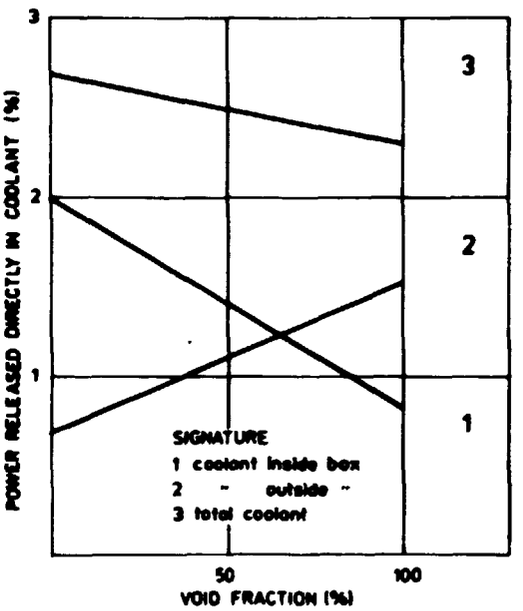

Fig. 5.2.2. Fraction of total power directly to the coolant.

5.3. Hydraulics

The Loop

A schematic diagram of the hydraulic loop is given in fig. 5.3.1. The loop consists of seven parts, i.e., an upper plenum, two downcomers, two lower plena, a core with parallel coolant channels, and a riser. Steam is

removed from the loop at the top of the upper plenum, while feed-water injection and the pump are placed in one of the downcomers. The loop parts can be divided into a variable number of sections.

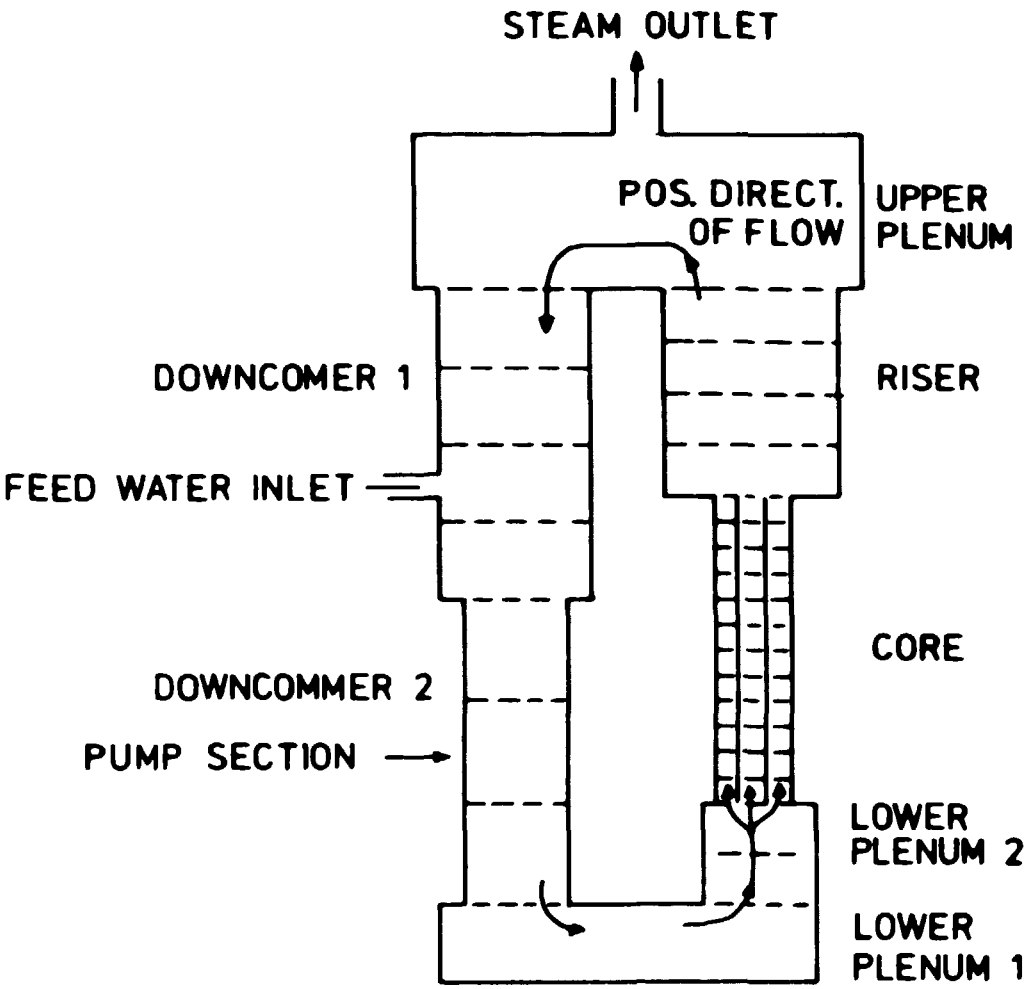

Fig. 5.3.1. Model of the hydraulic loop.

Thermodynamic Functions

As in RODACC, subcooling or superheating of the steam are not incorporated in the program, so the steam temperature, T_s, and the pressure, p, are correlated and the steam thermodynamic quantities can be calculated as a function of the pressure only, while the liquid quantities are functions of both the water temperature, T_f, and the pressure.

The functions are expanded in Taylor series with coefficients calculated at some reference temperature $(T)_r$ and reference pressure $(p)_r$. The following symbols are used

$(T_s)_r$: saturation temperature at the reference pressure $(p)_r$

$(p_s)_r$: saturation pressure at the reference temperature $(T)_r$

The quantities $(\rho_g)_r$, $(h_{fg})_r$ and $(h_{fs})_r$ are all calculated at the thermodynamic point $((p)_r, (T_s)_r)$ and they represent the steam density, the specific heat of evaporation, and the specific enthalpy of saturated water, respectively. The reference fluid density, $(\rho_f)_r$, and the reference specific fluid enthalpy, $(h_f)_r$, are calculated at the pressure $(p_s)_r$ and the temperature $(T)_r$. Using the expressions

$$dp = p - (p)_r \tag{5.3.1}$$

$$dT = T - (T)_r \tag{5.3.2}$$

$$dT_s = T_s - (T_s)_r \tag{5.3.3}$$

the thermodynamic quantities at the temperature T and pressure p are approximated to

$$T_s = (T_s)_r + \left(\frac{dT_s}{dp}\right)_r dp \tag{5.3.4}$$

$$p_s = (p_s)_r + \left(\frac{dp_s}{dT}\right)_r dT \tag{5.3.5}$$

$$\rho_g = (\rho_g)_r + \left(\frac{d\rho_g}{dp}\right)_r dp \tag{5.3.6}$$

$$h_{fg} = (h_{fg})_r + \left(\frac{dh_{fg}}{dp}\right)_r dp \tag{5.3.7}$$

$$\rho_f = (\rho_f)_r + \left(\frac{\partial \rho_f}{\partial T}\right)_r dT + 1/2 \left(\frac{\partial^2 \rho_f}{\partial T^2}\right)_r (dT)^2 + \left(\frac{\partial \rho_f}{\partial p}\right)_r (p-p_s) \tag{5.3.8}$$

$$h_f = (h_f)_r + \left(\frac{\partial h_f}{\partial T}\right)_r dT + 1/2 \left(\frac{\partial^2 h_f}{\partial T^2}\right)_r (dT)^2 + \left(\frac{\partial h_f}{\partial p}\right)_r (p-p_s) \tag{5.3.9}$$

$$h_{fs} = (h_{fs})_r + \left(\frac{dh_{fs}}{dT_s}\right) dT_s + \left(\frac{d^2 h_{fs}}{dT_s^2}\right) (dT_s)^2 \tag{5.3.10}$$

The steam specific enthalpy and the steam specific internal energy are then defined to

$$h_g = h_{fs} + h_{fg} \tag{5.3.11}$$

$$e_g = h_g - \frac{p}{\rho_g} . \qquad (5.3.12)$$

The dynamical viscosity of water, η_f, and the thermal conductivity of water, λ_f, are only calculated as functions of the system pressure p_o

$$\eta_f = (\eta_f)_r + (\frac{d\eta_f}{dp})_r (p_o - (p)_r) \qquad (5.3.13)$$

$$\lambda_f = (\lambda_f)_r + (\frac{d\lambda_f}{dp})_r (p_o - (p)_r) . \qquad (5.3.14)$$

A numerical calculation scheme for the reference quantities is presented in appendix A.

Thermodynamic Correlations

Most of the correlations used in the hydraulic part of DANAID originate from RAMONA[8], and many of them were presented in the description of RODACC, chapter 4.4.

In RAMONA the specific internal energy of water is calculated as

$$e_f = C_p (T_f - T_{so}) \qquad (5.3.15)$$

where C_p is calculated for saturated liquid as function of the pressure p and T_{so} is a reference temperature. Equation 5.3.15 is a rather poor approximation to e_f, and therefore in DANAID the internal energy is based on the enthalpy function

$$e_f = h_f - \frac{p}{\rho_f} . \qquad (5.3.16)$$

When C_p is needed, it is then calculated as

$$C_p = (\frac{\partial e_f}{\partial T})_p . \qquad (5.3.17)$$

The correlation between the velocities of steam and fluid is

$$v_g = S v_f + v_o \qquad (5.3.18)$$

$$S = S_1 + S_2 a^r \qquad (5.3.19)$$

$$v_o = - S_g \cos \varphi . \qquad (5.3.20)$$

where S_1, S_2, S_g, and r are input constants, while φ is the angle between the positive flow direction and vertical.

In RAMONA the thermodynamic quantities are not calculated as functions of the local pressure and temperature, but this is done in DANAID.

At loop-part borders the pressure is generally changed due to expansion or restriction losses, and the pressure change (Δp) can be calculated when the coolant velocity is known. The corresponding temperature change (ΔT) is then calculated from the relationship

$$w_g h_g(p) + w_f h_f(T, p) = w_g h_g(p+\Delta p) + w_f h_f(T+\Delta T, p+\Delta p) , \qquad (5.3.21)$$

where the mass flow rates w_g and w_f are assumed constant over the loop-part border.

The total evaporation rate Φ within each node is calculated as a sum of two terms, a surface evaporation term Φ_{SF} and a bulk fluid evaporation term Φ_B

$$\Phi = S_H \Phi_{SF} + \Omega \Phi_B \qquad (5.3.22)$$

S_H represents the heated surface area, Ω the volume of coolant.

Φ_B is defined through equations 4.4.11 to 4.4.12, while in RAMONA Φ_{SF} is derived as

$$\Phi_{SF} = \frac{Q}{h_{fg} + C_p(T_s - T_f)\frac{\rho_f}{\rho_g} + (T_{ca} - T_s)(\frac{\rho_f}{\rho_g} - 1)\frac{C_p}{2}} . \qquad (5.3.22)$$

Q is the heat flux to the coolant through S_H and T_{ca} is the temperature of the fuel cladding.

During a control-rod-ejection accident, the flux level exceeds the level in normal reactor states by some decades, thus it seems reasonable to examine whether the amount of radiolytic gas produced is sufficient to significantly influence the neutronic cross sections.

Along the path of the neutrons and the gamma radiation some water molecules are ionized and some are decomposed; then there are free electrons, H-atoms and OH-molecules in the track. The radicals are expected to react with each other, or with the water molecules, after the following schemes

$$2e^- + 2H_2O \rightarrow H_2 + 2OH^- \qquad (5.3.23)$$

$$H + H \rightarrow H_2 \qquad (5.3.24)$$

$$OH + OH \rightarrow H_2O_2 \qquad (5.3.25)$$

$$H + OH \rightarrow H_2O, \qquad (5.3.26)$$

because both H_2 and H_2O_2 molecules have been observed in the track, while recombinations are due to the reactions

$$H_2O_2 + H \rightarrow H_2O + OH \qquad (5.3.27)$$

$$H_2 + OH \rightarrow H_2O + H\ . \qquad (5.3.28)$$

According to [19], the time constants involved in the recombination processes are so small that a steady state is obtained at pulses with a duration of more than 1 ms. An energy deposition of 100 eV gamma energy should result in an H_2 production of 0.44 molecules, while 100 eV deposited from neutrons result in 1.12 molecules of H_2. Approximately 90% of the direct energy deposition to the coolant results from neutrons and 10% from gamma radiation, therefore 1.05 H_2-molecules are produced when 100 eV is deposited, or 1.1×10^{-7} mol per Joule. In a control-rod-ejection accident the direct power deposition to the coolant has a maximum level of $3 \times 10^6 \frac{W}{l}$, which means that 3×10^3 J/l is deposited within 1 msec. Corresponding to this energy deposition rate 0.33×10^{-3} moles/l of radiolytic gas are produced, and the volume fraction of the gas becomes (assuming ideal gas)

$$\alpha = \frac{nRT}{p} = 2 \times 10^{-7}\ . \qquad (5.3.29)$$

This is far below the normal steam production and it can be concluded that radiolytic gas production is negligible in neutronic calculations.

The heat transfer correlations used are the Colburn correlation for the non-boiling region and the Jens and Lottes correlation for the boiling region.

As in RAMONA, the steam load is calculated as

$$w_{sl} = \begin{cases} \rho_g \sqrt{\frac{K_p}{\rho_g}(p_o - p_{sec})} & \text{if } p_o \geq p_{sec} \\ 0 & \text{if } p_o < p_{sec} \end{cases} \qquad (5.3.30)$$

where K_p and p_{sec} are constants and p_o is the time-dependent system pressure. The feed-water temperature and the feed-water mass flow are kept constant during the transient, the temperature must be given as input, and the mass flow is made equal to the steam load in the initial static condition.

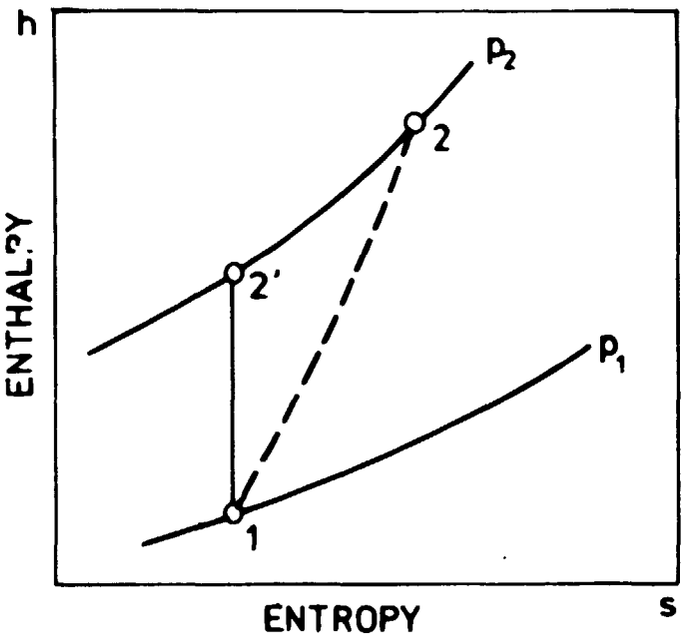

Fig. 5.3.2. Schematic entropy-enthalpy diagram for the pump process.

To the pump is ascribed an isentropic efficiency factor η_p, defined as

$$\eta_p = \frac{h_{2'} - h_1}{h_2 - h_1} \quad , \tag{5.3.31}$$

where the enthalpies are defined through the s-h-diagram in fig. 5.3.2. Indexes 1 and 2 refer to the state before and after the pump, respectively. According to [11] the flow in a pump is adiabatic and for an adiabatic isentropic process the thermodynamic state is described by

$$dQ = de + pd\left(\frac{1}{\rho}\right) = 0 \tag{5.3.32}$$

which is tantamount to

$$dh = \frac{1}{\rho}\, dp \, . \tag{5.3.33}$$

In principle, the mass density is a function of both the pressure and the enthalpy, but the function is not generally known. The assumption that ρ is constant during the reversible process (which is equal to accepting the

the internal energy as a constant) yields

$$h_{2'} - h_1 = \frac{p_2 - p_1}{\rho_1} \quad . \tag{5.3.34}$$

Using eqs. 5.3.31 and 5.3.34, the coolant enthalpy after the pump becomes

$$h_2 = h_1 + \frac{1}{\eta_p} \frac{p_2 - p_1}{\rho_1} \quad . \tag{5.3.35}$$

In DANAID the pump is characterized by

$$p_2 - p_1 = a_o + a_1 v_f + a_2 v_f^2 \quad , \tag{5.3.36}$$

where v_f is the velocity of the fluid in the pump.

When w is the coolant mass flow through the pump, the total power delivered from the pump to the coolant is

$$Q_{pump} = w\,(h_2 - h_1) \, . \tag{5.3.37}$$

Basic Thermodynamic Equations

The energy balance, the steam mass balance and the momentum equation are written and solved for each node.

A very compressed calculation scheme is given below; details can be found in the description of the RAMONA program

$$\text{steam mass } \frac{dm_g}{dt} \rightarrow m_g \rightarrow m_f \rightarrow \alpha \rightarrow W \rightarrow v_f \rightarrow v_g \rightarrow W_g \rightarrow W_f$$

$$\text{energy } \frac{dE}{dt} \rightarrow E \rightarrow e_f \rightarrow T_f \rightarrow \Phi \tag{5.3.38}$$

$$\text{momentum } \frac{dp}{dt} \rightarrow p \rightarrow T_s$$

The symbols used in the scheme and not previously defined are

m : coolant mass
W : coolant volume flow
E : coolant internal energy
f : fluid index
g : gas = steam index
s : saturation index

5.4. Fuel Thermodynamics

The fuel thermodynamic calculations are performed on an averaged rod within each neutronic node. The model used is very much the same as that used in RAMONA, therefore only the basic assumptions will be described here.

The fuel rod is divided into annular zones of equal volume, but nuclear heat is generated homogeneously over a cross section of the rod. Volume expansions of the fuel are neglected and consequently the density is kept constant. The volume occupied by the gas gap and the cladding is assumed infinitely small, and the heat capacities are neglected. In the runs presented in this report the specific heat of the fuel is constant, but in earlier runs the relatively accurate polynomium expression

$$C_F = \sum_{i=1}^{5} a_i T_F^{i-1} \qquad (5.4.2)$$

was used. With

$$a_1 = .13005 \times 10^{3}$$
$$a_2 = .71466$$
$$a_3 = -.94009 \times 10^{-4}$$
$$a_4 = .48958 \times 10^{-5}$$
$$a_5 = -.79200 \times 10^{-10}$$

and T_F inserted in ^{o}C, the unit of C_F becomes $J/kg^{o}C$. During a rod-ejection accident initiated from the hot startup condition the fuel-temperature range is rather broad, thus it may seem a serious error to maintain C_F unchanged during the transient. However, T_F is almost a step function of the time, because the temperature is increased within 25 ms and a slight deviation from the real temperature increase is insignificant. However, it is important that the final fuel temperature is correct. Choice of the specific heat as

$$C_F = \frac{1}{T_{F,max} - T_{F,min}} \int_{T_{F,min}}^{T_{F,max}} C_F(T)dT \qquad (5.4.3)$$

results in a correct time interval for heating and in a correct final temperature and energy content. Because $C_F(T)$ is an increasing function,

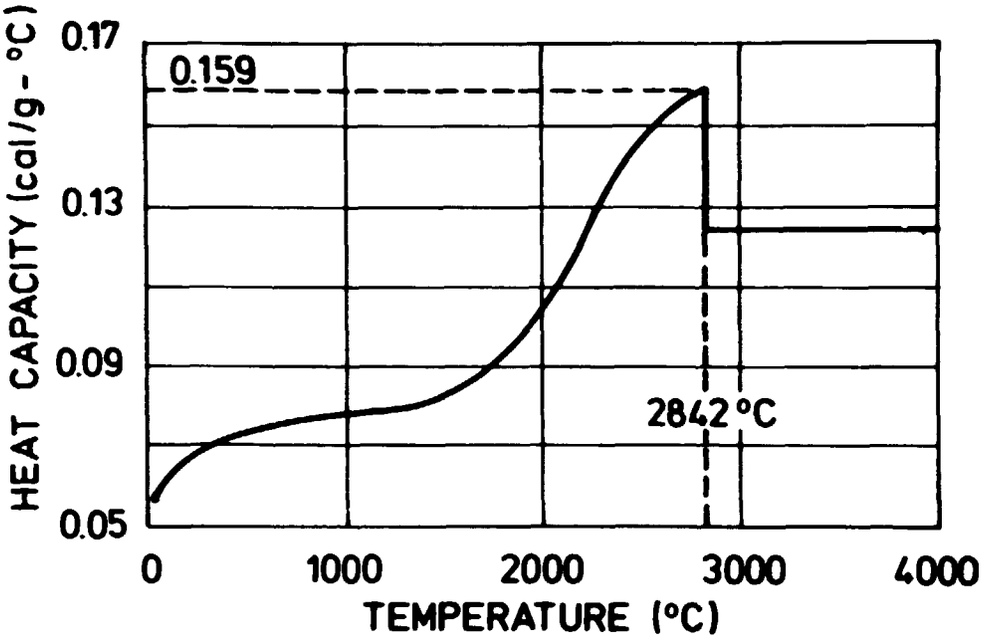

Fig. 5.4.1. UO_2 specific heat capacity as a function of temperature.

it is a slightly conservative assumption to keep C_F constant. A main disadvantage of the method described above is that detailed information about the fuel temperature interval must be known beforehand.

Axial heat conductivity is neglected in the fuel rod. The cladding is assumed an ideal heat conductor, while the conductivity of the gas gap is calculated as a function of the averaged fuel temperature within the node

$$K_{gap} = a_o + a_1 T_F + a_2 T_F^2 . \qquad (5.4.4)$$

The thermal conductivity of uranium dioxide is structure-sensitive, properly depending on a number of factors such as temperature, density, stoichiometric composition, preparation technology, burn-up, etc.[20]. However, for one particular piece of fuel the most reasonable temperature dependency seems to be

$$\lambda_F = \frac{\epsilon_1}{1 + \epsilon_2 T_F} , \qquad (5.4.5)$$

where ϵ_1 and ϵ_2 are constants.

The temperature assigned to each fuel zone has been taken as the volume-averaged temperature of that zone and the temperature on the

boundary between two zones is calculated from a linear temperature distribution between the centres in the two zones.

The fuel thermodynamic model is coupled to the neutronics through the power deposition in the rod and to the hydraulics through the heat transport from the cladding to the coolant. Feed back from the fuel model to the neutronics is the fuel average temperature.

6. TRANSIENTS ANALYSED BY MEANS OF DANAID

The DANAID program involves heavy computer costs, and consequently it was necessary to restrict the number of runs performed on a full-size core to two only, a rod ejection run, and a rod drop run. The influence of essential parameters was then examined by means of a small imaginary reactor.

6.1. Core Configuration

The basis for the full-size reactor model is the ASEA-ATOM reactor Oskarshamn 1. The core contains 448 fuel boxes arranged as 112 neutronic channels in the pattern shown in fig. 6.1.1. Consequently each channel must consist of 4 fuel boxes, or 256 fuel rods, and one control rod.

The control rod removed from the core is the same in the two full-size transients analysed. The rod selected from the four central rods is that that has the maximum reactivity worth, because rapid removal of this rod is believed to result in an accident with most potential consequences.

For computer savings, the 112 hydraulic channels were collapsed into nine groups only. As shown in fig. 6.1.1, the groups make up an annular geometry surrounding the accidentally removed rod. The coolant outside the fuel boxes is contained in one moderator channel only covering the whole core cross section.

A reactor core with only 37 neutronic channels was used for the parameter studies. Applying symmetry properties to this core, it can be represented by 8 channels only, fig. 6.1.2. The ejected control rod is positioned in the central channel for the whole analysis.

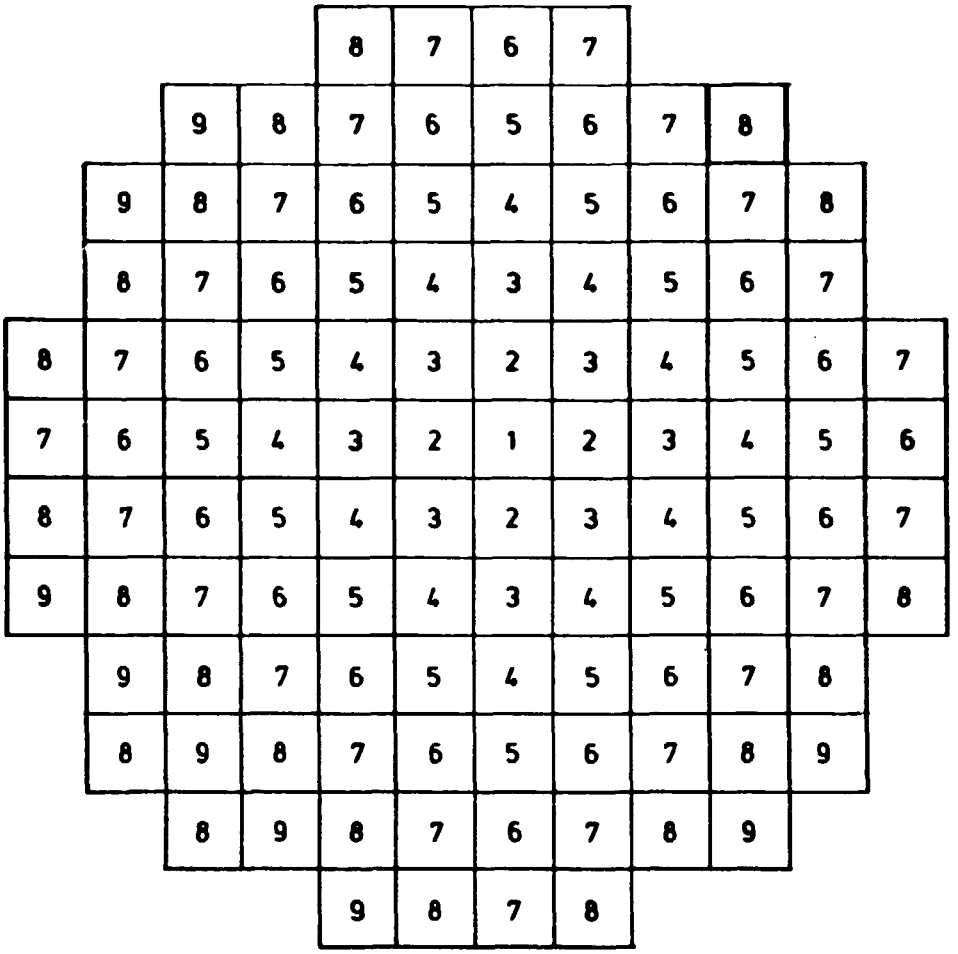

Fig. 6.1.1. Hydraulic channel configuration for full-size reactor analysis.

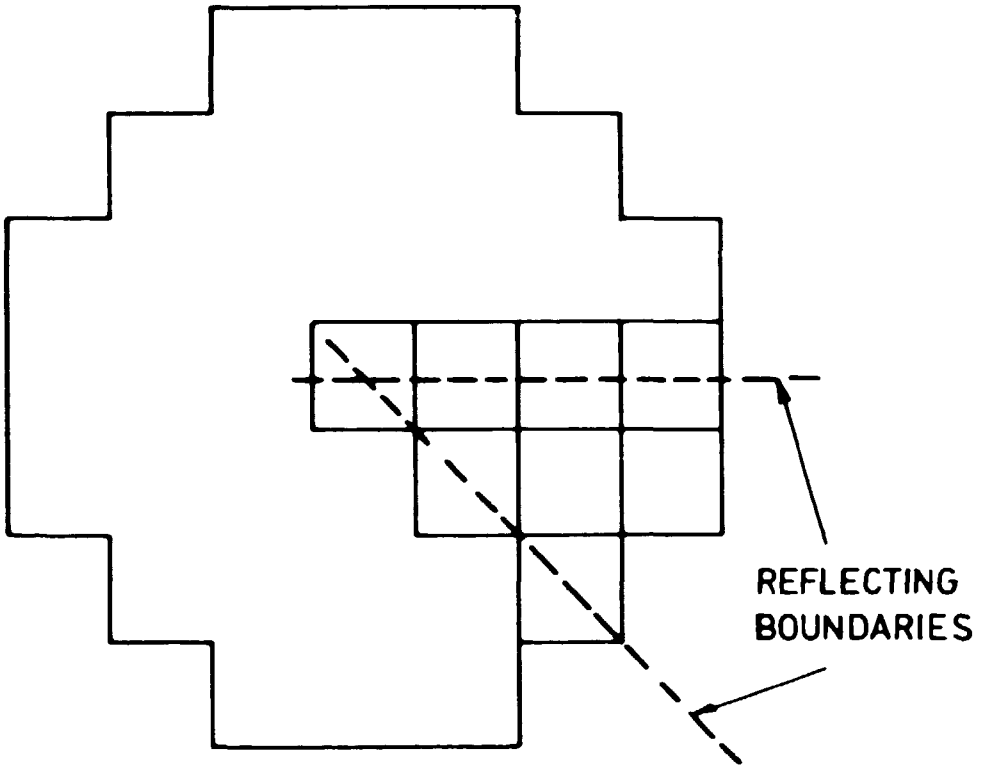

Fig. 6.1.2. Channel configuration for the reduced reactor core.

6.2. Initial Reactor State

The potential consequences of a reactivity accident are mainly a function of the reactivity insertion rate. Due to the reactor feedback mechanisms, the total amount of reactivity inserted plays a minor role, provided that it exceeds a certain threshold. For control rod accident categories, the reactivity insertion rate depends on the control rod reactivity worth and on how rapidly the rod is removed from the core.

In fig. 6.2.1 the maximum rod worth is given as a function of the reactor power for a typical boiling water reactor (General Electric BWR/6) with normal control rod patterns. From the figure it is obvious that special interest must be paid to reactor states in the low power range.

In appendix B of this report an expression is evaluated for the control rod ejection time, t_{rem},

$$t_{rem} = t^{o}_{rem} \left(\frac{P_s(\rho_o) - P_{con}}{P_s(\rho) - P_{con}} \frac{\rho}{\rho_o} \right)^{1/2} \qquad (6.2.1)$$

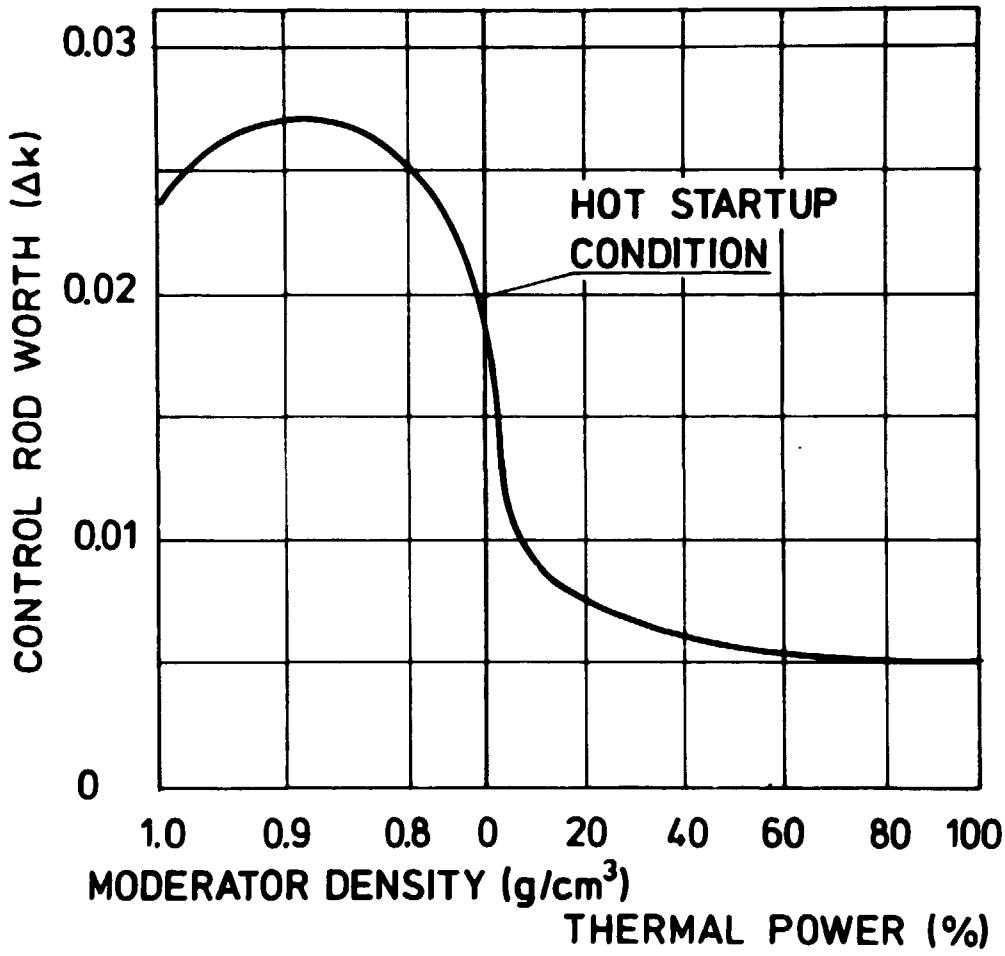

Fig. 6.2.1. Maximum control rod worth at various normal operating states.

where t^{o}_{rem} is the removal time at hot start up, ρ is the coolant density ($\rho = \rho_o$ at hot start up), p_{con} the containment pressure, and $p_s(\rho)$ the saturated water pressure as a function of coolant density. Equation 6.2.1 is only valid in the low power range, where the coolant can be treated as saturated. By means of fig. 6.2.1 and eq. 6.2.1, the average reactivity insertion rate can be calculated as a function of the coolant density. In table 6.2.1 the insertion rate is specified relative to that at hot start up.

Table 6.2.1

Relative reactivity insertion rates

ρ g/cm^3	$\Delta k/t_{rem}$ relative
0.74	1.00
0.80	0.89
0.88	0.50

It is evident from the table that the reactivity insertion rate is maximum in the hot start-up condition. Therefore rod ejection accidents are believed to have the worst potential consequences when they are initiated from a reactor in this power range, i. e. a critical reactor at operating pressure, saturated temperature, and with an initial power fraction of 10^{-6} of that rated. The hot start-up state is characterized by a fractional control rod density of 50%. The rods are arranged in a checkerboard configuration with half of them fully inserted and the rest fully out. In fig. 6.1.1 odd numbered channels have rods inserted and channels with even numbers have control rods withdrawn. The steam load and the feed water injection rate is very small at hot start-up and the pump operates at approximately 30% of rated pump power.

The potential consequences of a rod drop accident are probably not maximum at hot start-up, but at a lower power because the rod drop removal time does not depend so much on the vessel pressure. However, the intention of the rod drop calculation in this report is not to estimate the largest potential consequences of such an accident, but to compare the calculational model to other models, and with this purpose in mind the rod drop analysis can be performed on a reactor at any power level provided that a similar analysis is available. Now, rod drop calculations from the hot start-up range are available, and therefore both the two full-size reactor analyses performed in this report were initiated from this power level.

The results of the calculations are presented in the next sections.

6.3. Standard Rod Ejection Analysis

From a reactor at hot start-up the control rod in the hydraulic channel no. 1, fig. 6.1.1, is ejected from the core with the standard control rod ejection velocity, i. e. the velocity function calculated by RODACC and given in fig. 4.5.3. Results of the calculation are discussed below.

Fig. 6.3.1 shows the power generation as a function of the time since accident initiation. Five curves are plotted in the figure. The term "total power" refers to the total nuclear power generated at that particular moment. The total power is the sum of the power released promptly after the fission process ("prompt power") and the delayed power; the latter is not explicitly shown in the plot. The delayed power fraction is very small, therefore the total power and the prompt power nearly merge. The power to the coolant is represented by the convective heat generation ("conv. power") and the power deposit directly in the coolant ("direct power"). Also the total power to coolant, i. e. the sum of the convective power and the directly deposited power, is shown in the figure.

During the first 100 ms after the break, no change in power generation can be observed. Then power rapidly increases by 8 decades, corresponding to a peak power of more than 100 times the nominal level. During the power increase the reactor period is approximately 5.5 ms. It is seen that the peak power is reached before the control rod is fully out of the core, which happens after 308 ms. This is more clearly demonstrated by the rod ejection calculations based on a small reactor core, where the appearance of the peak is earlier, and this supports the assertion that the reactivity insertion rate is more significant than the total amount of reactivity inserted. The power peak is very slim, and soon the production rate is lower than the nominal level.

At steady state the direct power to the coolant is only a small fraction of the total coolant power, but during the power increase the direct power overrides the convective power by more than a decade, thus it is important to have an accurate model for the fission power directly released into the coolant. Although this power fraction depends on the coolant density, which certainly changes during the ejection, the fraction has been kept constant at the value corresponding to zero void. This is due to the fact that most of the neutron kinetic energy, which is normally deposited in the internal box coolant, will, when the internal coolant density is low, be transmitted to the external coolant. However, the outside coolant is rather poorly represented in DANAID - only one channel for the whole reactor cross section - and energy deposition in this channel would lack spatial dependency, resulting in a weak moderator feedback effect. Deposition of most of the energy in the internal channel results in a too high void fraction in this channel and a strong feedback mechanism, but then the outside coolant has a good moderator effect because it contains no steam, which it normally would in such accidents. Therefore the best approximation to the real problem is believed to be a high relative energy deposition in the internal channel. After the power peak the direct power deposition drops and becomes insignificant.

The convective power is mostly a step-function with a steady level before and after the peak. The final level is 6 decades above the initial, i.e. approximately at the nominal value, but the power distribution is not as in a normal full power reactor state (fig. 6.3.2).

Fig. 6.3.3 plots the inserted reactivity, the rod worth, as a function of time. Up to approximately 0.2 s after accident initiation the total reactivity of the core merges with the rod worth, but as soon as the fuel temperature and the coolant void fraction are increased, the reactivity drops drastically. Due to the very high power directly delivered to the coolant, the delay in the moderator feed back relative to the Doppler feed back set point is not significant.

During the power increase the reactivity is approximately a stepwise linear function as shown in fig. 6.3.3. In the first step the control rod reactivity insertion is dominant; subsequently the reactivity insertion and both the two feedback mechanisms are significant. In the last step the fuel temperature has reached its final level and consequently the reactivity is only changed by the moderator feed back and by the removal of the control rod. From the gradient of the straight lines drawn in fig. 6.3.3, it is possible to extimate the time derivative of the three reactivity effects

$$\dot{\rho}_c = 0.004\ s^{-1} \qquad (6.3.1)$$

$$\dot{\rho}_V = -0.31\ s^{-1} \qquad (6.3.2)$$

$$\dot{\rho}_D = -0.69\ s^{-1} \qquad (6.3.3)$$

Thus the Doppler feedback mechanism is approximately twice as strong as the moderator feedback. The control rod reactivity insertion is insignificant when the feedback mechanisms are active.

When a control rod is partially inserted in a node, it is treated as if it was totally inserted but with a reduced control effect. This way of representing the rod results in small ripples on the reactivity curve if a node border is passed. The two cuts on the reactivity curve in fig. 6.3.3 are also due to this effect; the first one corresponds to the total removal of the ejected rod from the core and the second to the scram insertion initiation. Apart from the cuts, the events do not influence on the reactivity.

Because of the highly peaked power distribution the convective power level corresponds to a maximum section average fuel temperature of 1270°C. With a local formfactor of 1.20, the maximum rod temperature becomes 1524°C. As discussed in section 5.4, the final fuel temperature is sensitive to the choice of specific heat capacity of the fuel. In appendix C is evaluated an iterative procedure for correction of the fuel temperature due to changes in the heat capacity. The procedure is based on point kinetics and both moderator feedback and Doppler feedback mechanisms are incorporated. With this procedure the temperature of the hottest rod section becomes

$$T_{F\,max} = 1616^{\circ}C$$

corresponding to a peak enthalpy of

$$h_{F\,max} = 120\ cal/g\ .$$

Experimentally based fuel rod failure thresholds[5] are given in table 6.3.1. It is seen that the calculated fuel enthalpy is well below the failure thresholds, thus from this point of view the fuel integrity should not be altered.

Table 6.3.1

Fuel Failure Enthalpy Thresholds

	peak enthalpy
- cladding	170 cal/g
- incipient fuel melting	269 cal/g
- fully molten fuel	336 cal/g
- prompt fuel dispersal	425 cal/g

Table 6.3.2[22] shows characteristic relations (according to General Electric Company) between the reactivity insertion rate, the minimum period, the peak enthalpy, and the principal shutdown mechanism.

Table 6.3.2

Characteristics of Nuclear Excursion

range	reactivity insertion rate $/s	minimum period ms	peak enthalpy cal/g	principal shut down mechanisms
low	$\langle$ 2,5	$\rangle$ 4	$\langle$ 120	Doppler effect moderator "
medium	2-25	5-2	100-425	Doppler effect
high	$\rangle$ 20	$\langle$ 1.5	$\rangle$ 380	Doppler effect core disassembly

The characteristics of the standard rod ejection transient analysed in this report are a minimum period of 5.5 ms and a peak fuel enthalpy of 120 cal/g, which corresponds pretty well to the lower part of the medium range, but the reactivity insertion rate, 10 $/s, fits better to the middle of this range.

The void fraction shown in fig. 6.3.3 corresponds to the hot channel exit, but it is not the exit void only that increases rapidly. This is clearly

demonstrated by fig. 6.3.4, where the steam content in each section of the central channel is given at different times. The rapid steam production rate causes the coolant to be ejected from both ends of the channel, fig. 6.3.5. It could be interesting to see how long a time it would take before good cooling conditions were re-established, in the hot channel, but the DANAID code cannot handle sections with very small mass contents without starting to oscillate. However, from fig. 6.3.5 it can be assessed that it would probably take several seconds before the channel is refilled with water. Within the assessment, it must be remembered that on the containment isolation signal the pump speed is even further reduced from 30% to 20% of nominal speed, and that the relief valves will start to blow. These effects are not included in the DANAID analysis. Thus, even if DANAID could handle totally voided sections, it would be too expensive to use such a code for these calculations. Now, DANAID overestimates the heat conduction to the coolant because the convective heat correlations are based on nucleate boiling, but the channel would definitely be voided nevertheless.

The water velocity distribution inside the hot channel is shown in fig. 6.3.6 and the heat flux in fig. 6.3.7. The high heat fluxes combined with large steam qualities and mass fluxes result in burn-out of the rods. Fuel rod performance in the absence of good cooling conditions is analysed in section 7.1.

The pressure increase and the water level increase is shown in fig. 6.3.8. The pressure increase is not significant and it will be further reduced when the relief valves start to blow. The effect of the valves is not considered in the model, because the delay time of the valves after the isolation signal is approximately 0.3 s, and consequently the effect is negligible within the time range of a DANAID analysis.

The influence on the transient of the discharge coolant flow from the ruptured control rod drive house thimble was analysed and found insignificant. However, in the analysis it was assumed that the discharge was from the lower plenum, but if the communication from the hot channel via the control rod guide tube to the ruptured area results in a reduced coolant density in the hot channel, this might result in an earlier moderator feedback. The influence of such communication has not been examined.

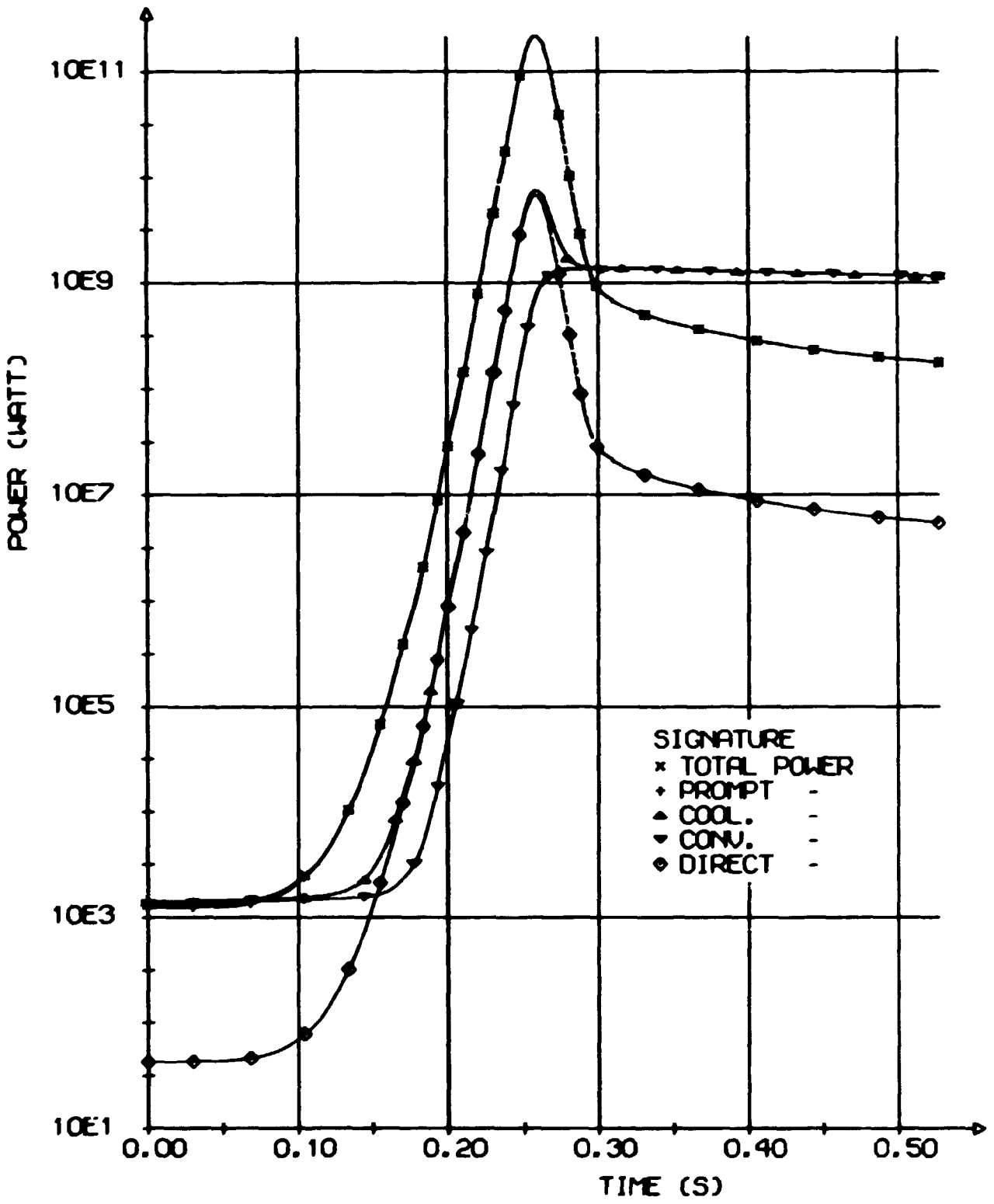

Fig. 6.3.1. Rod ejection transient power generation.

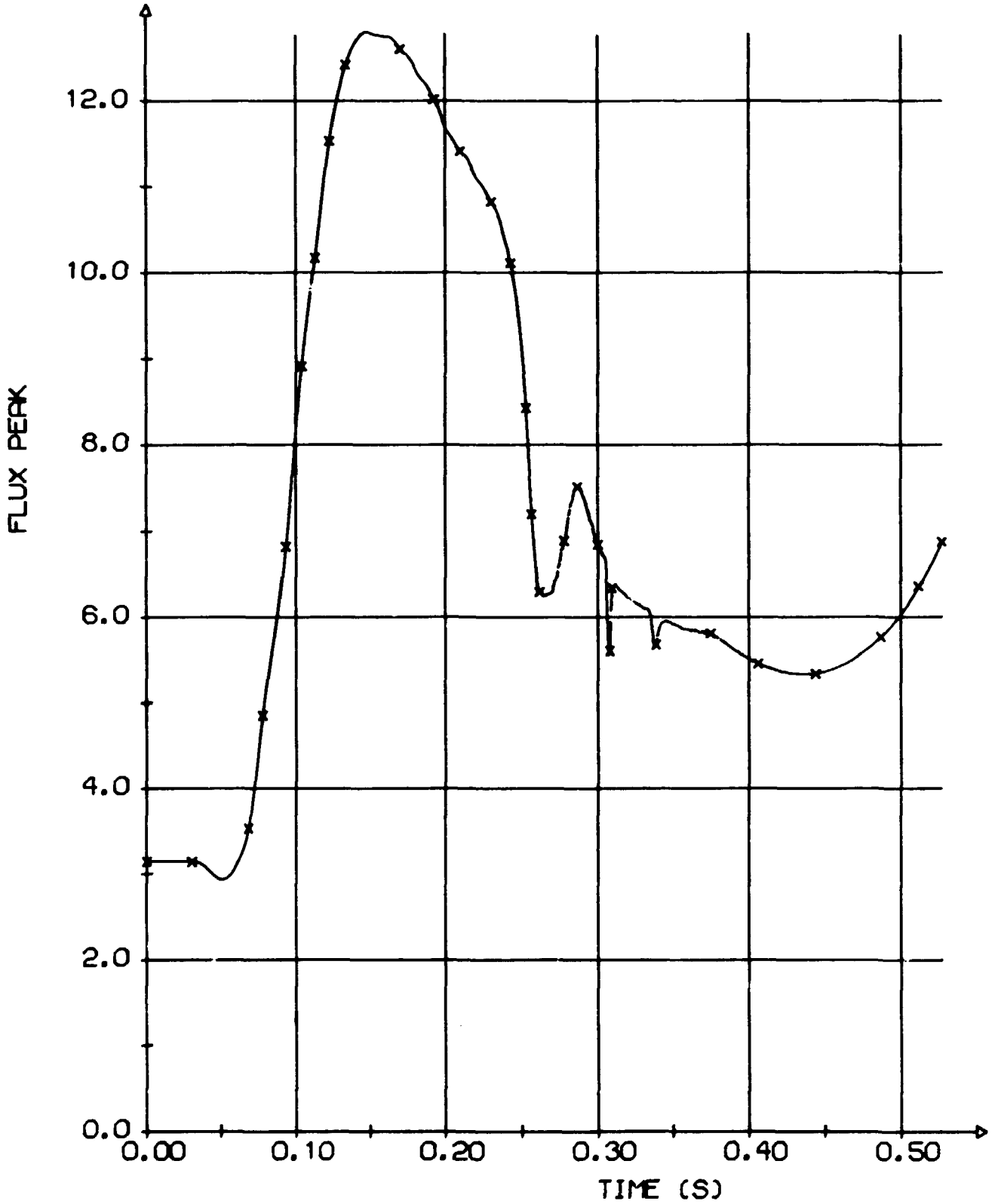

Fig. 6.3.2. Rod ejection peak to average flux ratio.

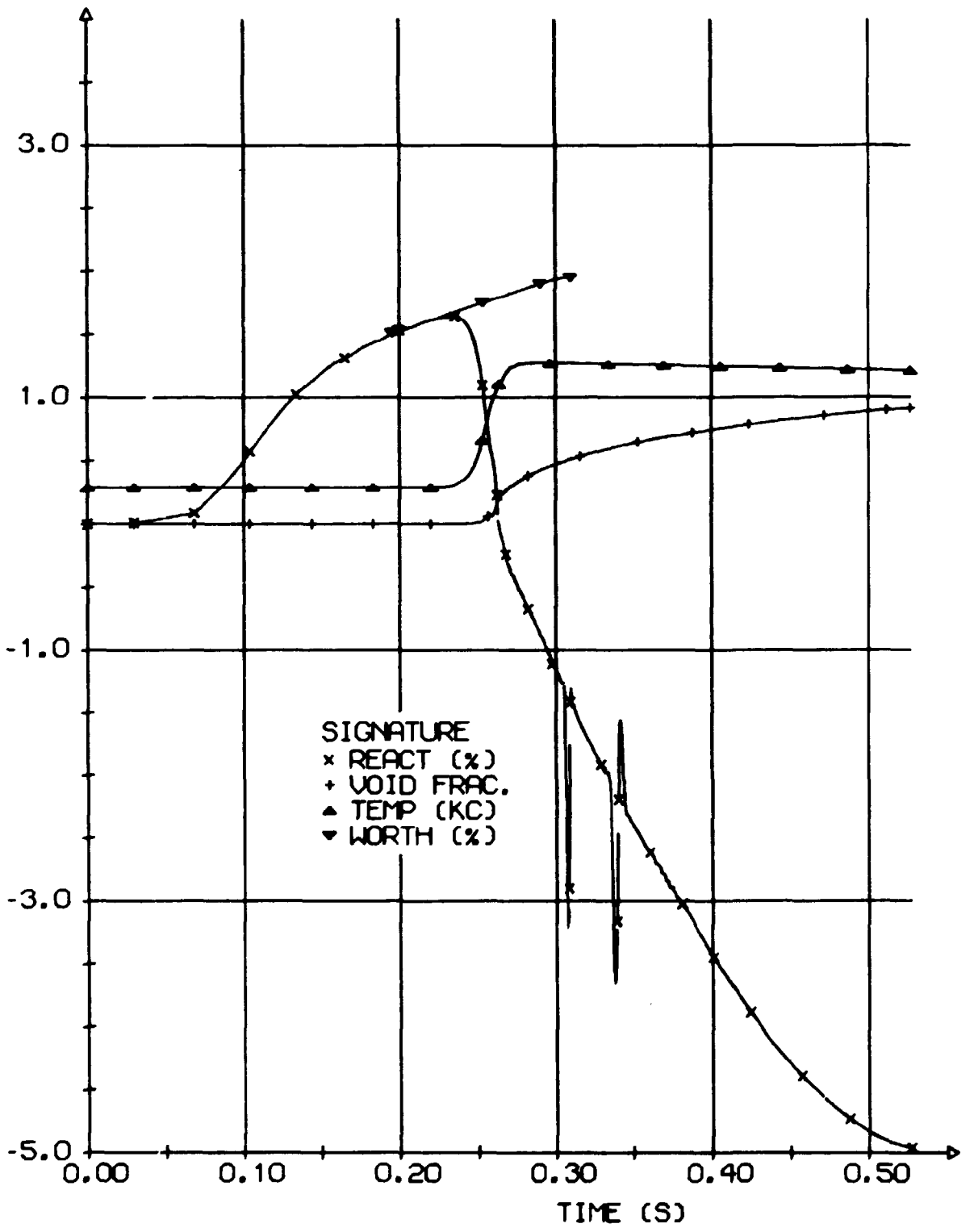

Fig. 6.3.3. Rod ejection net reactivity. Demonstration of feedback mechanisms.

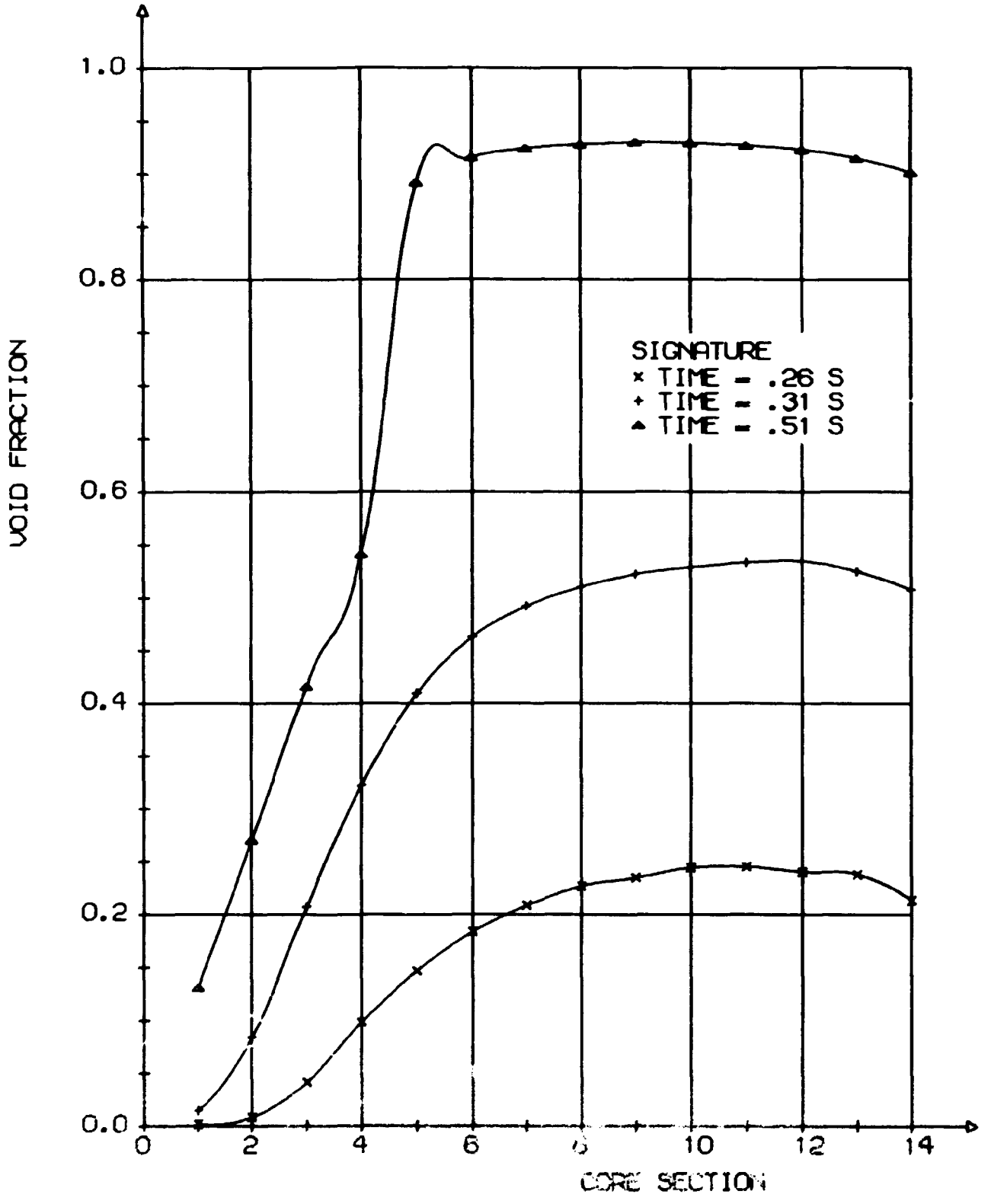

Fig. 6.3.4. Hot channel void fraction distribution.

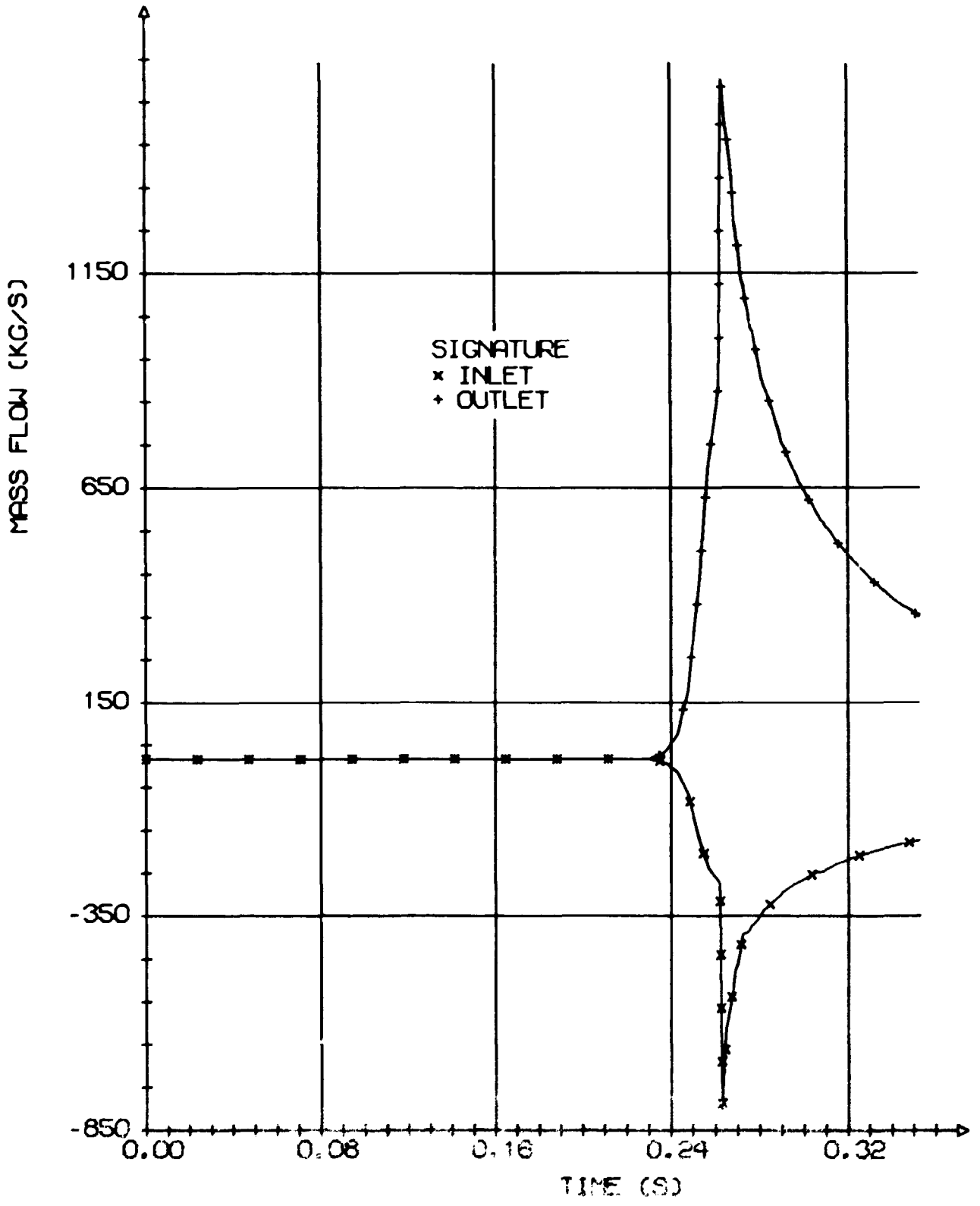

Fig. 6.3.3. Hot channel coolant inlet and outlet mass flows.

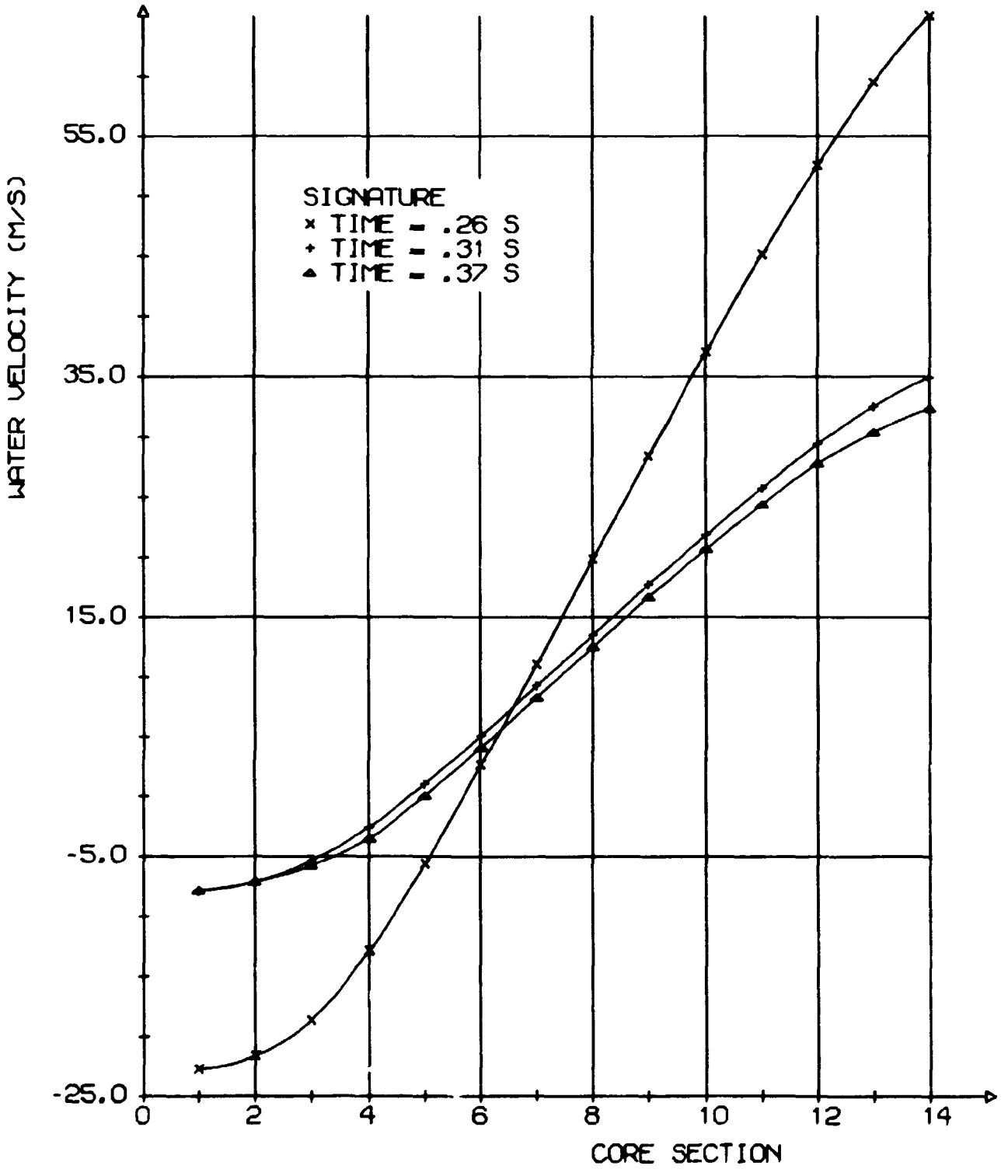

Fig. 6.3.6. Hot channel water velocity distribution.

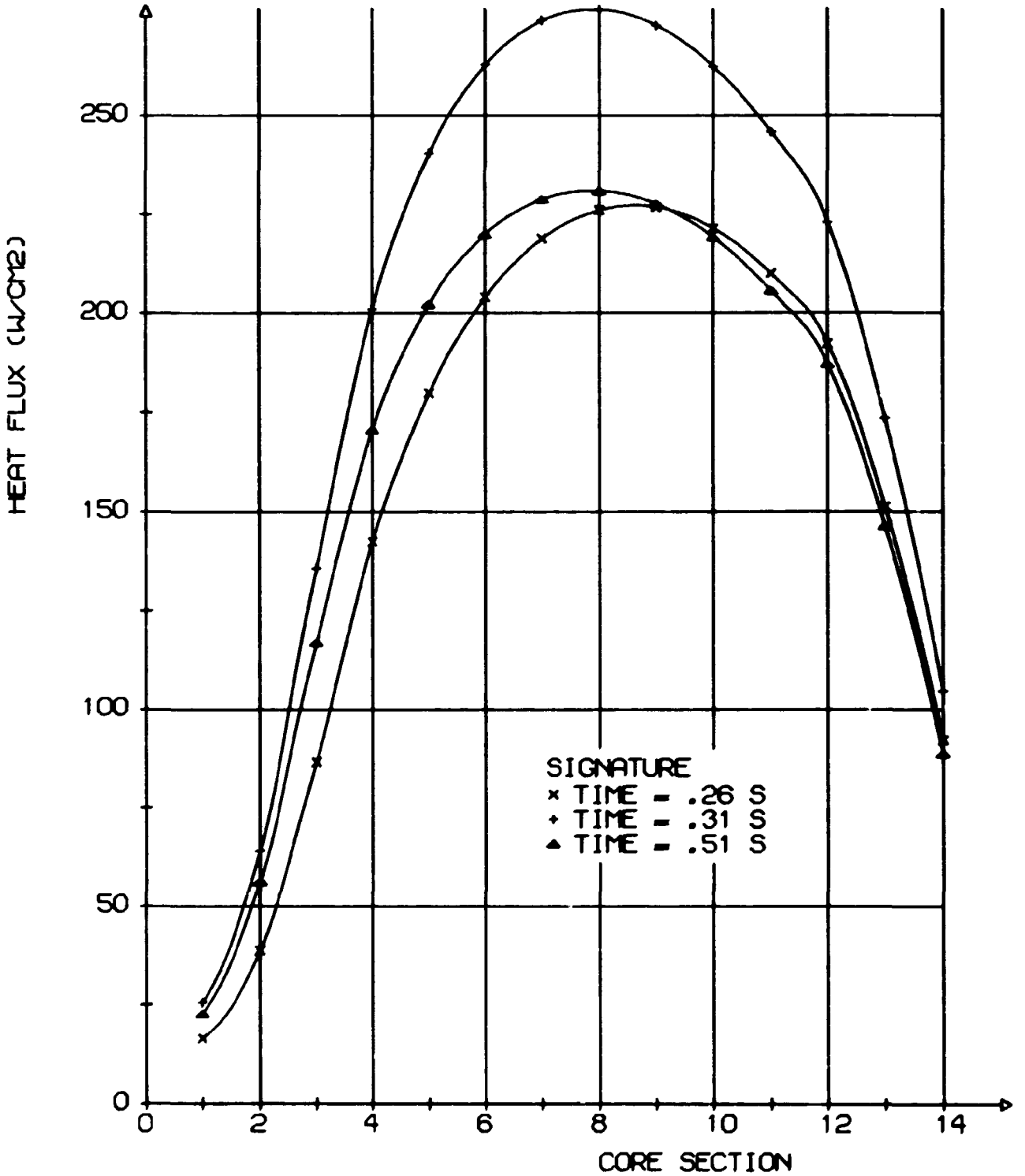

Fig. 6.3.7. Hot channel heat flux distribution.

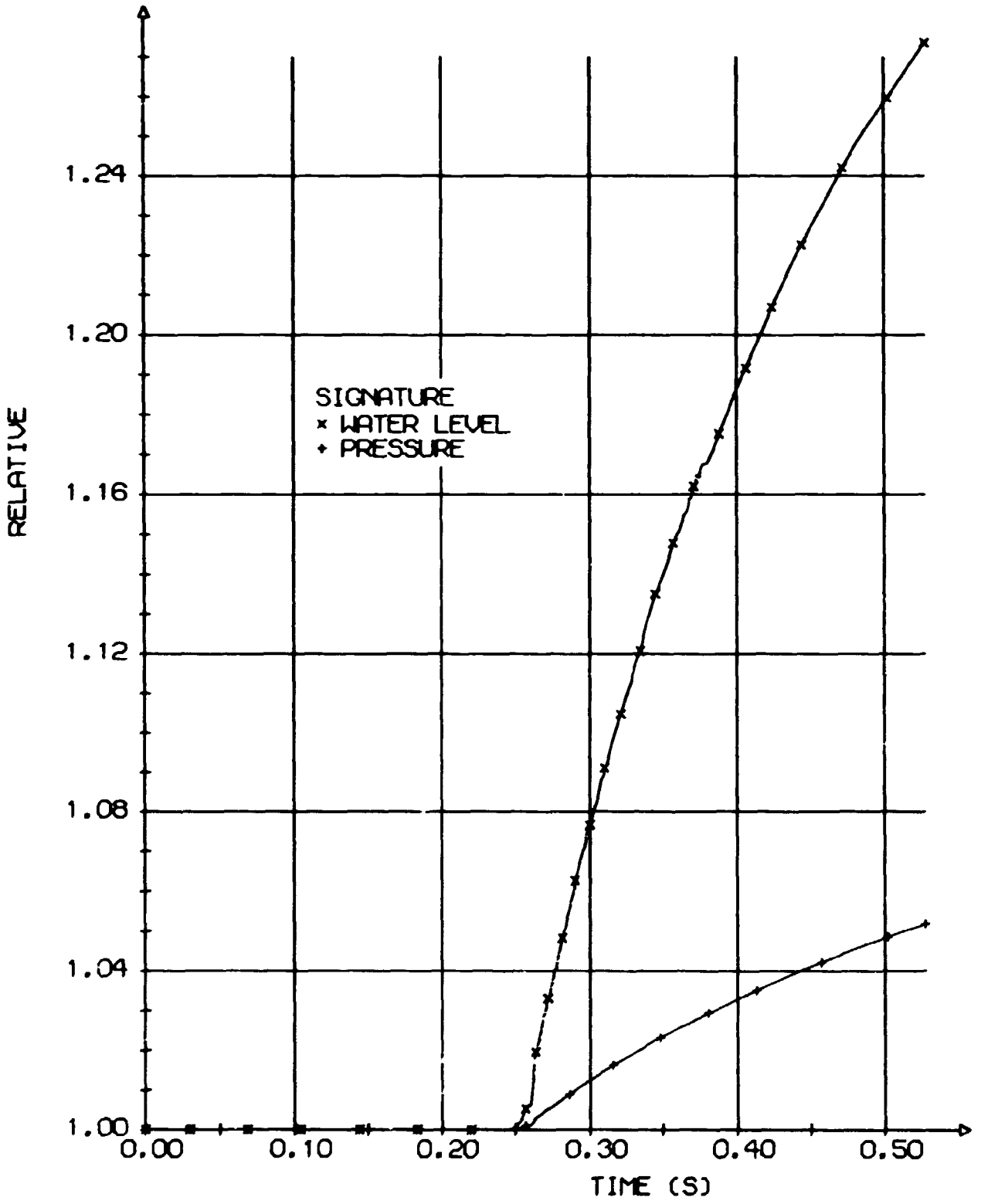

Fig. 6.3.8. Water level and reactor pressure relative to initial value.

6.4. Standard Rod Drop Analysis

Results of the rod drop analysis are presented in figures in this section.

The rod drop power peak is considerably delayed compared to the rod ejection peak (approximately 1.3 s), but because of the slow reactivity insertion rate the peak reactivity becomes less than 1% $\Delta k/k$, while in the rod ejection case it exceeds 1.6% $\Delta k/k$ (in both cases it should be recalled that the static rod worth was approx. 2.0% $\Delta k/k$). Once again the Dopler feedback and moderator feedback slow down the power burst.

Contrary to rod ejection accidents, the scram rods do move before the excursion is over, but from fig. 6.4.2 it is obvious that the negative scram reactivity insertion rate is much too slow to influence the results. For the transients analysed in this report, the scram signal has been set at the time of a 20% increase in the average nuclear power and no credit has been given to the delay time in the instrumentation system. This is probably too optimistic, but according to reference 3 the scram instrumentation should be very fast in the low power range. Normally, the delay times for such instrumentation systems are 0.1 s. Rod movement is started 0.2 s after the trip signal and all rods, except the one accidentally removed, are inserted.

The power peaking factor is very much the same in the two transients, but because of a lower total power in the rod drop case, the peak fuel temperature and enthalpy only become 772°C and 50.6 cal/g, respectively. Again the hot channel maximum exit void is pretty high, but not alarming, and the axial void distribution is not so uniform. Even during this slow excursion, the steam production rate is high enough to cause flow reversal in the hottest channels.

Because the dropping rod is only half removed at the time of the power peak, the axial power distribution is very peaked in the upper core part (fig. 6.4.8)

In the rod drop accident the burn-out limit is not exceeded and the fuel integrity is maintained.

The purpose of this rod drop transient analysis was to compare the DANAID model to other dynamical large core reactor models. However, the results of analysis of nuclear excursions in large power reactors are not frequently published, and the published results are generally of older date and based on a point kinetics approach. It is not unexpected that literature studies[23] show that point kinetics are unable to describe the

the spatial dependency in a realistic manner. The poor representation of the spatial effects results in a poor incorporation of the very important feedback mechanisms.

One of the more recently published (1972) studies[5], from the General Electric Company, uses an adiabatic, point kinetic model with some consideration of spatial effects. The model is described below.

The neutron flux is separated as

$$\Phi(\underline{r}, t) = \Phi^t(\underline{r})\, F(t) \qquad (6.4.1)$$

where $\Phi^t(\underline{r})$ is the fundamental mode spatial flux at selected points in time. The shape function will reflect space- and time-varying nuclear properties at each time point. The eigenvalue of the fundamental mode solution for $\Phi^t(\underline{r})$ provides the reactor average effect of these changing properties in time. By relating this change in eigenvalue to the time-dependent reactor multiplication factor k(t), this parameter is used in the point reactor kinetics equations.

$$P(t) = \frac{1}{\tau}\left[\frac{k(t)-1}{k(t)} - \beta\right] P(t) + \sum_{j=1}^{N} \lambda_i C_i(t) \qquad (6.4.2)$$

$$C_i(t) = \frac{1}{\tau}\beta_i P(t) - \lambda_i C_i(t) \qquad (6.4.3)$$

$$\dot{h}(t) = K\,[\,P(t) - P(o)\,] \qquad (6.4.4.)$$

where

- $P(t)$ = average power fraction
- $C_i(t)$ = average effective precursor density for delay group i
- $h(t)$ = average fuel enthalpy
- τ = prompt neutron generation time
- β_i = delayed neutron fraction, $\beta = \sum_{i=1}^{N} \beta_i$
- λ_i = decay constant for delay group i
- N = number of delay groups
- K = factor converting average power fraction to average fuel enthalpy rate

Integrating the kinetics equations yields fuel enthalpy, which may be related to fuel temperature and to the effect of Doppler feedback. Thermal-hydraulic effects are ignored.

The method uses two-dimensional calculations of fundamental mode flux and power for several average fuel enthalpy increments. For each increment the enthalpy distribution at the end of the step n+1 is estimated by

$$h_i^{n+1} = h_i^n + \tilde{P}_i^{n+1} \Delta h^n \qquad (6.4.5)$$

where

h_i = fuel enthalpy distribution
$\tilde{P}_i$ = estimated (extrapolated) normalized power distribution
Δh = increment of average enthalpy.

The detailed nodal power distribution is used in the above equation to produce the nodal enthalpy distribution, which is related to fuel temperature. A Doppler feedback relation converts the temperature distribution into changes in nuclear properties on a nodal basis. Using these properties, the fundamental mode spatial flux, power and associated eigenvalue are obtained for the succeeding step. The reactor average kinetics equations provide time-dependent results during the step using

$$k(t) = k(o) + \Delta k_C(t) + \Delta k_S(t-t_S) + \Delta k_F(t) \qquad (6.4.6)$$

where $\Delta k_C(t)$ represents the perturbation causing the excursion, Δk_S represents reactor scram, t_S is the time when average power reaches the scram set point, and feedback is represented by

$$\Delta k_F(t_o) = \frac{1}{\lambda^o} \left\{ \lambda^n + (\lambda^{n+1} - \lambda^n) \frac{h(t)-h^n}{\Delta h^n} \right\} - 1.0 , \qquad (6.4.7)$$

where

λ^n = fundamental mode eigenvalue at the end of step n

h^n = average enthalpy at the end of step n .

Because the model is adiabatic, moderator effects are not included and it is difficult from the description to judge how valid the treatment of the Doppler feedback is, but it is obvious that the model predicts results that are significantly different from the results predicted by DANAID. Fig. 6.4.10 shows the net reactivity for two transients analysed by DANAID and

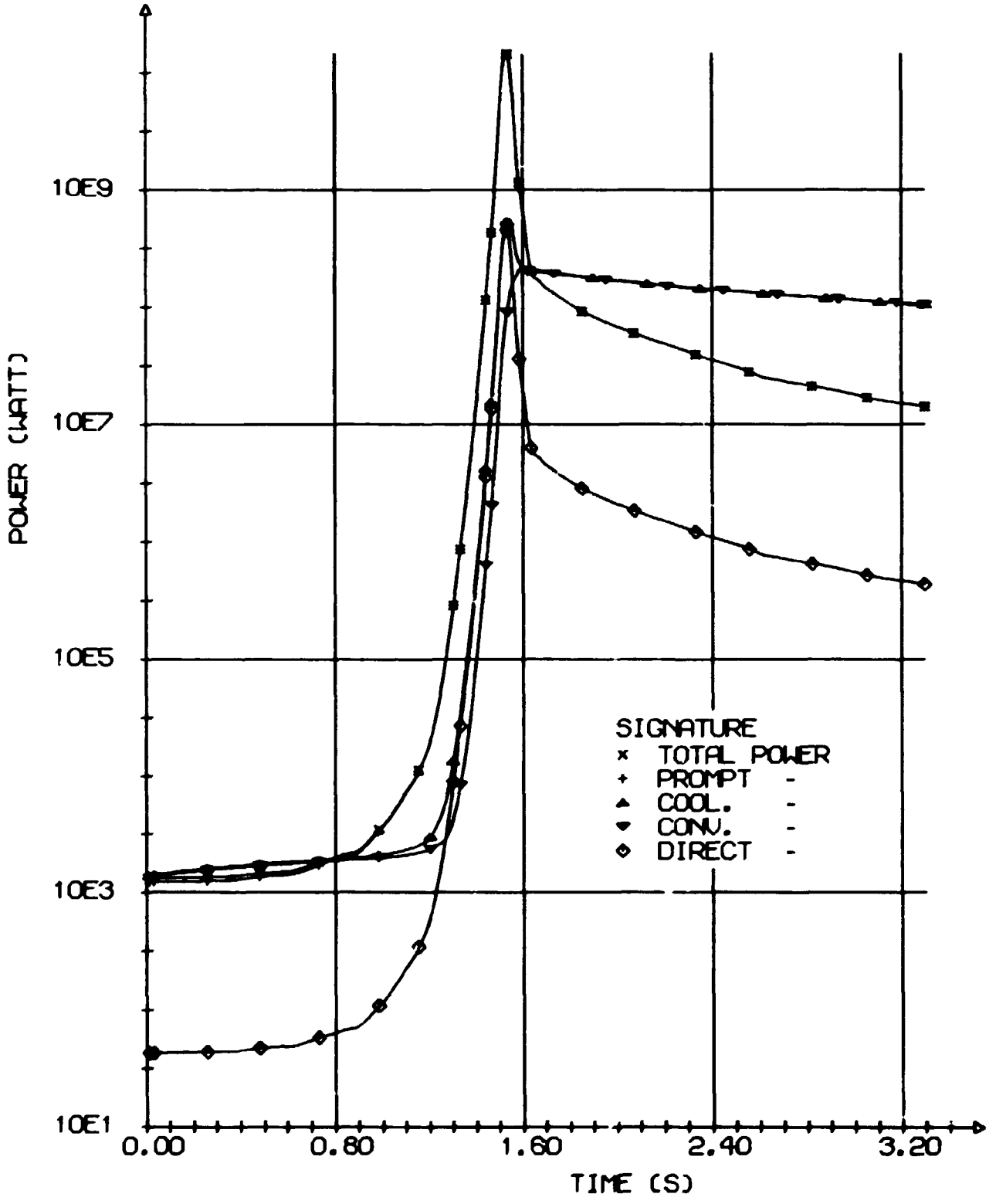

Fig. 6.4.1. Rod drop transient power generation.

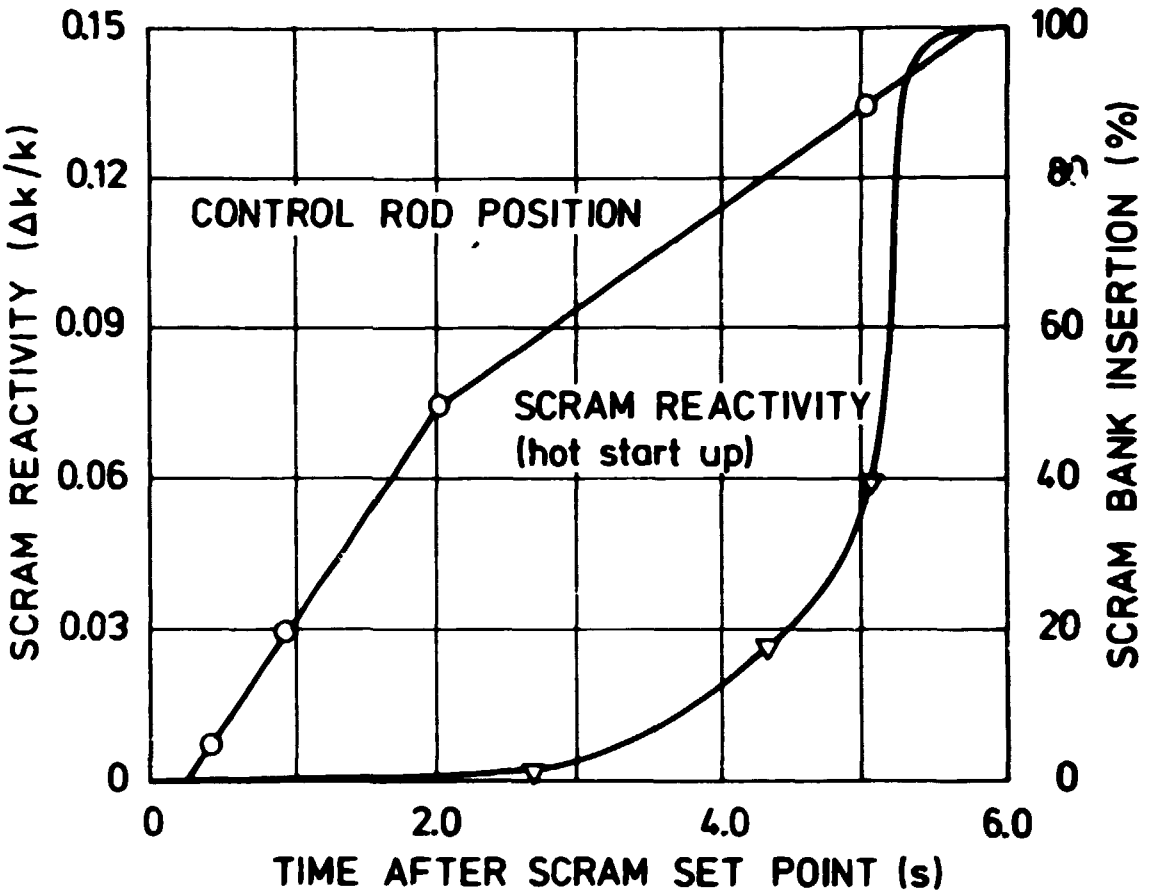

Fig. 6.4.2. Scram characteristics assumed for transient analysis.

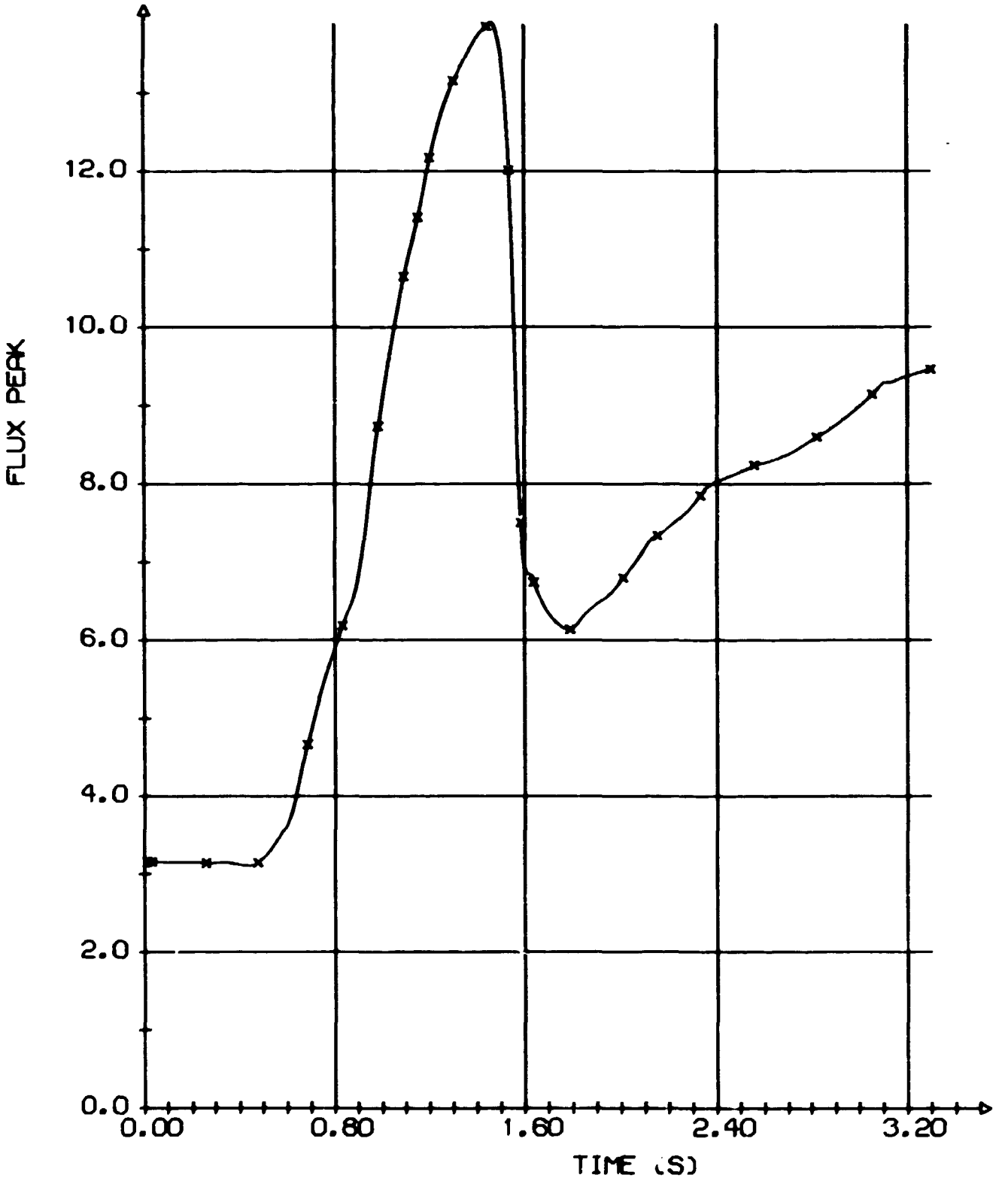

Fig. 6.4.3. Rod drop transient peak to average flux ratio.

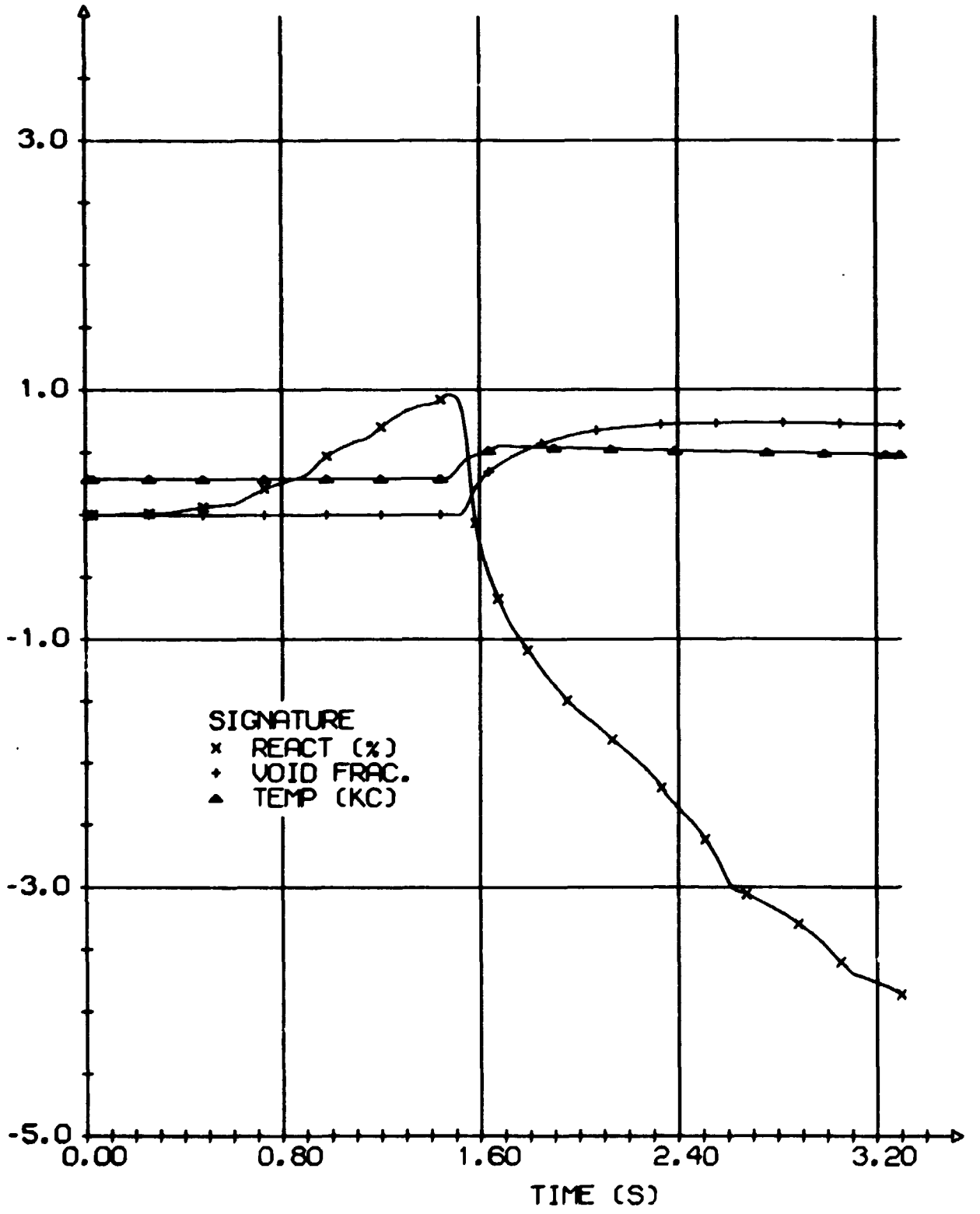

Fig. 6.4.4. Rod drop net reactivity. Demonstration of feedback mechanisms.

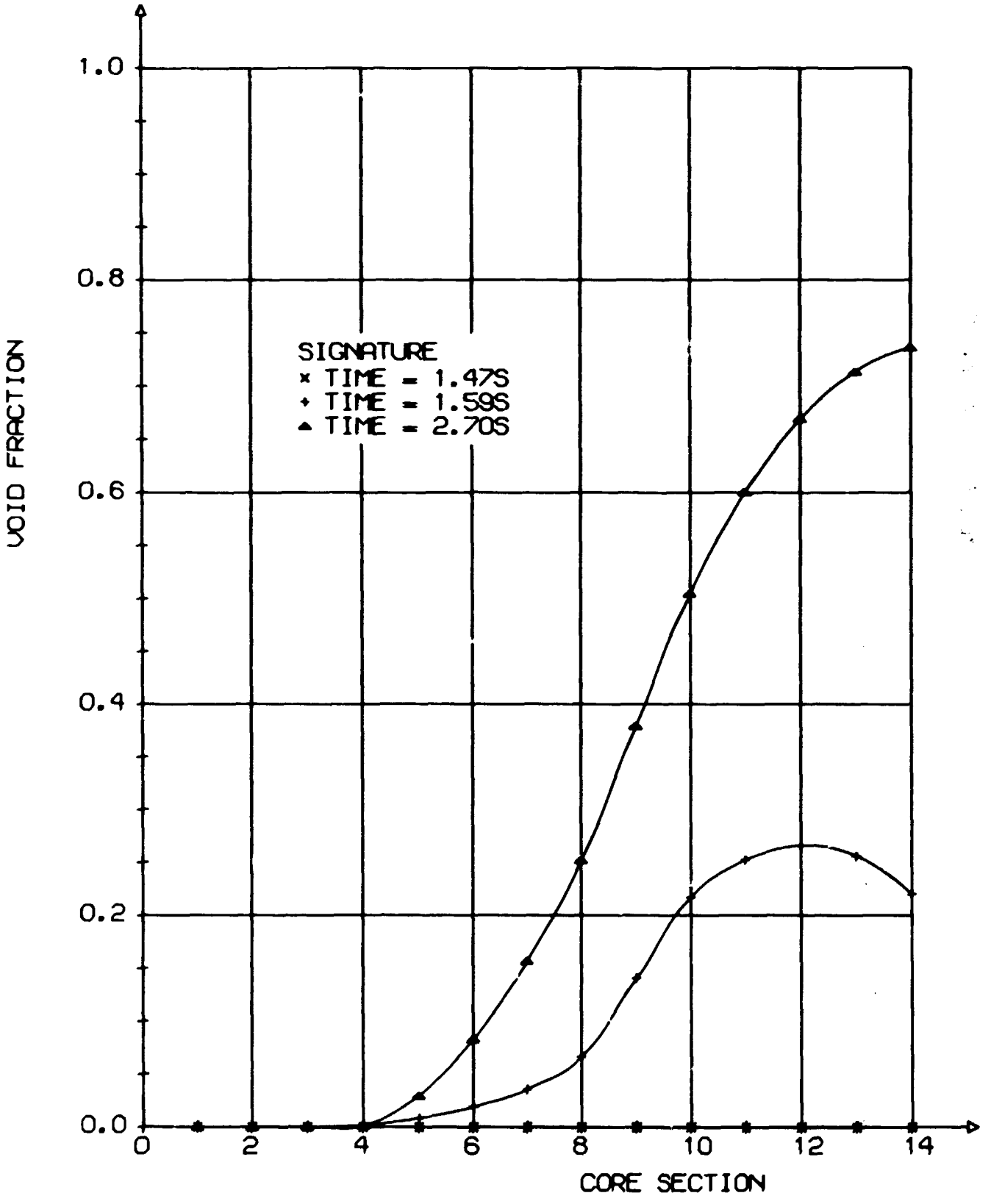

Fig. 6.4.5. Hot channel void fraction distribution.

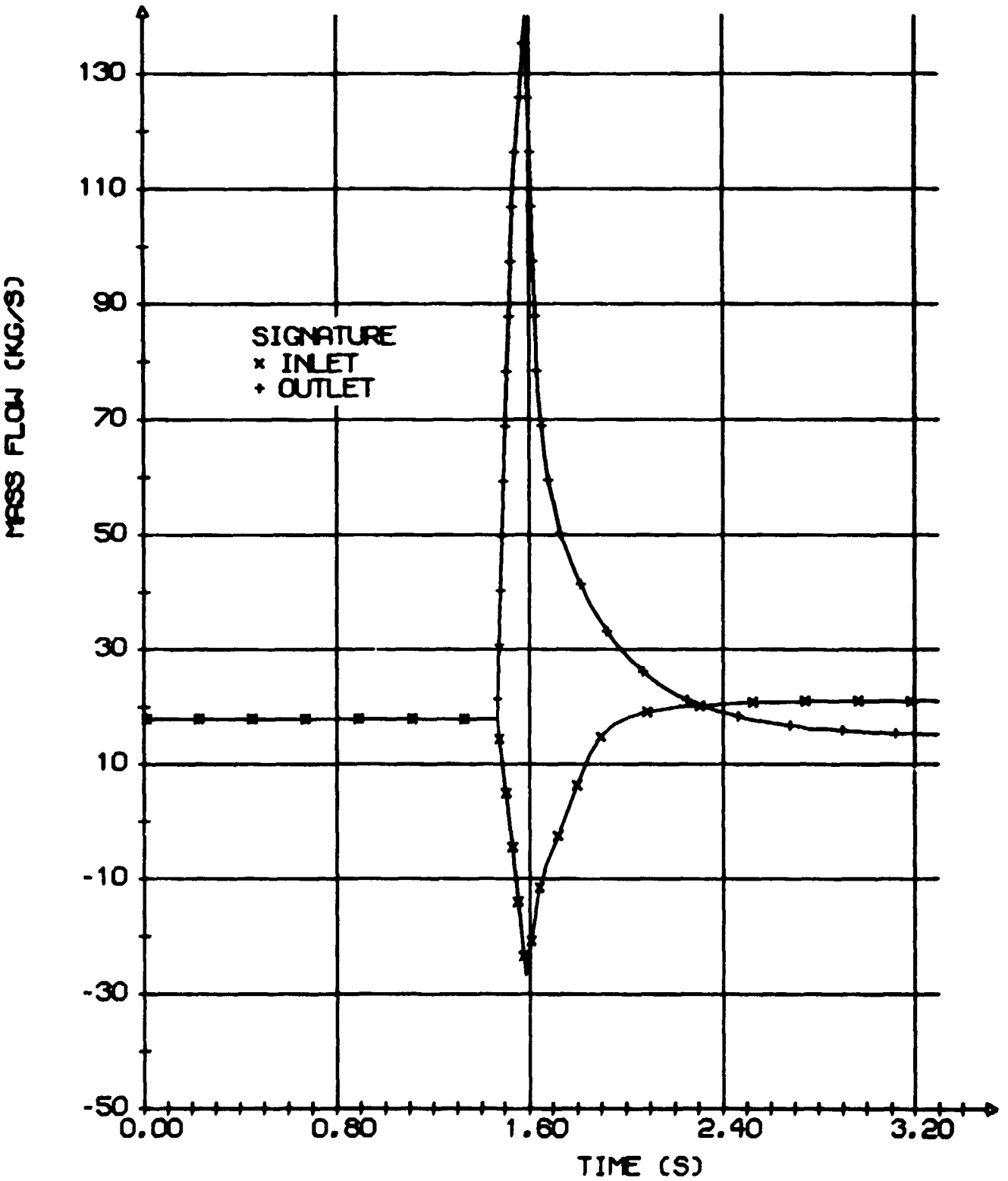

Fig. 6.4.6. Hot channel coolant inlet and outlet mass flows.

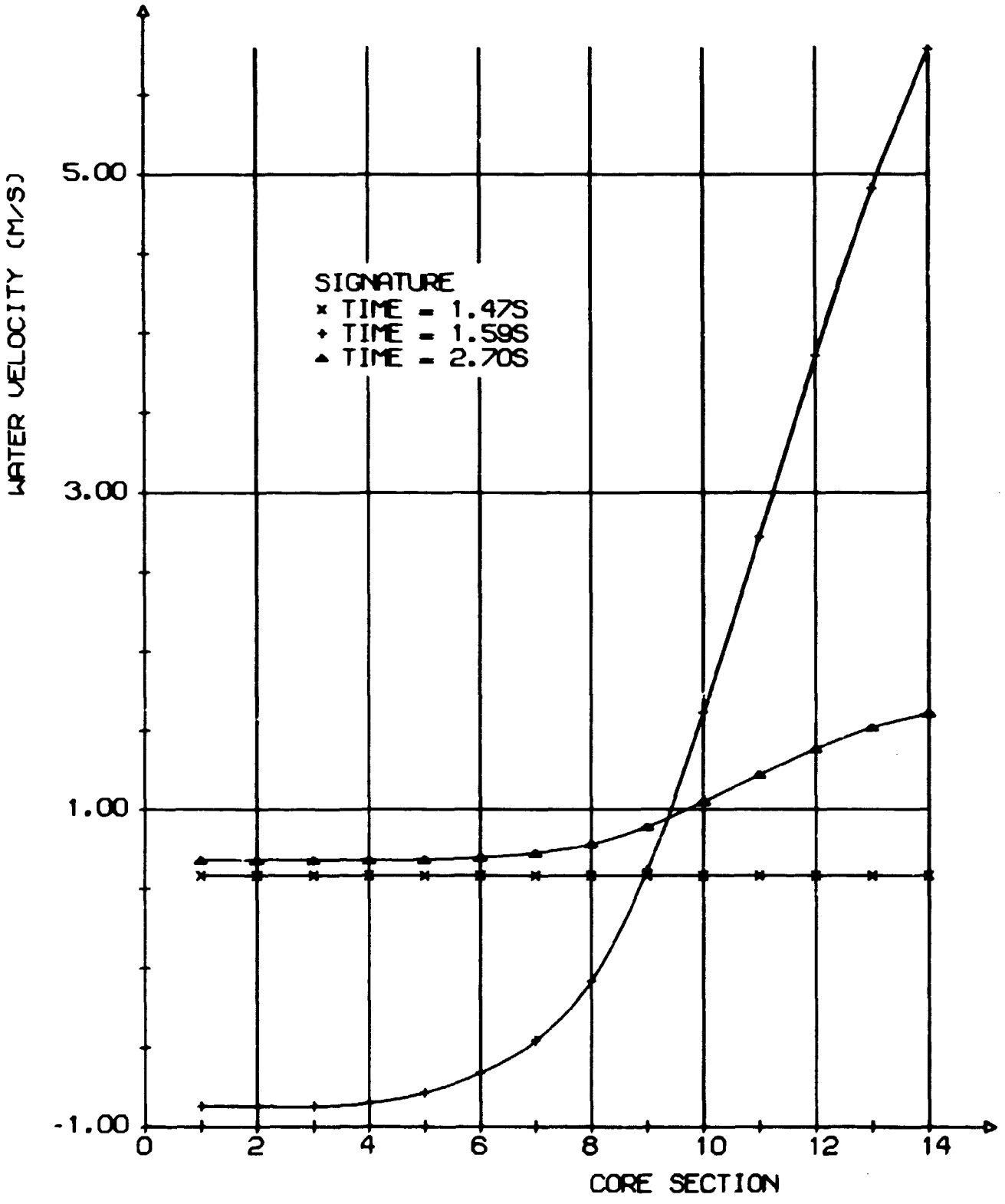

Fig. 6.4.7. Hot channel water velocity distribution.

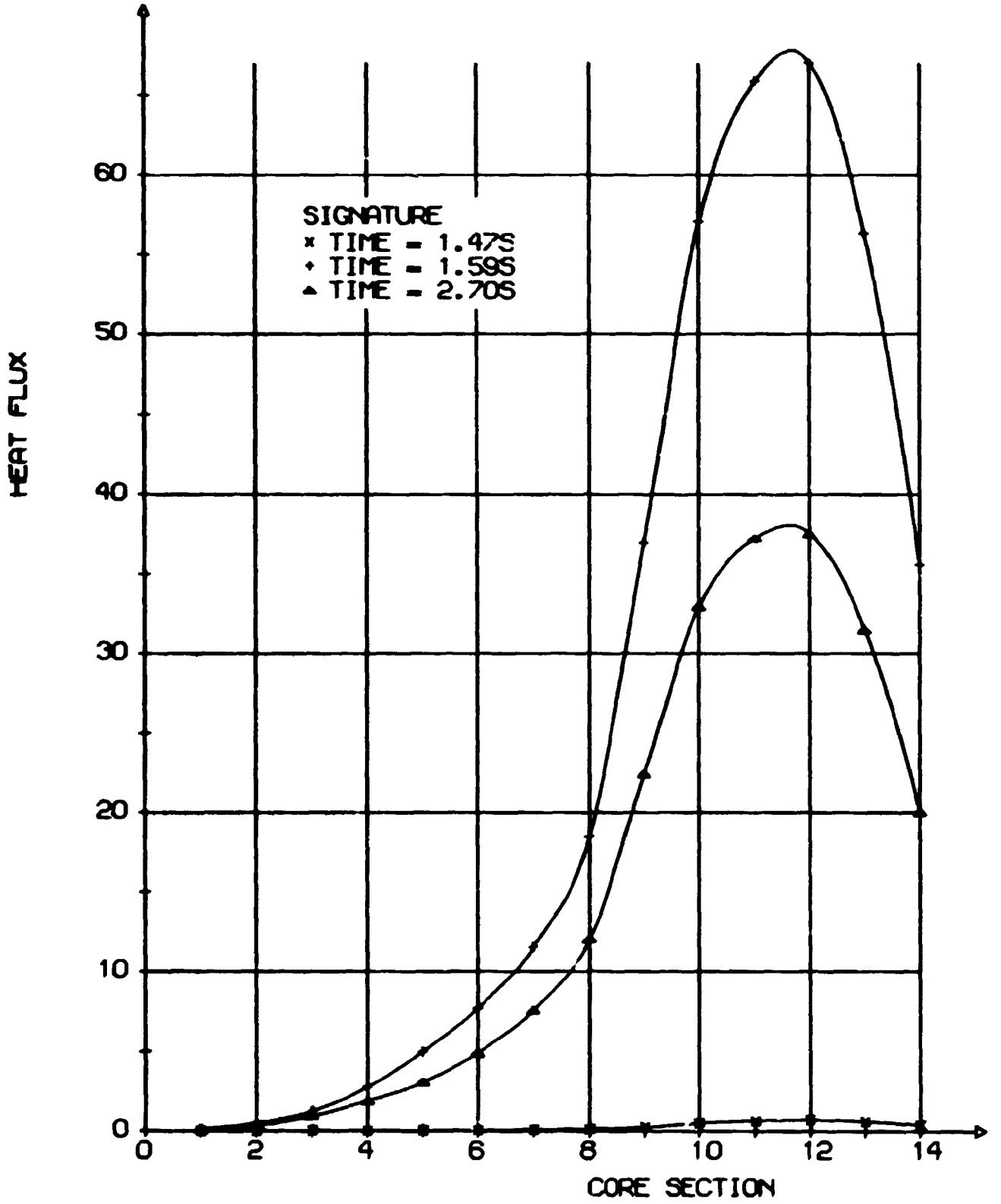

Fig. 6.4.8. Hot channel heat flux distribution.

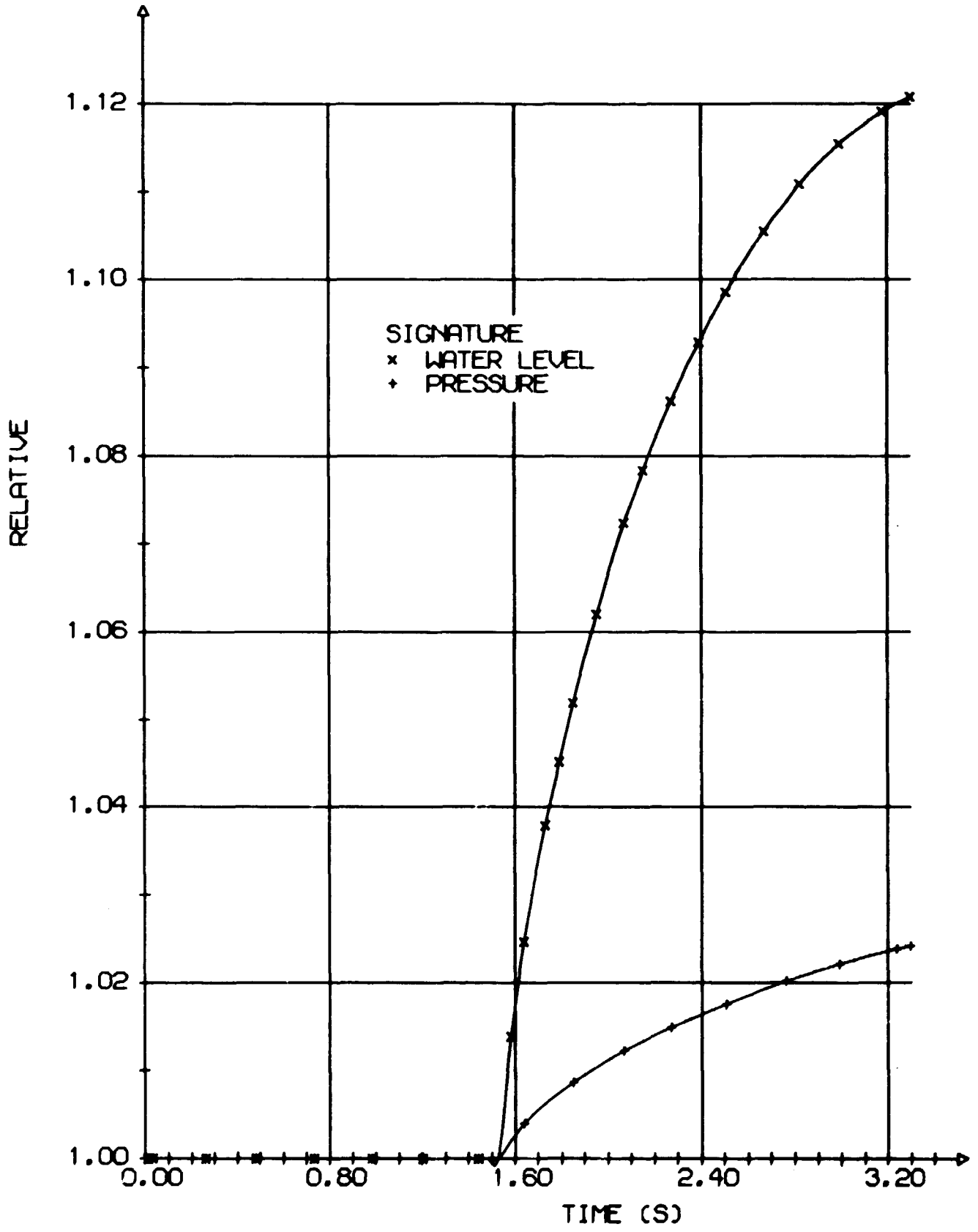

Fig. 6.4.9. Water level and reactor pressure relative to initial value.

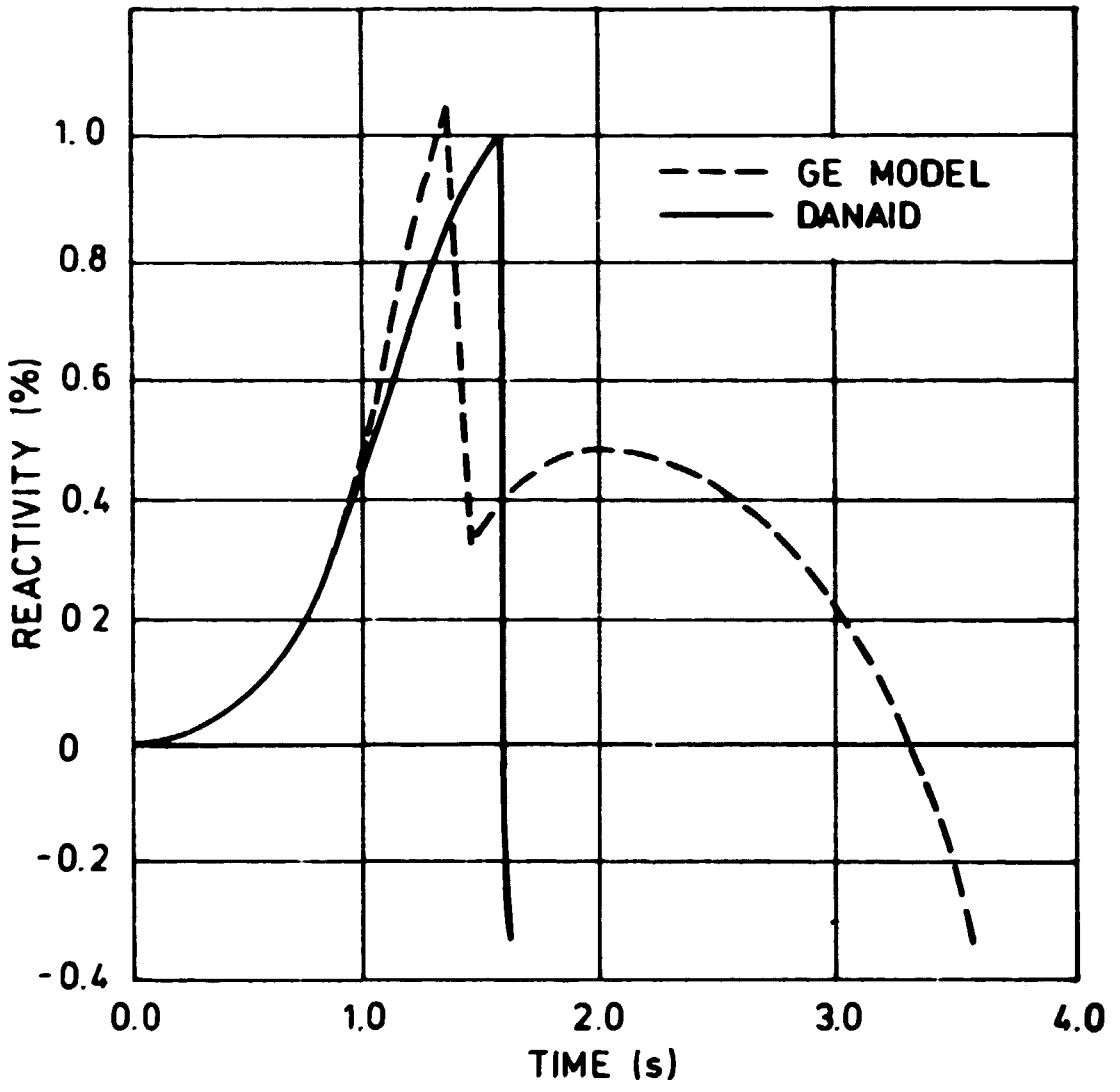

Fig. 6.4.10. Rod drop transient net reactivity. Comparison of DANAID to General Electric model.

the model described above, respectively. The transients are not identical, but they are both applied to large boiling water reactors, and the reactivity insertion rate is not very different in the two cases (slightly lower in the DANAID case). It is seen that the prediction of the power peak is in good agreement, but that the reactor feedback is much stronger in DANAID than in the point model. The difference cannot be explained alone by the lack of

moderator feedback in the GE model, it must also be due to differences in the Doppler reactivity. Because of the weak feedback mechanisms, the GE model predicts much higher fuel peak enthalpies than DANAID does.

It could be interesting to compare DANAID to analyses performed with more detailed reactor models, but as far as I know such results are not published.

6.5. Parameter Studies

The influence of some of the essential parameters was analysed by means of the small core described in section 6.1.

For relating the results of the small core calculations to the large core, a small core analysis was performed with the standard rod ejection characteristics (same rod worth, rod velocity, initial power level, etc.). Figs. 6.5.1 to 6.5.5 show that the most significant difference in the two cores is that the response from the small reactor is approximately 30 ms in advance of the large core response.

As expected, a reduced reactivity worth of the ejected rod results in a slower transient and a smaller power peak, fig. 6.5.6. Another way to decrease the reactivity insertion rate is to reduce the control rod velocity, the same result being obtained, fig. 6.5.7.

Fig. 6.5.8 shows how the hot channel outlet flow depends on the conductivity of the gas gap between the fuel and the cladding. The dependency is very weak, which indicates that it is a good approximation to use an adiabatic fuel model for the power peak calculation, but the direct power deposition in the coolant must be incorporated.

Finally, an analysis was made of a rod ejection transient from an initial power level of 10% of that rated, figs. 6.5.9 and 6.5.10. As expected, the rod ejection accident initiated from the hot start-up power range is the most severe with a peak fuel enthalpy that is twice the value of the transient initiated from 10% of rated power.

Thus the study reveals the dependency of the parameters, which was expected. It could be interesting to see how sensitive the result of the transient is to changes in the Doppler feedback mechanisms and in the coolant evaporation correlations, but such analyses have not yet been performed.

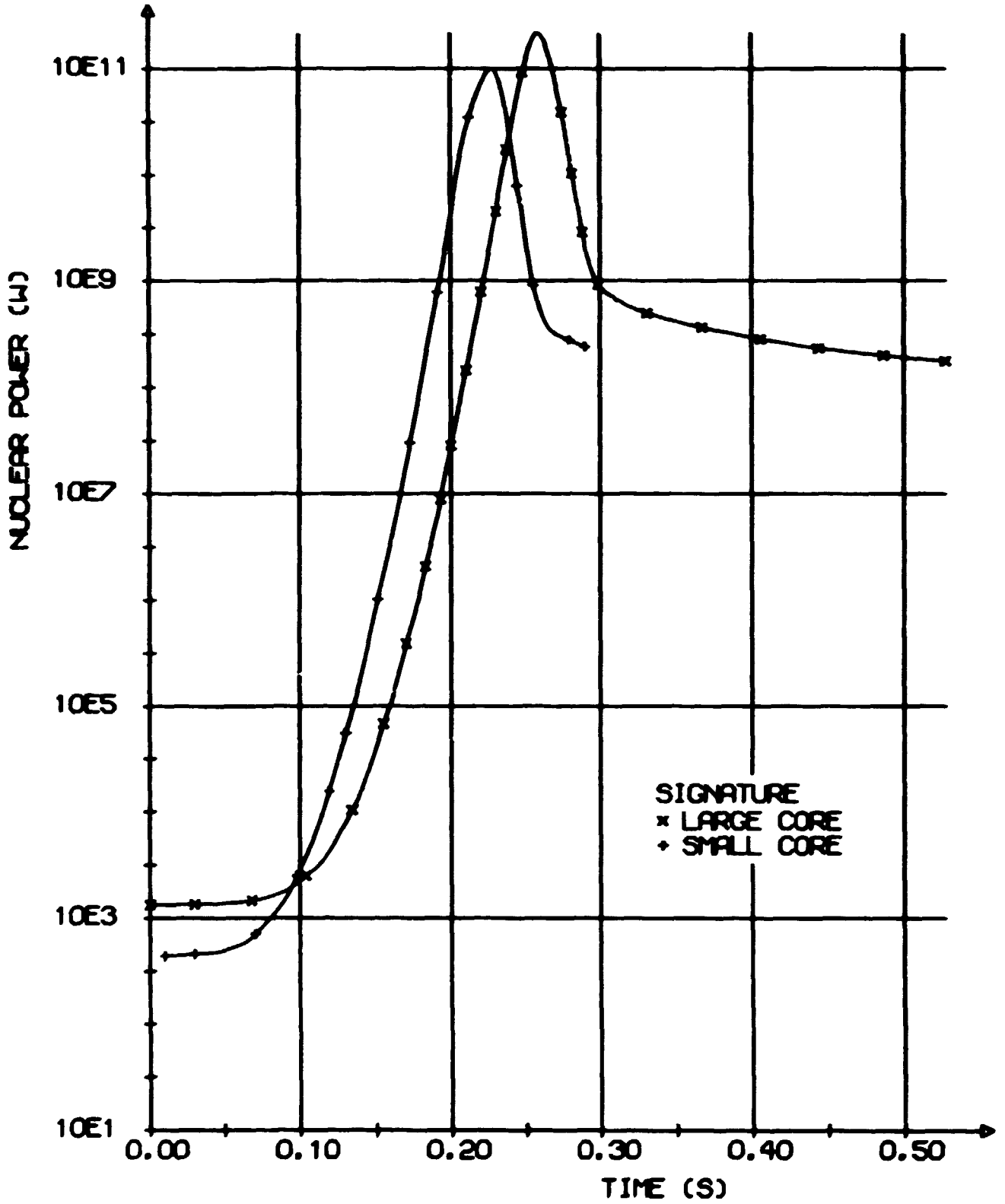

Fig. 6.5.1. Nuclear power production. Comparison of large core to small core.

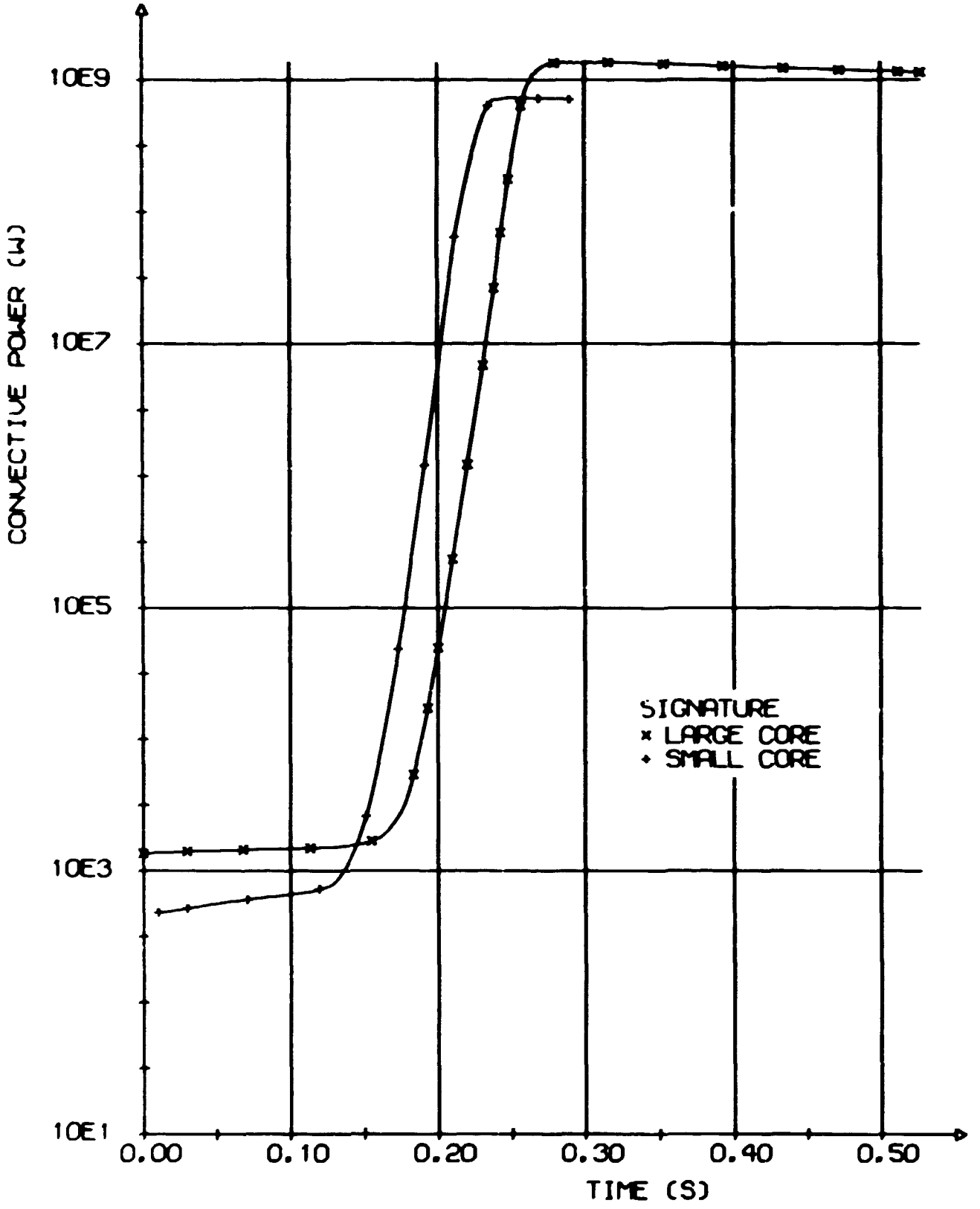

Fig. 6.5.2. Convective power production. Comparison of large core to small core.

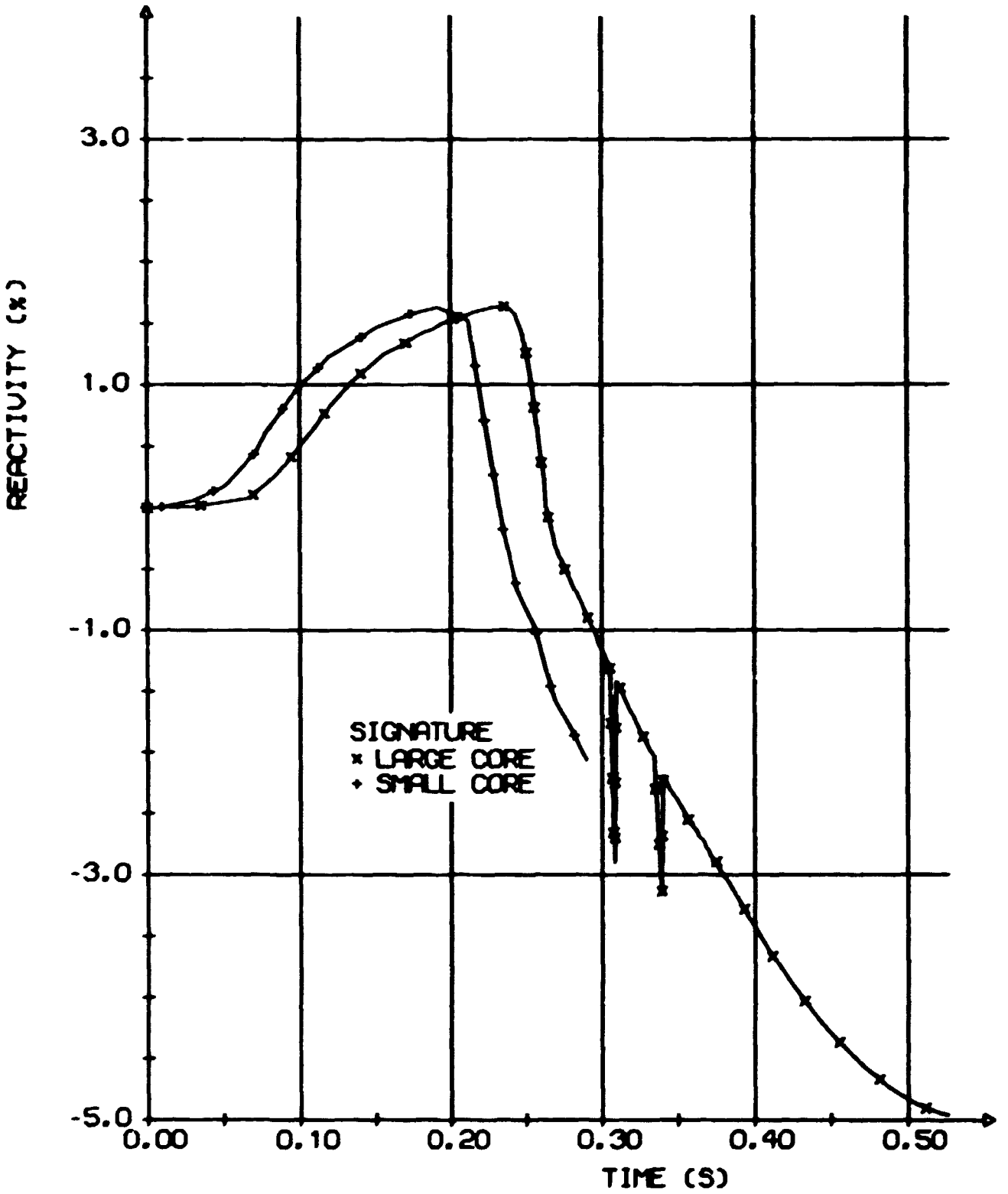

Fig. 6.5.3. Net reactivity. Comparison of large core to small core.

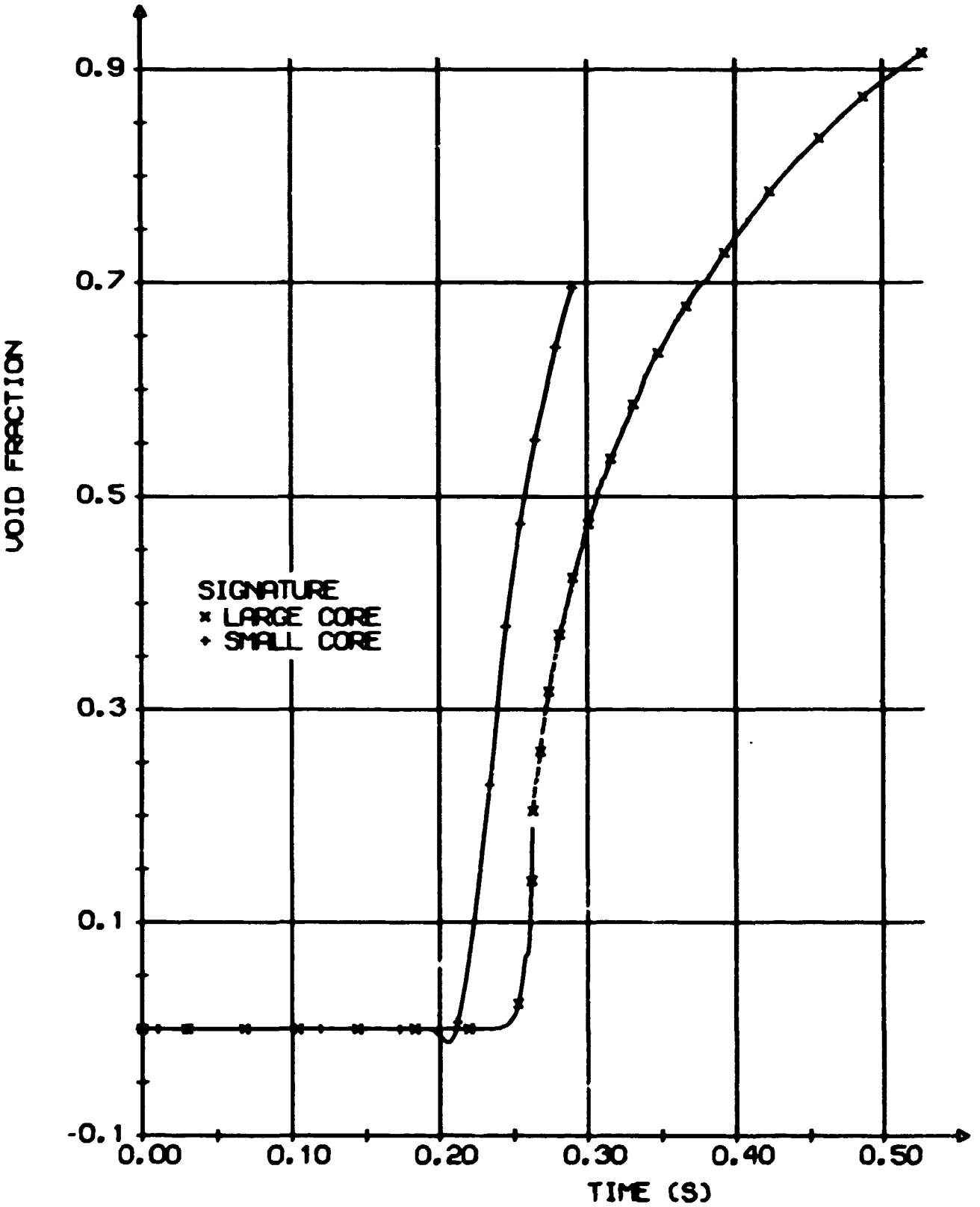

Fig. 6.5.4. Hot channel exit void fraction. Comparison of large core to small core.

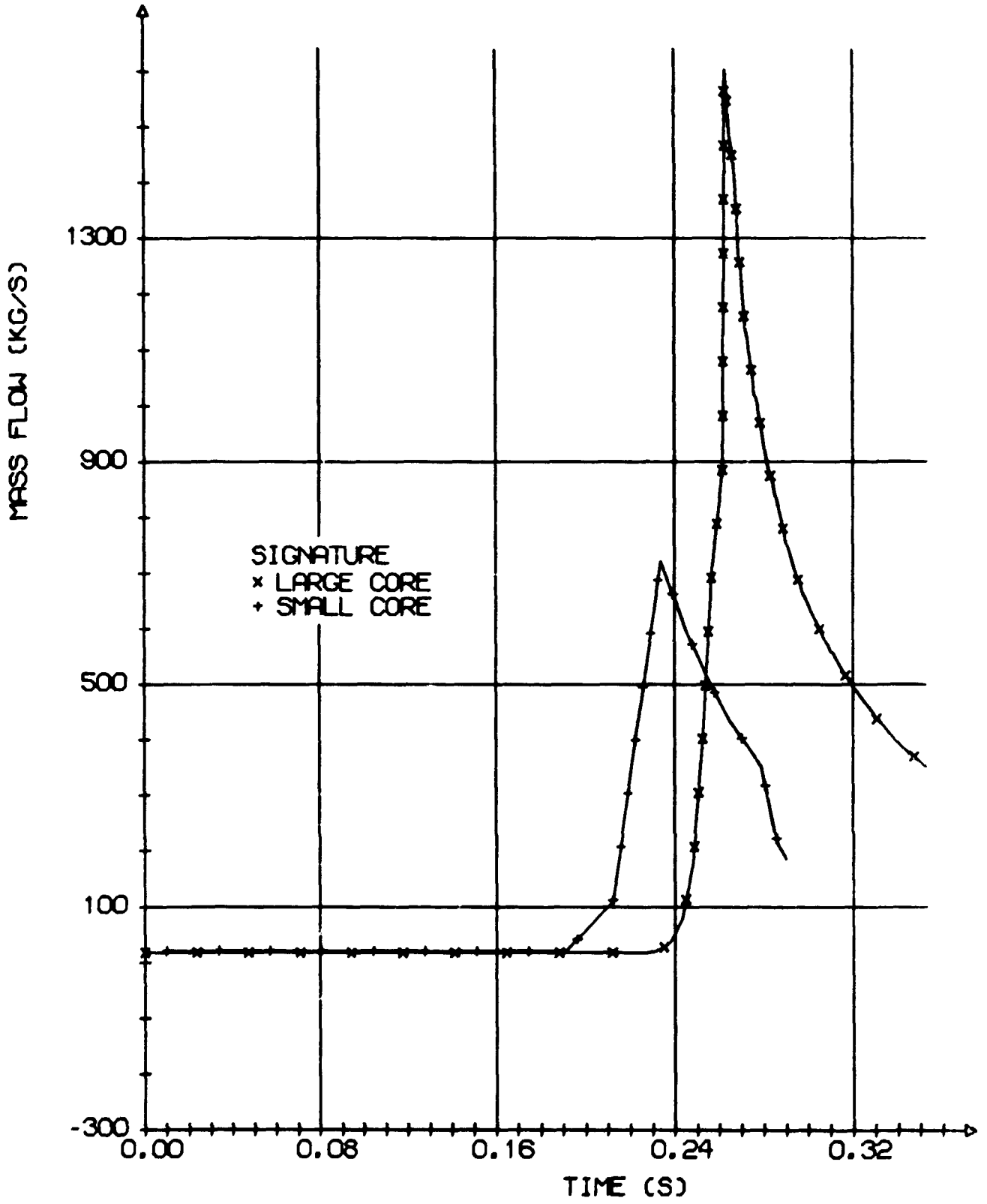

Fig. 6.5.5. Hot channel exit coolant mass flow. Comparison of large core to small core.

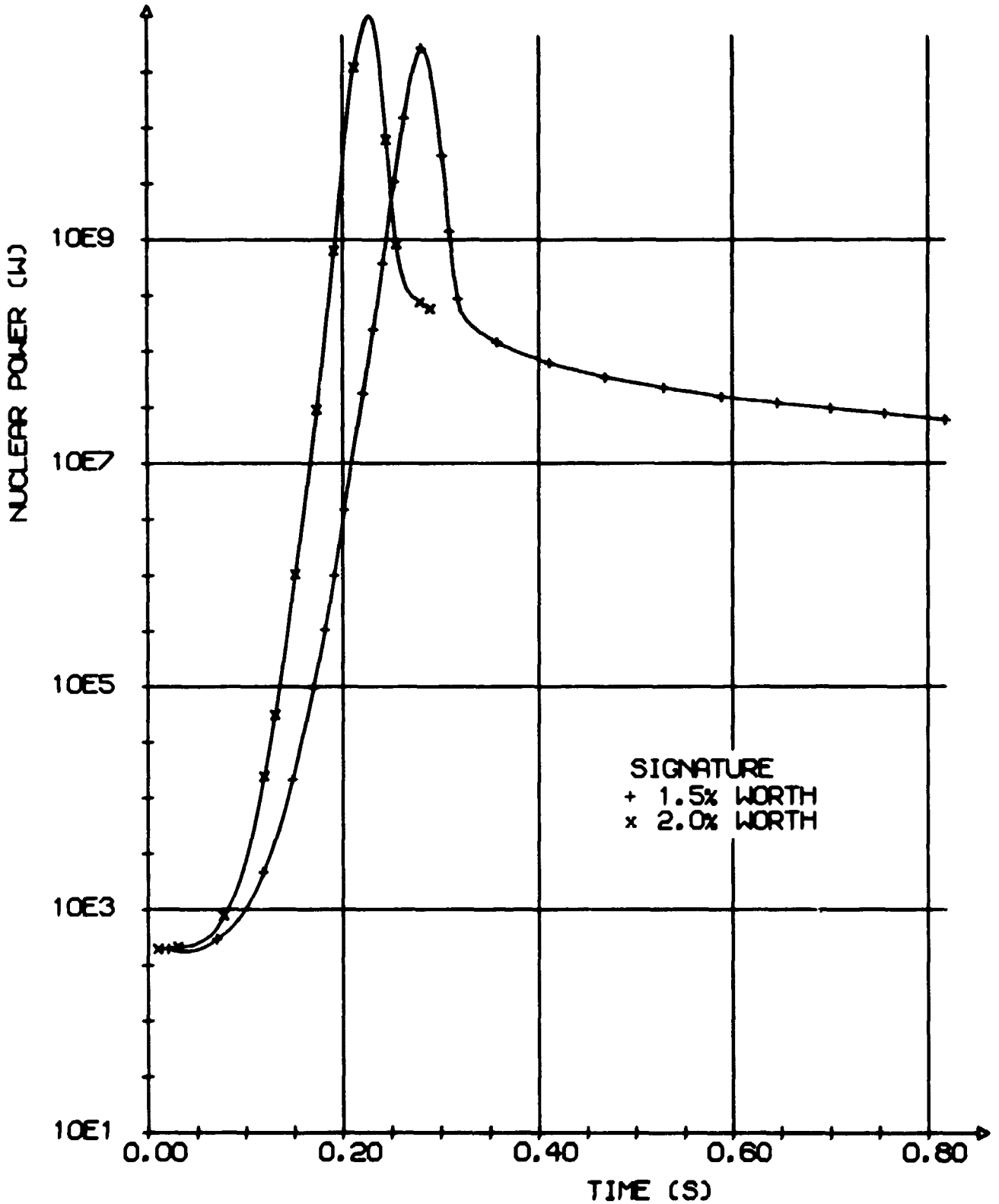

Fig. 6.5.6. Nuclear power production. Dependency on control rod worth.

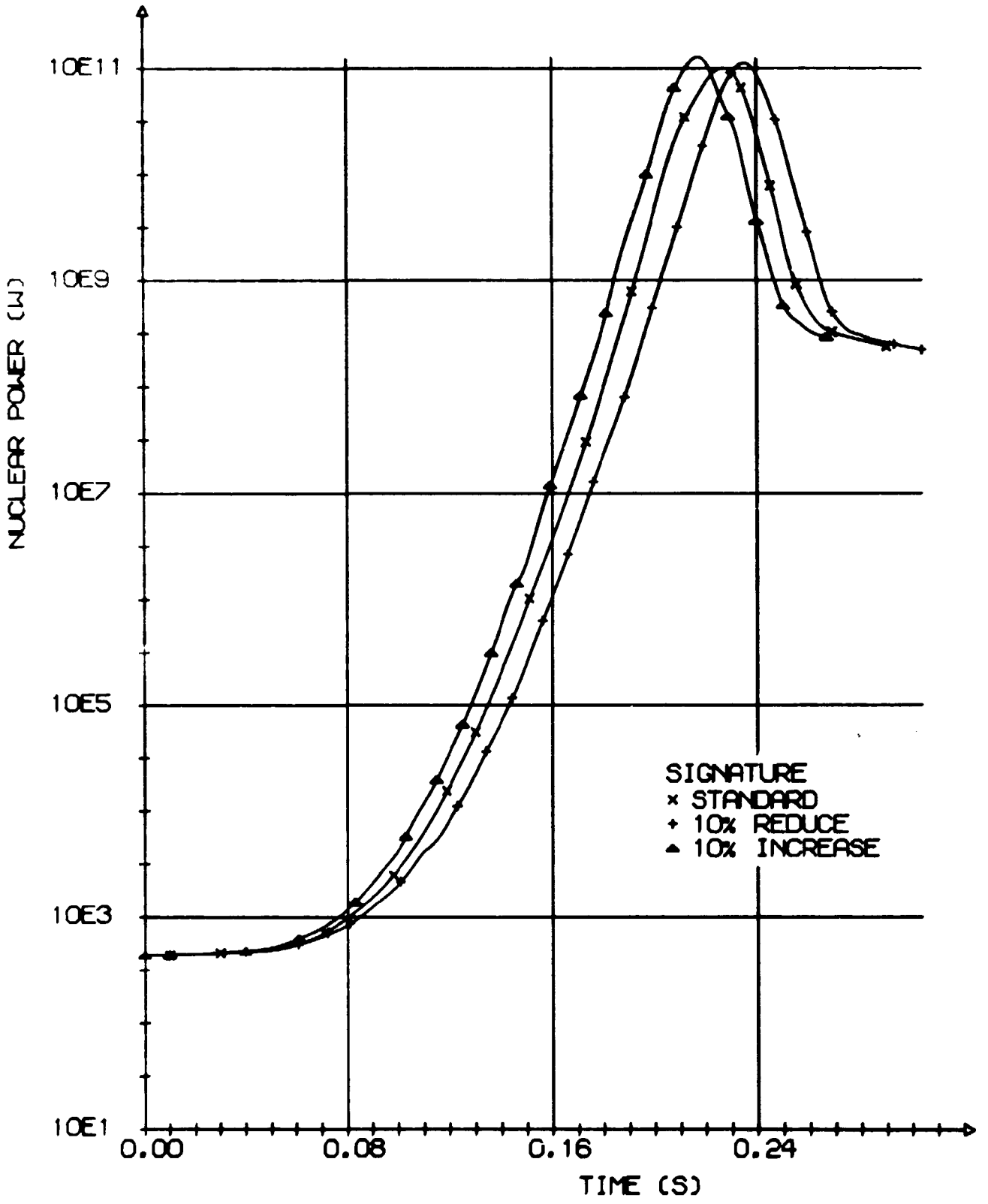

Fig. 6.5.7. Nuclear power production. Dependency on control rod velocity.

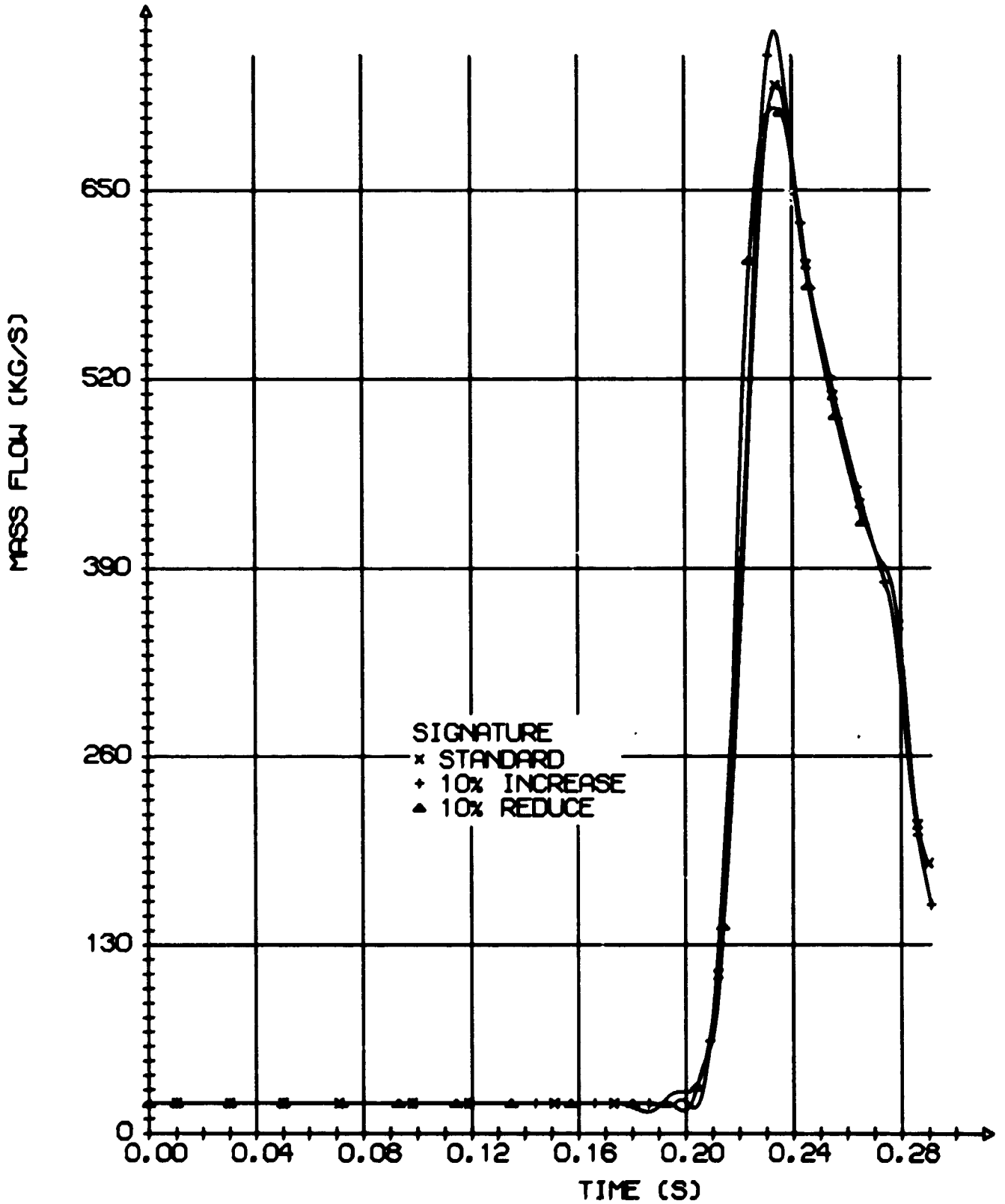

Fig. 6.5.8. Hot channel coolant outlet flow. Dependency on fuel-clad gap conductivity.

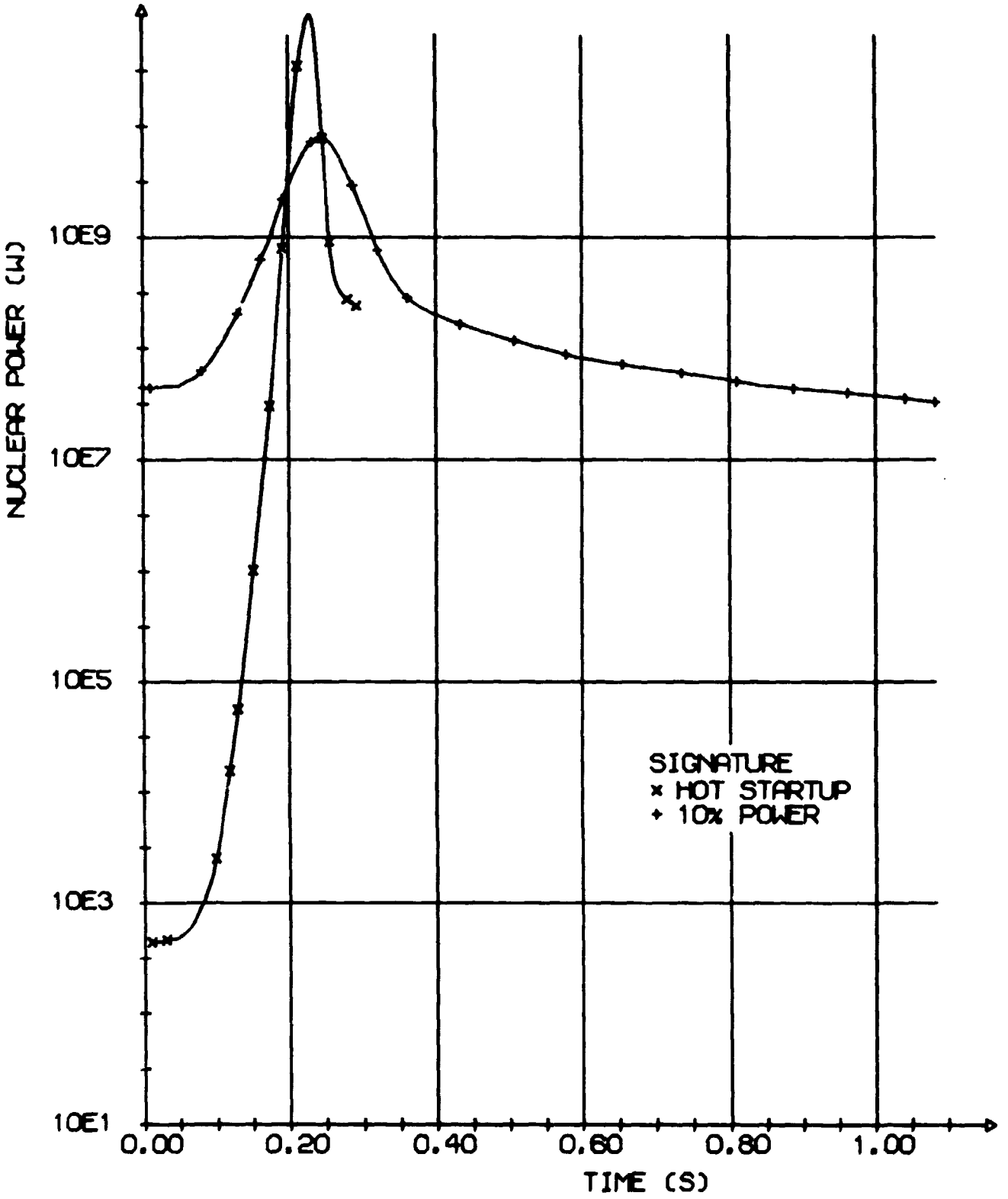

Fig. 6.5.9. Nuclear power production. Dependency on initial power level.

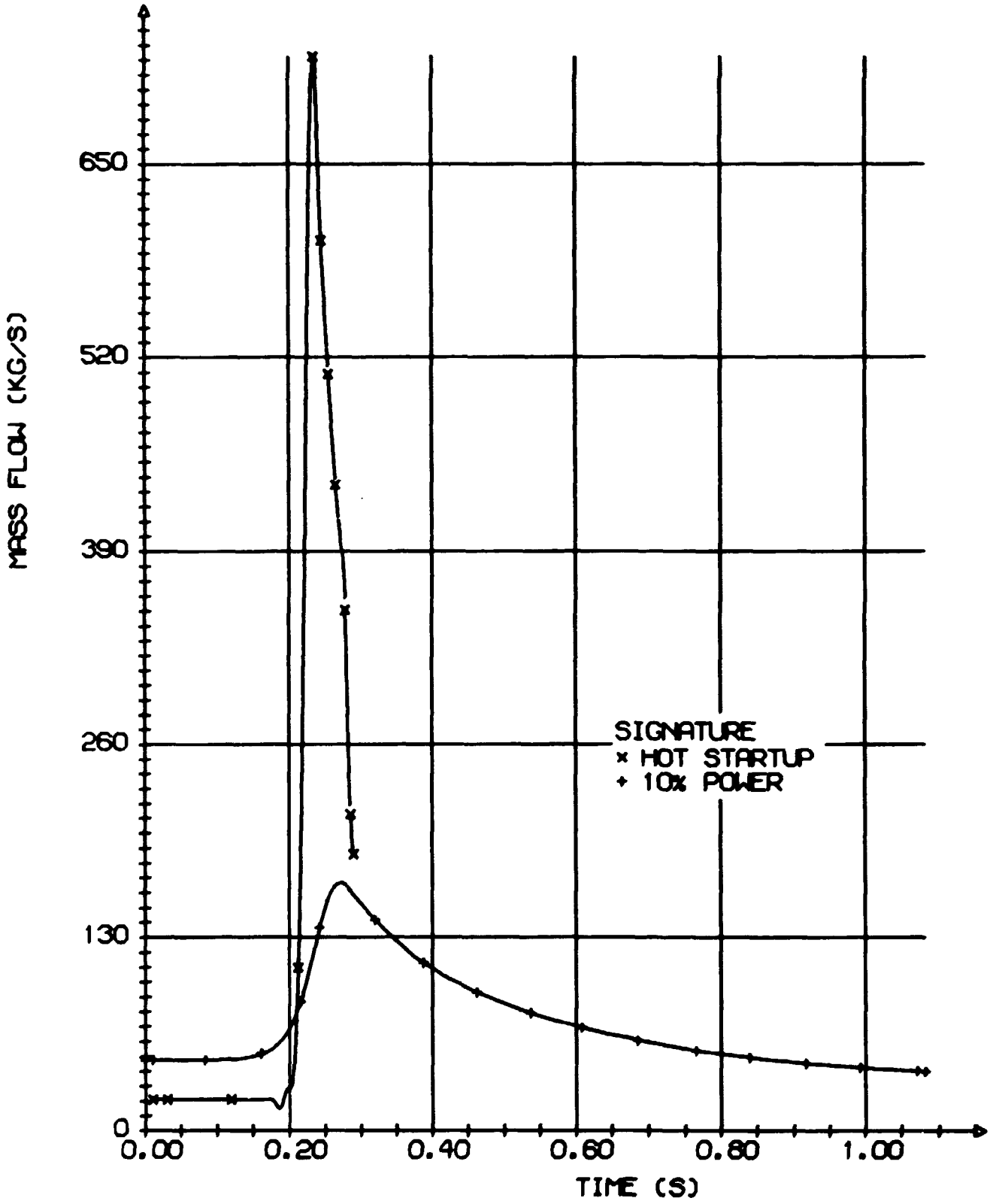

Fig. 6.5.10. Hot channel coolant outlet flow. Dependency on initial power level.

6.6. Conclusion of DANAID Analysis

The conclusion of the transient analysis is that the boiling water reactor is characterized by feedback mechanisms strong enough to slow down nuclear power bursts long before the reactor protection system interacts. The main feedback results from the fuel temperature increase, but because of the direct power deposition in the coolant moderator feedback is essential too.

The calculated maximum fuel enthalpies apply to all transients below the fuel failure thresholds, but for the rod ejection transients burn-out occurs in central channels. This cannot be described by DANAID.

Because of the direct power to the coolant, the coolant mass flow increases rapidly and might be a potential risk for the internals of the core. This cannot be described by DANAID.

The DANAID program is well qualified for transient analysis of nuclear excursions in the range of the rod drop transient analysed here, although a model for the annular flow regime ought to be included. For such transients, the computer time is reasonable.

For power bursts like the rod ejection transients, only the first part of the transient can be described by DANAID. After the power peak the built-in correlations for the cladding to coolant heat transfer do not describe the physical phenomena correctly. It is not a simple task to make DANAID adequate for a complete analysis of such transients. In this case the program should incorporate cladding to coolant interaction models, core spray models, fuel melt models, etc., etc. Furthermore it is not realistic to use DANAID rod ejection for transients in a time scale of more than 0.3-0.4 s because of its poor ratio of real time to computer time.

Thus the last part of a rod ejection transient must be analysed by means of much simpler models.

7. FINAL REACTOR PERFORMANCE

For the rod ejection transient, some of the mathematical models used in DANAID are inadequate to describe the real physical phenomena that occur after the fuel temperature increase. These occurrences should be analysed by a core melt program, but in lack of such a model some simple calculations were performed.

7.1. Fuel Rod Performance

Immediately after the fuel temperature rise occurs in rod ejection transients, the central channel convective heat transfer from the cladding to the coolant is very near the burn-out limit. The critical heat flux[24] is given in fig. 7.1.1 as a function of the coolant mass flux, the pressure and the stagnation steam quality, which is the ratio of steam mass to total coolant mass.

In rod ejection transients the stagnation steam quality is rapidly increased and very soon the burn-out limit is exceeded. When good cooling of the fuel rod is maintained, as it is in the DANAID model throughout the transient, the cladding temperature is not significantly high ($\sim 320^{\circ}C$), but when the loss-of-coolant condition occurs, the fuel temperature distribution within the rod is flattened out and the cladding temperature rapidly increases.

In the radial dimension the temperature distribution within the fuel rod is governed by

$$\rho_F \, C_F \frac{\partial T_F}{\partial t} = \frac{1}{r} \frac{\partial}{\partial r} \left(r k_F \frac{\partial T_F}{\partial r} \right) + q \qquad (7.1.1)$$

where

T_F = fuel temperature
ρ_F = mass density
C_F = specific heat capacity
k_F = heat conductivity
q = power density.

Equation 7.1.1 cannot be solved analytically because of the source term q. However after the power burst the nuclear power is significantly decreased, thus in a first approximation q can be neglected. Furthermore, ρ_F, C_F and k_F are assumed temperature independent. Then eq. 7.1.1 becomes

$$\varkappa \left[\frac{\partial^2 T_F}{\partial r^2} + \frac{1}{r} \frac{\partial T_F}{\partial r} \right] = \frac{\partial T_F}{\partial t} \qquad (7.1.2)$$

with

$$\varkappa = \frac{k_F}{\rho_F C_F} \, . \qquad (7.1.3)$$

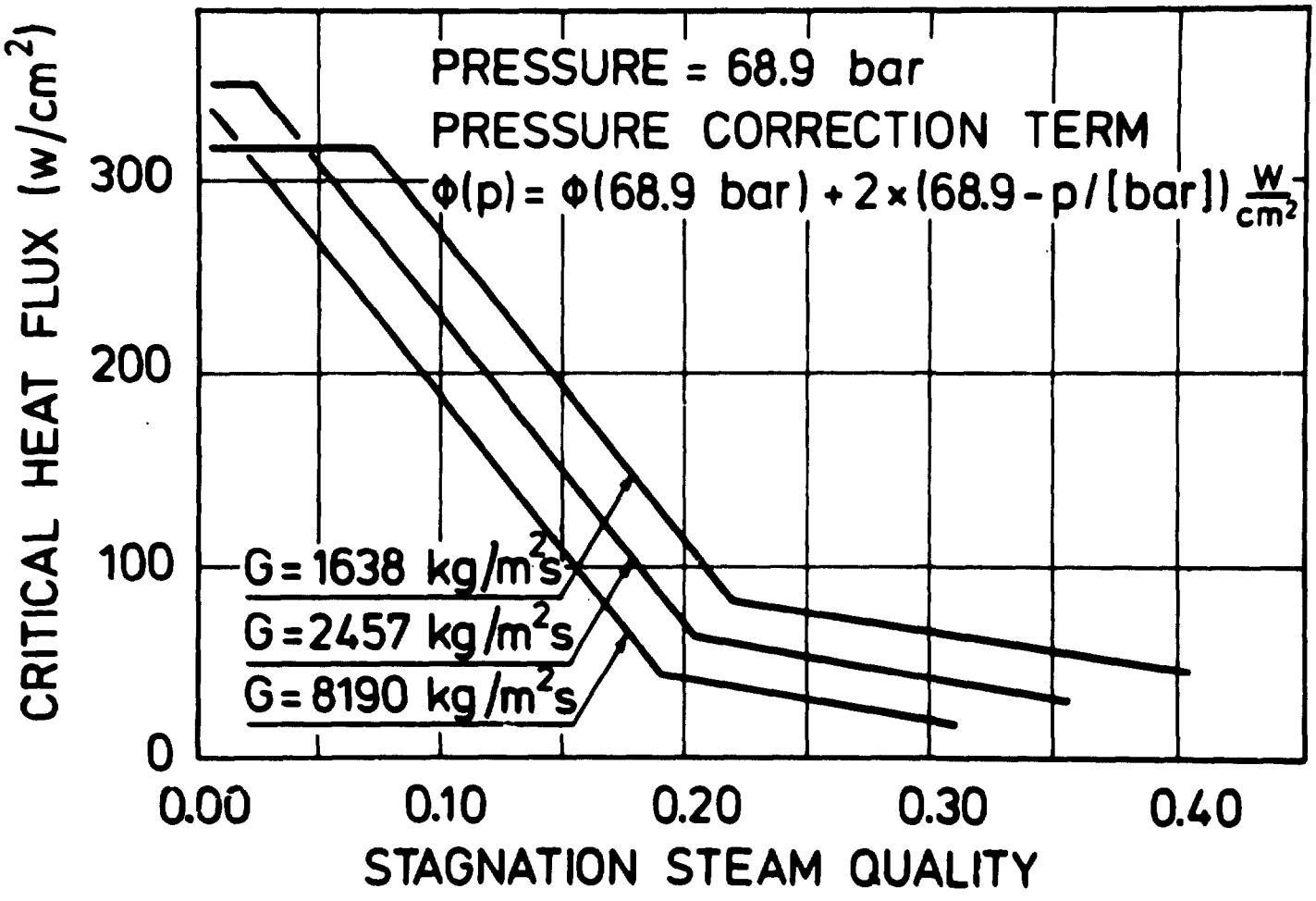

Fig. 7.1.1. Recommended curves of burn out limit.

The most suitable (and simple) boundary condition for a burn-out calculation is the adiabatic condition

$$\left(\frac{\partial T_F}{\partial r}\right)_{r=r_F} = 0 \qquad (7.1.4)$$

where r_F is the radius of the fuel pellet. The full solution to the problem is given in appendix D.

$$T_F(r,t) = \sum_{i=1}^{\infty} A_i \exp\left[-\pi\left(\frac{\lambda_i}{r_F}\right)^2 (t-t_o)\right] J_o\left(\lambda_i \frac{r}{r_F}\right). \qquad (7.1.5)$$

The coefficients A_i must be determined from the temperature distribution to $t=t_o$, where t_o is the time when the good cooling condition is lost. J_o is the Bessel function of first kind and zero order and λ_i, $i = 1, 2 \ldots$ are the roots to the Bessel function of first kind and first order,

$$J_1(\lambda_i) = 0 \qquad i = 1, 2, \ldots \qquad (7.1.6)$$

It is not difficult from eq. 7.1.5 to show that $A_1 = \bar{T}_F$ is the volume average fuel temperature (see appendix D). The average temperature is time independent because power production and heat transfer to the cladding are neglected.

The purpose of the fuel temperature calculation was to estimate the cladding temperature increase after burn-out. When the cladding temperature has been calculated, the change in the average fuel temperature due to power production and heat transmission to the cladding can be expressed as

$$\frac{d\bar{T}_F}{dt} = \frac{Q_F + A_F \Phi_{gap}}{\Omega_F \rho_F C_F}, \qquad (7.1.7)$$

where Q_F is the power production inside the node, A_F is the surface area of the fuel, Φ_{gap} the heat flux to the canning (see below), Ω_F the fuel volume, ρ_F the fuel density, and C_F the specific heat capacity. The actual mean fuel temperature may be inserted in the expression for the canning temperature.

The surface temperature of the fuel pellet is given from eq. 7.1.5.

$$T_{FS}(t) = \sum_{i=1}^{\infty} A_i J_o(\lambda_i) \exp\left[-\pi\left(\frac{\lambda_i}{r_F}\right)^2 (t-t_o)\right] J_o(\lambda_i). \qquad (7.1.8)$$

Using the cladding temperature T_{ca}, the heat flux from the fuel to the cladding, which was neglected above, can be expressed

$$\Phi_{gap}(t) = K_{gap}(T_{FS} - T_{ca}). \qquad (7.1.9)$$

The gap conductivity, K_{gap}, is calculated in DANAID only as a function of the mean fuel temperature, which is constant here (no power production and adiabatic model). The heat transfer from the cladding to the surroundings, mostly the shroud, is governed by radiation[1)]

$$\Phi_{rad}(t) = K_{rad}(T_{ca}^4 - T_o^4) \qquad (7.1.10)$$

T_o is the temperature of the surroundings. The radiation factor K_{rad} is proportional to the radiation interchange factor F, which is calculated assuming the radiating and receiving surfaces are parallel planes; thus

$$F = \left(\frac{1}{\varepsilon_{rad}} + \frac{1}{\varepsilon_{rec}} - 1\right)^{-1} \qquad (7.1.11)$$

where

ε_{rad} = emissivity of the radiating surface

ε_{rec} = emissivity of the receiving surface.

Because of the high mean fuel temperature, the contact area between the fuel pellet and the cladding is large. Thus the heat conductivity from the fuel to the cladding is significant. In combination with the poor heat transfer from the rod to the surroundings, this means that the cladding temperature is largely the same as the fuel surface temperature. Consequently the cladding temperature is substituted with the fuel surface temperature in the expression for Φ_{rad}.

The energy balance for the cladding becomes

$$d\,\rho_{ca}\,C_{ca}\,\frac{dT_{ca}}{dt} = \Phi_{gap} - \Phi_{rad} \qquad (7.1.12)$$

where

d = the thickness of the cladding

ρ_{ca} = the cladding density

C_{ca} = the specific heat of the cladding.

Assuming d, ρ_{ca} and C_{ca} constant, and using only the first two terms in the expression for T_{FS}, the solution to eq. 7.1.12 is

$$T_{ca}(t) = \bar{T}_F - \frac{k_{rad}}{k_{gap}} (\bar{T}_{FS}^4 - T_o^4) + \Delta e^{-\alpha(t-t_o)} \qquad (7.1.13)$$

with

$$\Delta = T_{FS}(t_o) - \bar{T}_F(t_o)$$

$$\alpha = \pi \left(\frac{\lambda_2}{r_F}\right)^2$$

$$k_{gap} = \frac{K_{gap}}{d\rho_{ca}C_{ca}}$$

$$k_{rad} = \frac{K_{rad}}{d\rho_{ca}C_{ca}}$$

In the evaluation of 7.1.13 the fact that $\alpha \ll k_{gap}$ has been used. The cladding temperature as a function of $t-t_o$ is given in table 7.1.1.

Table 7.1.1

Hot Region Cladding Temperature as a Function of Time Since Burn-out Set Point

$t-t_o$ s	T_{ca} °C
0	318
1	615
2	820
3	960
4	1057
5	1124

For rewetting of the fuel rod, the canning temperature should not exceed the temperature threshold T_{wet} given by

$$\frac{T_{wet}}{T_{crit}} = 0.13 \frac{p}{p_{crit}} + 0.84, \qquad (7.1.14)$$

where p, p_{crit}, and T_{crit} are the actual pressure (N/m^2), the critical pressure (N/m^2), and the temperature (^oC) at the critical point, respectively. The value of T_{wet} is approximately 330°C, which is exceeded by the cladding temperature long before the channel is refilled with fluid. However, if the cladding temperature is below the so-called sputtering temperature, T_{sp}, some cooling can be established. The sputtering temperature is a function of the coolant saturation temperature, T_s (^oC), and the actual pressure (N/m^2)

$$(T_{sp} - T_{sat})^{-1} = 9.0945 \cdot 10^{-4} + 3.6963 \cdot 10^{3} p^{-1}. \qquad (7.1.15)$$

The approximate value of T_{sp} is 990°C, but even this high temperature is believed to be exceeded by the cladding temperature before good cooling conditions can be re-established.

An accepted threshold for the cladding to perferate is at an oxidation of 17% by weight. This threshold is exceeded by the fuel rods in the hot channel.

Not only channel 1 in fig. 6.1.1 is voided, but also channel 2 that contains 16 fuel boxes. The maximum average fuel temperature in this channel is not as high (1050°C) as in channel 1. However, the power shape inside this channel is very skewed, consequently the fuel temperature in the fuel boxes nearest to the central channel is high (maximum average temperature of 1100°C) and these rods will probably fail too. Additionally, some rods inside the outer boxes of channel 2 are believed to perforate.

Thus it is estimated that radioactivity originating from 800-1200 fuel rods will be released into the coolant.

8. CONCLUSION

The rapid removal of a high worth control rod from an initially critical boiling water reactor has been analysed. The power burst is terminated by the built-in feedback mechanisms. The Doppler effect is especially strong, but because of the direct power deposition in the moderator, resulting from the neutron slow-down power, the moderator feedback is also significant and rapid.

Removal of a 2% $\Delta k/k$ rod with a velocity corresponding to the maximum drop velocity of a General Electric control rod should not result in any significant damage to the reactor system.

The rod ejection accident that has most potential consequences is initiated from the hot start-up condition. The result of this transient is high fuel temperatures, but the maximum fuel enthalpy is far from the fracture threshold. However, the central channels are voided and the radioactivity from 800-1200 fuel rods will be released to the coolant. A significant amount of energy is transmitted to the coolant, but the potential damage resulting from this effect has not yet been examined in detail. However it is estimated that the reactor vessel will not be destroyed.

9. ACKNOWLEDGEMENTS

I am indebted to P. Skjerk Christensen, Research Establishment Risø, for much help in both theoretical and practical matters, and to Alex Jensen, also from Risø, for assistance in solving computer problems.

APPENDIX A

Thermodynamic Functions

The thermodynamic functions given in chapter 5.3 are based on some reference quantities calculated as rational functions of either the reference temperature or the reference pressure.

The rational functions are of the general type

$$Y_{ji}(X) = \frac{\sum_{k=1}^{i} a_{ki} X^{j-k}}{\sum_{k=1}^{j} a_{j+ki} X^{j-k}} ,$$

where i is the item of the particular function in the calculation scheme, table A-1, and 2j the number of coefficients used for that function; j must be either 3 or 6 depending on i. In the program the functions are calculated as

$$Y_{ji}(X) = \text{H20APP}(X, 2j, i)$$

where H20APP is the Fortran function listed at the end of this appendix. The coefficients are aggregated in the block data subroutine also listed in this appendix. For evaluation of the coefficients, the Fortran program H20TP[21] from the Risø code complex was taken as base. H20TP calculates the thermodynamic functions according to the same principles as used in[17] and the coefficients were fitted with the program LSFIT[18]. Compared to steam tables[17], the accuracy of the pressure-dependent functions is better than 1 o/oo for pressures in the range of 1 to 100 bar. The accuracy of expressions 5.3.8 and 5.3.9 for ρ_f and h_f, respectively, is better than 1 o/oo for pressures in the range of 2 to 100 bar and subcoolings down to 100°C, when the reference temperature was chosen to be 20°C above the actual temperature, and better than 5 o/oo in the pressure range 1 to 140 bar with the same subcooling.

Table A-1

Identification number for thermodynamic functions

Function Symbol	Identification Number	Number of Coefficients
ρ_f	1	12
p_s	2	12
h_f	3	12
T_s	4	12
h_{fg}	5	12
ρ_g	6	12
η_f	7	12
λ_f	8	12
$\frac{\partial \rho_f}{\partial p}$	1	6
$\frac{\partial h_f}{\partial p}$	2	6
$\frac{\partial \rho_f}{\partial T}$	3	6
$\frac{\partial p_s}{\partial T}$	4	6
$\frac{\partial h_f}{\partial T}$	5	6
$\frac{\partial^2 \rho_f}{\partial T^2}$	6	6
$\frac{\partial^2 h_f}{\partial T^2}$	7	6
$\frac{\partial T_s}{\partial p}$	8	6
$\frac{\partial h_{fg}}{\partial p}$	9	6
$\frac{\partial \rho_g}{\partial p}$	10	6
$\frac{\partial \eta_f}{\partial p}$	11	6
$\frac{\partial \lambda_f}{\partial p}$	12	6

```
      FUNCTION H2OAPP(X,N,IFUNK)
C     CALCULATES THERMODYNAMIC FUNCTIONS OF WATER AND STEAM
C     INPUT QUANTITIES:
C     X              INDEPENDENT VARIABLE (EITHER TEMPERATURE/[DEG.C]
C                                          OR     PRESSURE/[N/M**2])
C     N              NUMBER OF COEFFICIENTS IN FUNCTION EXPRESSION (6/12)
C     IFUNK          FUNCTION NUMBER IN DATA BLOCK
      COMMON/H2O     / H2O1(12,8),H2O2(6,12)
      NHALF=N/2
      IF(N.EQ.12) GOTO 1000
      DO 500 I=1,3
      COUNT=COUNT*X + H2O2(I,IFUNK)
      DENOM=DENOM*X + H2O2(I+NHALF,IFUNK)
  500 CONTINUE
      H2OAPP=COUNT/DENOM
      RETURN

 1000 CONTINUE
      DO 1500 I=1,6
      COUNT=COUNT*X + H2O1(I,IFUNK)
      DENOM=DENOM*X + H2O1(I+NHALF,IFUNK)
 1500 CONTINUE
      H2OAPP=COUNT/DENOM
      RETURN
      END
```

```
      BLOCK DATA
      COMMON/H2O   / H2O1(12,8),H2O2(6,12)
      DATA((H2O1(I,J),I=1,12),J=1, 8)/
CC     TEMPERATURE DEPENDENT FUNCTIONS WITH 12 COEFFICIENTS
CC                COEFFICIENTS FOR ROFS
     1  -.2556071821446-13,  -.3207664673396-11,   .3207142469646-05,     ROFS
     2  -.2145707648746-02,   .1190637682466+00,   .8893358834726+02,     ROFS
     3  -.1121402149746-15,   .1757239139836-11,  -.1064784833526-08,     ROFS
     4  -.1570257993646-05,   .1164261284756-03,   .8902000000006-01,     ROFS
CC                COEFFICIENTS FOR PSAT
     1   .1585011047056-06,  -.1518383566806-06,  -.1234847188806-03,     PSAT
     2   .3458671336406-01,  -.3550722832866+01,   .1331828090566+03,     PSAT
     3  -.3989184013326-16,   .1759502673566-13,   .2783052285406-11,     PSAT
     4  -.5572996818086-09,   .3615572889166-06,   .2781299233346-03,     PSAT
CC                COEFFICIENTS FOR HSAT
     1  -.1068066001326-09,  -.8929706248486-08,  -.3674753065386-05,     HSAT
     2  -.4205117322026-03,   .5163224588556+01,  -.1864731652086+01,     HSAT
     3   .6374649005846-17,  -.2057624597646-13,  -.6894875972006-11,     HSAT
     4  -.8281928787206-09,  -.3954084765516-07,   .1225338701476-02,     HSAT
CC     PRESSURE  DEPENDENT FUNCTIONS WITH 12 COEFFICIENTS
CC                COEFFICIENTS FOR TSAT
     1   .2815897194176-33,   .4314169114316-26,   .5212332040796-20,     TSAT
     2   .5270175281776-15,   .2889541762836-11,  -.1947113553756-08,     TSAT
     3   .5063007544086-36,   .1607123559656-28,   .3421159316856-22,     TSAT
     4   .6601841298486-17,   .1060637451096-12,   .1012436809196-09,     TSAT
CC                COEFFICIENTS FOR HFG
     1   .1043444366486-32,  -.2664278064346-25,  -.1264148682246-19,     HFG
     2   .7025654474086-11,  -.1145205169576-03,   .1755454052866+04,     HFG
     3   .3024251982226-43,   .2361198102176-36,  -.2649820691296-30,     HFG
     4  -.6392260126166-22,  -.1665106638996-14,   .8151759952646-03,     HFG
CC                COEFFICIENTS FOR ROG
     1   .4199377710456-35,  -.1011287963846-27,   .1751093565466-20,     ROG
     2   .5414898908706-15,   .7889737591846-06,   .6614480387926-01,     ROG
     3  -.9442972999286-42,  -.1076193884296-34,  -.9577530783846-28,     ROG
     4  -.2784281614986-21,   .1352952828916-13,   .1654553578636+00,     ROG
CC                COEFFICIENTS FOR ETHA
     1   .5666542196246-37,  -.1515108174616-29,   .1700964829596-24,     ETHA
     2   .3014713163956-15,  -.3054228198836-08,   .1887997925366-01,     ETHA
     3  -.3856218201136-38,   .3380913244516-31,   .1267655348756-23,     ETHA
     4   .1243073187996-16,  -.2353479833206-09,   .1036760416066+03,     ETHA
CC                COEFFICIENTS FOR WCOND
     1  -.7166315258906-36,  -.3094635277746-28,   .4766697790056-21,     WCOND
     2  -.2818532536836-14,  -.1237981410776-07,   .6882851920006+00,     WCOND
     3  -.4496249087756-42,  -.1105602276116-34,  -.7203979219046-27,     WCOND
     4  -.2841610002896-19,  -.7824107627126-12,   .9999990610086+00/     WCOND
```

```
      DATA((H2O2(I,J),I=1, 6),J=1,12)/
CC     TEMPERATURE DEPENDENT FUNCTIONS WITH  6 COEFFICIENTS
CC                COEFFICIENTS FOR DRODDP
     1    .8086167446 32E-08,    .128941034049E-07,   .1715987C8452E-03,      DRODDP
     2   -.1919833217 18E-01,    .706477096248E+01,  -.326936782877E-04,      DRODDP
CC                COEFFICIENTS FOR DHDP
     1    .2977619184 74E-05,   -.237852761225E-02,   .406272138014E+00,      DHDP
     2    .2675464142 78E-02,   -.224022945140E+00,   .462837603975E+03,      DHDP
CC                COEFFICIENTS FOR DRODDT
     1    .1560164759 12E-04,   -.753754795232E-02,  -.353150948321E+00,      DRODDT
     2   -.1112560755 42E-04,    .858089642936E-03,   .135570513537E+01,      DRODDT
CC                COEFFICIENTS FOR DPDT
     1    .1069946075 92E-01,   -.225066080164E+01,   .120022686052E+03,      DPDT
     2   -.6735076458 24E-07,    .383565245512E-04,  -.202569071169E-02,      DPDT
CC                COEFFICIENTS FOR DHDT
     1   -.1440921544 62E-02,    .646149923408E+00,   .185642763947E+01,      DHDT
     2   -.4212598931 18E-06,    .165762535841E-03,  -.156225344954E-04,      DHDT
CC                COEFFICIENTS FOR D2RFDT
     1   -.2097737305 76E-05,    .527554673180E-03,  -.925173277 12CE-01,     D2RFDT
     2   -.3221968672 84E-03,    .972394641112E-01,   .715811077672E+01,      D2RFDT
CC                COEFFICIENTS FOR D2HDT2
     1   -.2702313079 32E-05,    .124950173760E-01,  -.106200303671E+00,      D2HDT2
     2    .4347049166 97E-05,   -.522030293149E-02,   .132723583953E+01,      D2HDT2
CC     PRESSURE     DEPENDENT FUNCTIONS WITH  6 COEFFICIENTS
CC                COEFFICIENTS FOR DTDP
     1   -.2468799921 57E-17,    .384972003647E-09,   .632593320326E-03,      DTDP
     2    .3256630163 67E-11,    .247542995746E-04,  -.364177712315E+00,      DTDP
CC                COEFFICIENTS FOR DHFGDP
     1   -.1575038525 79E-14,    .747017662384E-08,  -.407152282892E+00,      DHFGDP
     2   -.7639260568 96E-13,    .982789958664E-06,   .108214782775E+01,      DHFGDP
CC                COEFFICIENTS FOR DRDGDP
     1   -.4108621324 22E-17,    .370942022916E-09,   .170918419259E-04,      DRDGDP
     2   -.3581660276 28E-11,    .842042084688E-04,   .376883899407E+00,      DRDGDP
CC                COEFFICIENTS FOR DETHDP
     1   -.7408638064 08E-19,    .149647132332E-11,  -.852903265768E-05,      DETHDP
     2   -.3036864110 61E-08,    .105650650782E+00,   .308798739719E+04,      DETHDP
CC                COEFFICIENTS FOR DWCCDP
     1    .7086837124 88E-18,   -.250479538533E-10,  -.104187349740E-04,      DWCCDP
     2    .5575200030 08E-11,    .105837572907E-02,  -.255251233415E+01/     DWCCDP
      END
```

APPENDIX B

Control Rod Ejection Times

In eq. 4.3.22 the control rod velocity during a rod ejection accident is given as

$$u = \begin{cases} u_o - u_1 \, tg \, (\frac{t_o - t}{\tau_1}) & t \leq t_o \\ u_o + u_2 \, tgh \, (\frac{t - t_o}{\tau_2}) & t > t_o \end{cases} \qquad (B.1)$$

where the quantities u_o, u_1, u_2, τ_1, τ_2, and t_o are defined through eqs. 4.3.11, 4.3.14, 4.3.15, 4.3.16, 4.3.17, and 4.3.23, respectively. By integration of u an implicite expression for the control rod removal time, t_{rem}, can be found

$$l = u_o t_{rem} + u_1 \tau_1 \ln \cos (\frac{t_o}{\tau_1}) + u_2 \tau_2 \ln \cosh (\frac{t_{rem} - t_o}{\tau_2}) \qquad (B.2)$$

where l is the removal distance, i.e. the height of the core.

To find an explicit expression for t_{rem}, some approximations must be made. Using

$$w_{leak} \propto (\rho \Delta p)^{1/2}, \qquad (B.3)$$

with ρ as the coolant density and Δp as the difference between the reactor vessel pressure and the containment pressure, the velocity dependency of ρ and Δp becomes

$$u_i \propto (\Delta p / \rho)^{1/2} \qquad i = 0, 1, 2 \qquad (B.4)$$

The time constant varies as

$$\tau_i \propto (\rho \Delta p)^{-1/2} \qquad i = 1, 2 \qquad (B.5)$$

and the time for initiation of relative flow reversal in the velocity limiter section

$$t_o = \tau_1 \, Arc \, tg \, (\frac{u_o}{u_1}) \propto (\rho \Delta p)^{-1/2}. \qquad (B.6)$$

The maximum theoretical control rod velocity during the ejection is $u_o + u_2$, thus a lower limit on the removal time is

$$t_{rem} > t_{min} = \frac{1}{u_o + u_2} , \tag{B.7}$$

and consequently

$$\frac{t_{rem} - t_o}{\tau_2} > \frac{t_{min}}{\tau_2} - \frac{t_o}{\tau_2} . \tag{B.8}$$

The right-hand side of (B.8) does not significantly depend on Δp. The ratio t_o/τ_2 is unaffected by changes in ρ too, while t_{min}/τ_2 increases linearly with ρ. Thus a lower limit on $(t_{min} - t_o)/\tau_2$ is 8.3, which is obtained in the hot start-up condition. Then it is a good approximation to use

$$\cosh\left(\frac{t_{rem} - t_o}{\tau_2}\right) = \frac{1}{2} \exp\left(\frac{t_{rem} - t_o}{\tau_2}\right) \tag{B.9}$$

and t_{rem} can be expressed explicitly as

$$t_{rem} = \frac{1 + u_2 \tau_2 \ln 2 + u_2 t_o - u_1 \tau_1 \ln \cos\left(\frac{t_o}{\tau_1}\right)}{u_o + u_2} . \tag{B.10}$$

In the nominator of (B.10) the term 1 overrides the others, thus

$$t_{rem} = t^o_{rem} \left(\frac{\Delta p_o}{\Delta p} \cdot \frac{\rho}{\rho_o}\right)^{1/2} , \tag{B.11}$$

where t^o_{rem}, $\Delta\rho_o$, and ρ_o refer to a reactor intially in the hot start-up range.

At low power no steam is removed from the vessel and no feed water is injected, the reactor coolant is thus isolated and the temperature distribution within the vessel is nearly uniform at the saturated level. Using this in eq. (B.11), the removal time becomes

$$t_{rem} = t^o_{rem} \left(\frac{p_s(\rho_o) - p_{con}}{p_s(\rho) - p_{con}} \cdot \frac{\rho}{\rho_o}\right)^{1/2} \tag{B.12}$$

where $p_s(\rho)$ is the pressure of saturated water with the density ρ, and p_{con} is the containment pressure.

Equation (B.12) expresses the control rod removal time in rod ejection accidents initiated from a reactor at low power. The removal time is a function of the coolant density only.

APPENDIX C

Sensitivity of the Fuel Temperature to Changes in the Heat Capacity

(A point kinetic approximation)

The main disadvantage of using a constant fuel heat capacity in the analysis of rapid and highly peaked transients is probably that the capacity must be averaged over a temperature range that is, of course, unknown before the calculation. When one computer run has been performed, a better choice of heat capacity can be made and a new run initiated with the corrected value. Such an iterative procedure would result in a correct solution to the problem. However, three-dimensional dynamic reactor calculations are expensive, and it would be satisfactory if it was possible in a simple way to get some idea of the error introduced by choosing an incorrect heat capacity.

In this appendix a simple method for correction of the final fuel temperature is evaluated. The method is based on point kinetics and is probably not very accurate, but if used in the way described below it is believed to show the sensitivity of the final fuel temperature to changes in the heat capacity.

The point kinetic equations are

$$\frac{d\Phi}{dt} = \frac{\rho - \beta}{\tau}\Phi + \sum_{i=1}^{N} \lambda_i C_i \qquad (C.1)$$

where

Φ = power production
ρ = reactivity
τ = neutron lifetime
β_i = delayed neutron fraction, $\beta = \sum_{i=1}^{N} \beta_i$
λ_i = decay constant
C_i = precursor density
N = number of delayed groups.

In the point model the power shape is time independent and therefore Φ and C_i can freely be chosen to represent either the whole reactor, or a specific part of it.

In DANAID the precursors are not updated in the dynamical part and,

because the initial power level is very low, this is approximately the same as totally neglecting the delayed neutrons. C_i can then be omitted from (C.1).

According to chapter 6.3, the reactivity in the peak power range is nearly a linear time-dependent function

$$\rho = \rho_o + \dot{\rho}_o(t-t_o) \tag{C.3}$$

with $\dot{\rho}_o$ as the constant (negative) slope of the reactivity curve.

Now, eq. (C.1) has the solution

$$\Phi(t) = \Phi_o \exp\left[\frac{\dot{\rho}_o}{2\tau}(t-t_o)^2 + 2\,\frac{\rho_o-\beta}{2\tau}(t-t_o)\right] \tag{C.4}$$

where $\Phi_o = \Phi(t_o)$. The energy production resulting from $\Phi(t)$ is

$$\Delta Q(t) = \int_{t_o}^{t} \Phi(t)dt = \frac{\sqrt{\pi}}{2}\,\Phi_o\,\frac{e^{u_o^2}}{\dot{u}_o}\,[\mathrm{erf}(u) + \mathrm{erf}(u_o)] \tag{C.5}$$

with

$$\dot{u}_o = \left(-\frac{\dot{\rho}_o}{2\tau}\right)^{1/2} \tag{C.6}$$

$$u_o = \frac{\rho_o-\beta}{(-2\dot{\rho}_o\tau)^{1/2}} \tag{C.7}$$

$$u = -u_o + \dot{u}_o(t-t_o)\,. \tag{C.8}$$

For calculation of the correction to the Doppler feed-back mechanism, due to changes in the fuel heat capacity, the main difficulty is to estimate in which time interval the gradient of the feed-back is constant, because the model is only valid in this interval. It seems as if the temperature-increasing time is very near to the half-time of the power peak (fig. 6.3.1 using straight lines), consequently this time interval has been chosen as basis in the procedure.

The time interval of interest is then

$$\Delta t = \frac{\rho_o-\beta}{-\dot{\rho}_o} \tag{C.9}$$

and the energy production becomes

$$\Delta Q = \frac{\sqrt{\pi}}{2} \quad \phi_o \frac{e^{u_o^2}}{u_o} \operatorname{erf}(u_o) \simeq \frac{\sqrt{\pi}}{2} \quad \phi_o \frac{c^{u_o^2}}{u_o} . \tag{C.10}$$

Neglecting the moderator temperature feed-back (or including it in the void feed-back), the reactivity can be written

$$\rho = \rho_o + \rho_C + \rho_D + \rho_V . \tag{C.11}$$

where ρ_C, ρ_D, and ρ_V are the reactivity insertion due to the removed rod, the Doppler feed-back, and the moderator feed-back, respectively. According to chapter 6.3, the single components of the reactivity insertion are assumed to depend linearly on time. Especially the Doppler feed-back is important, and it is calculated from the fuel temperature increase as

$$\rho_D = B_D \Delta T_F^{1/2} . \tag{C.12}$$

For a particular reactor configuration, B_D is a negative constant and $\Delta T_F^{1/2}$ is the increase in the square root of the fuel temperature T_F. The moderator feed-back is simply assumed to depend linearly on the energy production in the time t.

After a DANAID run, the final fuel specific enthalpy can be calculated as

$$h_{F_1} = h_{F_o} + C_{F_1} (T_{F_1} - T_{F_o}) \tag{C.13}$$

where T_{F_o} and h_{F_o} are the initial fuel temperature and enthalpy, respectively. C_{F_1} is the specific heat capacity used in the run. The correct specific enthalpy is known as a function of the temperature $h_F = h_F(T_F)$. A corrected temperature can be obtained from the inverse function h_F^{-1}

$$T_{F_{11}} = h_F^{-1} (h_{F_1}) \tag{C.14}$$

and a corrected heat capacity

$$C_{F_{11}} = \frac{h_{F_1} - h_{F_o}}{T_{F_{11}} - T_{F_o}} . \tag{C.15}$$

Because the convective heat during the power increase is more than two decades less than the power deposit in the fuel (fig. 6.3.1), the fuel rod heating can be treated as adiabatic. Thus, both the power deposit in the fuel and the power deposit in the coolant are constant fractions of the total power deposition.

The diagram presented in fig. C.1 shows how to combine the equations evaluated in this appendix for obtaining an iterative procedure that can yield a corrected fuel temperature.

Because the energy production is strongly dependent on $\dot{\rho}$ a severe perturbation of C_F might result in instability of the iterative procedure. In this case the procedure cannot give an estimate to the correct fuel temperature. However, the temperature is bounded on T_{F_I} and $T_{F_{II}}$ given by DANAID and eq. C.13, respectively.

The final result of the procedure is a corrected fuel temperature and a corrected heat capacity.

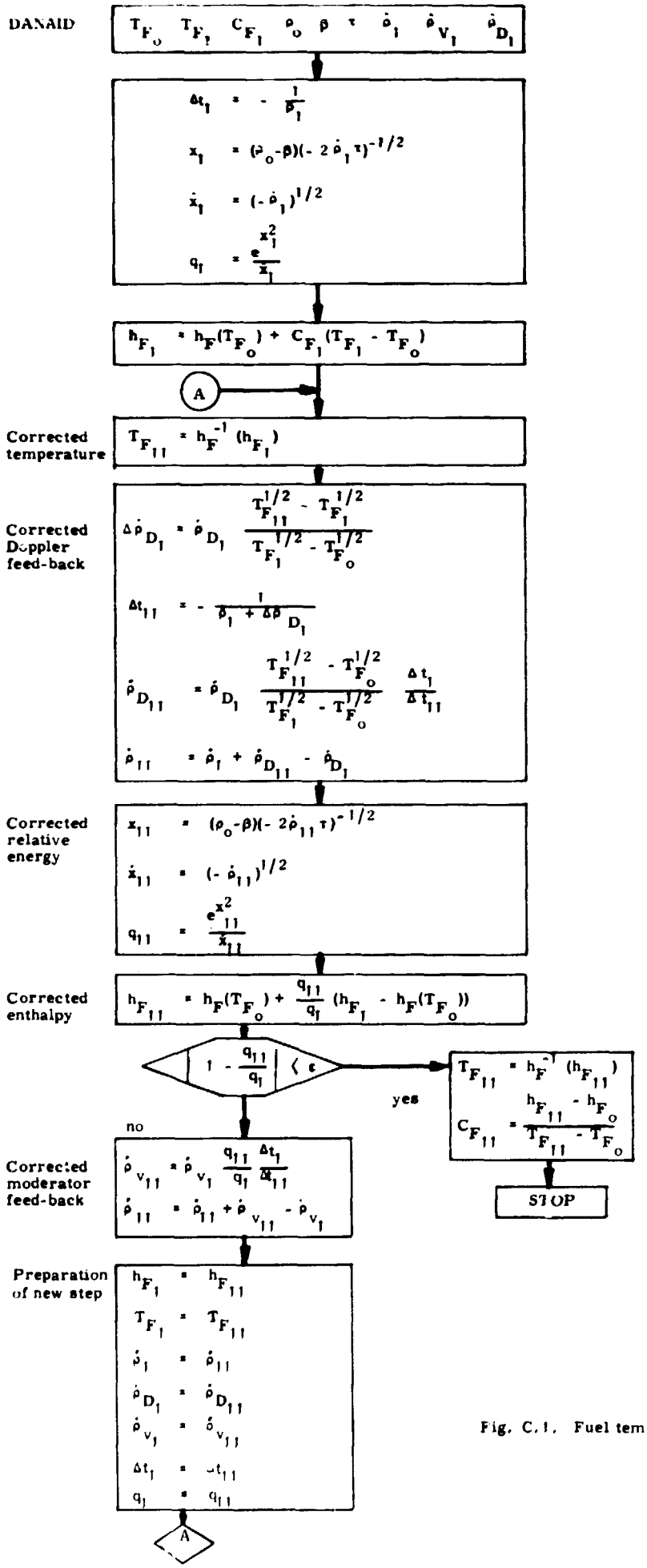

Fig. C.1. Fuel temperature correction diagram.

APPENDIX D

Solution of the Heat Conductivity Equation

Assuming constant thermodynamic properties and no power production, the fuel temperature T_F is governed by

$$\varkappa\left[\frac{\partial^2 T_F}{\partial r^2} + \frac{1}{r}\frac{\partial T_F}{\partial r}\right] = \frac{\partial T_F}{\partial t} \qquad \text{(D.1)}$$

where $\varkappa$ is the constant defined in eq. 7.1.3.

The solution to eq. D.1 can be obtained by means of the so-called separation method. The temperature is provisionally written as

$$T_F(r, t) = R(r) \cdot \tau(t) . \qquad \text{(D.2)}$$

Inserting this expression into eq. D.1 yields

$$\frac{1}{R(r)}\left[\frac{d^2R}{dr^2} + \frac{1}{r}\frac{dR}{dr}\right] = \frac{1}{\varkappa\tau(t)}\frac{d\tau}{dt} . \qquad \text{(D.3)}$$

The right-hand side of (D.3) is a function of t only and the left-hand side a function of r only, thus the two sides must be constant. Whether the constant is positive or negative cannot be determined now, but if the constant is chosen as positive, the solution to (D.3) will not fit the adequate boundary condition. Thus both sides of eq. (D.3) must be negative and the constant is written as $-p^2$.

The partial differential equation is now separated from the equations

$$\frac{d^2R}{dr^2} + \frac{1}{r}\frac{dR}{dr} + p^2 R(r) = 0$$

$$\frac{d\tau}{dt} + \varkappa p^2 \tau(t) = 0$$

with the solutions

$$R(r) = C_1 J_o(pr) + C_2 Y_o(pr) \qquad \text{(D.6)}$$

$$\tau(t) = \exp\left[\varkappa p^2(t-t_o)\right], \qquad \text{(D.7)}$$

where C_1, C_2, and t_o are arbitrary constants, and J_o and Y_o are the zero order Bessel functions of first and second kind, respectively.

Inserting the expressions for R(r) and $\tau(t)$ in eq. (D. 2) yields

$$T_F = \exp\left[-\alpha p^2 (t-t_o)\right] \left\{C_1 J_o(pr) + C_2 Y_o(pr)\right\} . \qquad (D.8)$$

The partial derivative of T(r, t), with respect to the spatial coordinate, is

$$\frac{\partial T_F}{\partial r} = \exp\left[-\alpha p^2 (t-t_o)\right] \left\{-C_1 p J_1(pr) - C_2 p Y_1(pr)\right\} \qquad (D.9)$$

J_1 and Y_1 are the first order Bessel functions of first and second kind, respectively.

Because symmetry is assumed for r = 0, one boundary condition is

$$\left(\frac{\partial T_F}{\partial r}\right)_{r=0} = 0 \qquad (D.10)$$

The characteristics of J_1 and Y_1 for zero argument are

$$J_1(0) = 0$$
$$Y_k(r) \xrightarrow[r \to o]{} -\infty \qquad (D.11)$$

This means that the arbitrary constant C_2 must be zero.

For an insufficiently cooled fuel rod, an adequate boundary condition at the fuel surface is

$$\left(\frac{\partial T_F}{\partial r}\right)_{r=r_F} = 0 \qquad (D.12)$$

where r_F is the radius of the fuel. Equation (D. 12) results in a limit to the parameter p, because only

$$p_i = \frac{\lambda_i}{r_F} \qquad i = 1, 2, \ldots , \qquad (D.13)$$

where λ_i satisfies

$$J_1(\lambda_i) = 0 \qquad i = 1, 2, \ldots , \qquad (D.14)$$

are allowed values of p.

The full solution to eq. (D.1) with the adiabatic boundary condition becomes

$$T_F(r, t) = \sum_{i=1}^{\infty} A_i \exp\left[-\pi p_i^2 (t-t_o)\right] J_o(\lambda_i \frac{r}{r_F}) . \qquad (D.15)$$

The coefficients A_i, $i = 1, 2, \ldots$ must be determined from the temperature distribution to $t = t_o$.

The life-time of the temperature signal corresponding to term i in $R_F(r, t)$ rapidly decreases with increasing i, because p_i^2 then rapidly increases.

With no power production and adiabatic boundary conditions, the average fuel temperature must be constant. This can easily be checked.

$$T(t) = \frac{\int_0^{r_F} 2\pi r\, T_F(r, t)\, dr}{\pi r_F^2} \qquad (D.16)$$

$$= \sum_{i=1}^{\infty} A_i \exp\left[-\pi p_i^2 (t-t_o)\right] \int_0^1 2x\, J_o(\lambda_i x)\, dx$$

$$= A_1$$

Thus A_1 is the average fuel temperature.

REFERENCES

1) Reactor Safety Study. An Assessment of Accident Risks in U.S. Commercial Nuclear Power Plants. WASH-1400 (NUREG-75/014) (1975) Main Report, Summary, App. 1-11.

2) Benecki, J.E., Impact Testing on Collet Assembly for Control Rod Drive Mechanism 7 RDB144A APED-5555 (1967) 31 pp.

3) BWR/6 Standard Safety Analysis Report. NEDO-10741 (DOCKET-STN-50-447) (1973) Loose Leaves.

4) Ølgaard, P.L., Forelæsningsnoter til atomkraftteknik: En-fase-tryk-tab og pumpeeffekt. Strålingsafskærmning I-III. (Danmarks Tekniske Højskole, Afdelingen for Elektrofysik, april 1973) ca. 80 pp.

5) Rod Drop Accident Analysis For Large Boiling Water Reactors. NEDO-10527 (March 1972) 74 pp.

6) Busch, J.S., Lynn, L.L., and Borilla, C.F., The Calculation of Pressure Drop and Flow Distribution within a Reactor Vessel in a Pressurized Water Nuclear System. WAPD-217 (1959) 39 pp.

7) Moody, F.J., Maximum Two-Phase Vessel Blowdown from PIPES. APED-4827 (1965) ca. 35 pp.

8) Bakstad, P. and Solberg, K.O., A Model for the Dynamics of Nuclear Reactors with Boiling Coolant with a New Approach to the Vapour Generating Process. KR 121 (1967) 68 pp.

9) Jackson, E.A., Equilibrium Statistical Mechanics. (Prentice Hall, London, 1968) 214 pp.

10) Becker, K., Hernborg, G., and Bode, M., An Experimental Study of Pressure Gradients for Flow of Boiling Water in a Vertical Round Ducts. AE-69 (Pr.1), AE-70 (Pr.2), AE-85 (Pt.3), AE-86 (Pt.4). (1962-1963).

11) Baehr, H.D., Thermodynamik. Eine Einführung in die Grundlagen und ihre technischen Anwendungen. 2. Umbearbeitete und erweiterte Auflage (Springer, Berlin, 1966) 445 pp.

12) Stacey, W.M., Space-Time Nuclear Reactor Kinetics. (Academic Press, New York, 1969) (Nuclear Science and Technology, 5) 180 pp.

13) Henry, A.F., Nuclear-Reactor Analysis. (MIT Press, Cambridge, Mass., 1975) 547 pp.

14) Suhr, P.B., Noter til forelæsningsnoter i reaktorfysik II. Diffusionsteori (1972) Unpublished Material.

15) Henry, A.F., A theoretical Method for Determining the Worth of Control Rods. WAPD-218 (1959) 50 pp.

16) Ølgaard, P.L., Forelæsningsnoter til atomkraftteknik: Strålingsafskærmning I-III. (Strålingskilder). (Danmarks Tekniske Højskole. Afdelingen for Elektrofysik, april 1973) 80 pp.

17) Properties of Water and Steam in Si-Units. Prepared by Ernest Smidt. (Springer, Berlin, 1969) 205 pp.

18) Dietrich, Ove W. and Rathmann, Ole S., Generalized Linear Least-Squares Fitting. Keyboard, 7, no. 4 (1975) 4-6.

19) Cohen, Paul, Water Coolant Technology of Power Reactors. (Gordon and Breach, New York, 1969) 439 pp.

20) Kolyadin, V.I. et al., The Thermal Conductivity of Uranium Dioxide. At. Energ., 36 (1974) 59-60 (Russ.).

21) Cortzen, F.W., H20TP, A Subroutine in Fortan for a Full Set of Light-Water Thermodynamic- and Transportproperties after the 1967 IFC Recommendations for Industrial Use. Risø-M-1844 (1976) 26 pp. Internal Report.

22) Branner, H.A. et al., Nuclear Excursion Technology. APED-5528 (1968) 42 pp.

23) Yasnisky, J.B., On the Use of Point Kinetics for the Analysis of Rod-Ejection Accidents. Nucl. Sci. Eng. 39 (1970) 241-256.

24) Janssen, E. and Levy, S., Burnout Limit Curves for Boiling Water Reactors. APED 3892 (1962) 22 pp.